

DTIC FILE COPY

2

RADC-TR-89-263  
In-House Report  
October 1989



AD-A228 689

# INCREMENTAL DIFFRACTION COEFFICIENTS FOR THE TRUNCATED HALF-PLANE AND THE CALCULATION OF THE BISTATIC RADAR CROSS SECTION OF THE DISK

Robert A. Shore and Arthur D. Yaghjian



APPROVED FOR PUBLIC RELEASE; DISTRIBUTION UNLIMITED.

ROME AIR DEVELOPMENT CENTER  
Air Force Systems Command  
Griffiss Air Force Base, NY 13441-5700

90 11 5 075

This report has been reviewed by the RADC Public Affairs Office (PA) and is releasable to the National Technical Information Service (NTIS). At NTIS it will be releasable to the general public, including foreign nations.

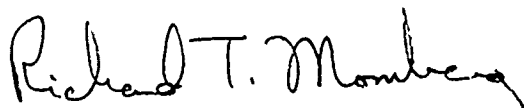
RADC TR-89-263 has been reviewed and is approved for publication.

APPROVED:



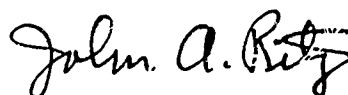
DANIEL J. JACAVANCO  
Chief, Antenna Systems Branch  
Antennas and Components Division  
Directorate of Electromagnetics

APPROVED:



RICHARD T. MOMBERG, Lt Col, USAF  
Deputy Director  
Directorate of Electromagnetics

FOR THE COMMANDER:



JOHN A. RITZ  
Directorate of Plans and Programs

If your address has changed or if you wish to be removed from the RADC mailing list, or if the addressee is no longer employed by your organization, please notify RADC (EEAS) Hanscom AFB MA 01731-5000. This will assist us in maintaining a current mailing list.

Do not return copies of this report unless contractual obligations or notices on a specific document requires that it be returned.

UNCLASSIFIED

SECURITY CLASSIFICATION OF THIS PAGE

## REPORT DOCUMENTATION PAGE

Form Approved  
OMB No. 0704-0183

1a. REPORT SECURITY CLASSIFICATION Unclassified			1b. RESTRICTIVE MARKINGS			
2a. SECURITY CLASSIFICATION AUTHORITY			3. DISTRIBUTION / AVAILABILITY OF REPORT Approved for public release; distribution unlimited			
2b. DECLASSIFICATION / DOWNGRADING SCHEDULE						
4. PERFORMING ORGANIZATION REPORT NUMBER(S) RADC-TR-89-263			5. MONITORING ORGANIZATION REPORT NUMBER(S)			
6a. NAME OF PERFORMING ORGANIZATION Rome Air Development Center		6b. OFFICE SYMBOL (If applicable) EEAS	7a. NAME OF MONITORING ORGANIZATION			
6c. ADDRESS (City, State, and ZIP Code) Hanscom AFB Massachusetts 01731-5000			7b. ADDRESS (City, State, and ZIP Code)			
8a. NAME OF FUNDING / SPONSORING ORGANIZATION		8b. OFFICE SYMBOL (If applicable)	9. PROCUREMENT INSTRUMENT IDENTIFICATION NUMBER			
8c. ADDRESS (City, State, and ZIP Code)			10. SOURCE OF FUNDING NUMBERS			
			PROGRAM ELEMENT NO. 62702F	PROJECT NO. 4600	TASK NO. 15	WORK UNIT ACCESSION NO. 07
11. TITLE (Include Security Classification) Incremental Diffraction Coefficients for the Truncated Half-Plane and the Calculation of the Bistatic Radar Cross Section of the Disk						
12. PERSONAL AUTHOR(S) Shore, R.A. and Yaghjian, A.D.						
13a. TYPE OF REPORT In-House		13b. TIME COVERED FROM Jan 88 to May 89		14. DATE OF REPORT (Year, Month, Day) 1989 October		
15. PAGE COUNT 112						
16. SUPPLEMENTARY NOTATION						
17. COSATI CODES			18. SUBJECT TERMS (Continue on reverse if necessary and identify by block number)			
FIELD	GROUP	SUB-GROUP	Incremental diffraction coefficients Strip Disk			
09	20					
19. ABSTRACT (Continue on reverse if necessary and identify by block number) In this report non-uniform current (PTD) high frequency incremental diffraction coefficients are derived for the perfectly conducting strip regarded as a truncated half-plane. An essential feature of the high frequency solution derived is that the diffraction at the trailing edge of the H-wave non-uniform leading edge current, which becomes appreciable near grazing incidence, is taken into account even when the leading and trailing edges of the incremental strips are not parallel. The incremental diffraction coefficients for the strip are then used to calculate bistatic radar cross section patterns of a perfectly conducting disk illuminated by a plane wave. Good agreement in general is obtained between the exact bistatic cross section patterns of the disk and the approximate bistatic cross section patterns obtained by adding the integral of the incremental diffraction coefficients around the edge of the disk to the physical optics scattered field.						
20. DISTRIBUTION/AVAILABILITY OF ABSTRACT <input checked="" type="checkbox"/> UNCLASSIFIED/UNLIMITED <input type="checkbox"/> SAME AS RPT. <input type="checkbox"/> DTIC USERS			21. ABSTRACT SECURITY CLASSIFICATION Unclassified			
22a. NAME OF RESPONSIBLE INDIVIDUAL Dr. Robert A. Shore			22b. TELEPHONE (Include Area Code) (617) 377-2058		22c. OFFICE SYMBOL RADC/EEAS	

DD FORM 1473, JUN 86

Previous editions are obsolete.

SECURITY CLASSIFICATION OF THIS PAGE  
UNCLASSIFIED



Accession For	
NTIS GRA&I	<input checked="" type="checkbox"/>
DTIC TAB	<input checked="" type="checkbox"/>
Unannounced	<input type="checkbox"/>
Justification	
By _____	
Distribution/	
Availability Codes	
Dist	Avail and/or Special
A-1	

## Contents

1. INTRODUCTION	1
2. THE FAR FIELDS RADIATED BY THE TRUNCATED CURRENTS OF A HALF-PLANE ILLUMINATED BY A PLANE WAVE	6
2.1 The TM Fields: Normal Incidence	7
2.2 The TM Fields: Oblique Incidence	9
2.3 The TE Fields: Normal Incidence	10
2.4 The TE Fields: Oblique Incidence	11
2.5 Modification of the TE Fields for the Trailing Edge	15
2.6 Calculations of the Two-Dimensional Bistatic Radar Cross Section of a Strip	17
3. NON-UNIFORM (PTD) INCREMENTAL DIFFRACTION COEFFICIENTS FOR THE TRUNCATED HALF-PLANE	37
4. SCATTERING OF A PLANE WAVE BY A PERFECTLY CONDUCTING DISK	44
4.1 Physical Optics Field	46
4.2 Transformation of the Local Coordinates of the Strip IDC's to the Global Coordinate System of the Disk	47
4.3 Choice of Incremental Strips	50
4.4 Calculations of the Bistatic Radar Cross Section of a Disk	51
REFERENCES	91
APPENDIX A: DERIVATION OF AN INTEGRAL OF THE FRESNEL INTEGRAL	93
APPENDIX B: DERIVATION OF INCREMENTAL STRIP PARAMETERS	95
B1. Incremental Strips Parallel to the X-axis	95
B2. Incremental Strips in the Direction of the Diffracted Rays	96
APPENDIX C: CONDITIONS FOR INCREMENTAL CURRENT STRIPS TO ACCURATELY PREDICT FIELDS DIFFRACTED FROM THE TRAILING EDGE	99
REFERENCE FOR APPENDIX C	101

## Illustrations

1a. Specular Scatter Cross Section Pattern of Disk, $ka = 15$ , for Plane-Wave Illumination with the Electric Field Polarized Perpendicular to the Plane of Incidence; ———: Exact, -----: PO, ----- : PO + Half-Plane IDC	3
1b. Specular Scatter Cross Section Pattern of Disk, $ka = 15$ , for Plane-Wave Illumination with the Electric Field Polarized Parallel to the Plane of Incidence; ———: Exact, -----: PO, ----- : PO + Half-Plane IDC	4
2. Geometry of the Truncated Half-Plane Illuminated by a Plane Wave	6
3a. Back Scatter Cross Section Pattern of Strip, $ks = 30$ , with TM (Perpendicular Polarized) Plane-Wave Illumination; ———: Exact, -----: PO + Approximate Nonuniform Current Field	18
3b. Back Scatter Cross Section Pattern of Strip, $ks = 30$ , with TE (Parallel Polarized) Plane-Wave Illumination; ———: Exact, -----: PO + Approximate Nonuniform Current Field	19
4a. Specular Scatter Cross Section Pattern of Strip, $ks = 30$ , with TM (Perpendicular Polarized) Plane-Wave Illumination; ———: Exact, -----: PO + Approximate Nonuniform Current Field	20
4b. Specular Scatter Cross Section Pattern of Strip, $ks = 30$ , with TE (Parallel Polarized) Plane-Wave Illumination; ———: Exact, -----: PO + Approximate Nonuniform Current Field	21
5a. Side Scatter Cross Section Pattern of Strip, $ks = 30$ , with TM (Perpendicular Polarized) Plane-Wave Illumination; ———: Exact, -----: PO + Approximate Nonuniform Current Field	23
5b. Side Scatter Cross Section Pattern of Strip, $ks = 30$ , with TE (Parallel Polarized) Plane-Wave Illumination; ———: Exact, -----: PO + Approximate Nonuniform Current Field	24

## Illustrations

6a.	Back Scatter Cross Section Pattern of Strip, $ks = 30$ , with TE (Parallel Polarized) Plane-Wave Illumination; ——— : Exact, ——— : PO + Approximate Nonuniform Current Field (No Trailing Edge Correction)	25
6b.	Specular Scatter Cross Section Pattern of Strip, $ks = 30$ , with TE (Parallel Polarized) Plane-Wave Illumination; ——— : Exact, ——— : PO + Approximate Nonuniform Current Field (No Trailing Edge Correction)	26
6c.	Side Scatter Cross Section Pattern of Strip, $ks = 30$ , with TE (Parallel Polarized) Plane-Wave Illumination; ——— : Exact, ——— : PO + Approximate Nonuniform Current Field (No Trailing Edge Correction)	27
7a.	Back Scatter Cross Section Pattern of Strip, $ks = 30$ , with TM (Perpendicular Polarized) Plane-Wave Illumination; ——— : Exact, ——— : PO	28
7b.	Back Scatter Cross Section Pattern of Strip, $ks = 30$ , with TE (Parallel Polarized) Plane-Wave Illumination; ——— : Exact, ——— : PO	29
8a.	Specular Scatter Cross Section Pattern of Strip, $ks = 30$ , with TM (Perpendicular Polarized) Plane-Wave Illumination; ——— : Exact, ——— : PO	30
8b.	Specular Scatter Cross Section Pattern of Strip, $ks = 30$ , with TE (Perpendicular Polarized) Plane-Wave Illumination; ——— : Exact, ——— : PO	31
9a.	Side Scatter Cross Section Pattern of Strip, $ks = 30$ , with TM (Perpendicular Polarized) Plane-Wave Illumination; ——— : Exact, ——— : PO	32
9b.	Side Scatter Cross Section Pattern of Strip, $ks = 30$ , with TE (Parallel Polarized) Plane-Wave Illumination; ——— : Exact, ——— : PO	33
10a.	Back Scatter Cross Section Pattern of Strip, $ks = 30$ , with TM (Perpendicular Polarized) Plane-Wave Illumination; ——— : Exact, ——— : Michaeli (1984)	34
10b.	Back Scatter Cross Section Pattern of Strip, $ks = 30$ , with TE (Parallel Polarized) Plane-Wave Illumination; ——— : Exact, ——— : Michaeli (1984)	35
11.	Back Scatter Cross Section Pattern of Strip, $ks = 30$ , with TE (Parallel Polarized) Plane-Wave Illumination; ——— : Exact, ——— : Ufimtsev (1969)	36
12a.	Back Scatter Cross Section Pattern of Strip, $ks = 3$ , with TM (Perpendicular Polarized) Plane-Wave Illumination; ——— : Exact, ——— : PO + Approximate Nonuniform Current Field	38
12b.	Back Scatter Cross Section Pattern of Strip, $ks = 3$ , with TE (Parallel Polarized) Plane-Wave Illumination; ——— : Exact, ——— : PO + Approximate Nonuniform Current Field	39
13a.	Specular Scatter Cross Section Pattern of Strip, $ks = 3$ , with TM (Perpendicular Polarized) Plane-Wave Illumination; ——— : Exact, ——— : PO + Approximate Nonuniform Current Field	40
13b.	Specular Scatter Cross Section Pattern of Strip, $ks = 3$ , with TE (Parallel Polarized) Plane-Wave Illumination; ——— : Exact, ——— : PO + Approximate Nonuniform Current Field	41

## Illustrations

14a.	Side Scatter Cross Section Pattern of Strip, $ks = 3$ , with TM (Perpendicular Polarized) Plane-Wave Illumination; ——— : Exact, - - - - - : PO + Approximate Nonuniform Current Field	42
14b.	Side Scatter Cross Section Pattern of Strip, $ks = 3$ , with TE (Parallel Polarized) Plane-Wave Illumination; ——— : Exact, - - - - - : PO + Approximate Nonuniform Current Field	43
15.	Geometry of Disk Illuminated by a Plane Wave	45
16a.	Back Scatter Cross Section Pattern of Disk, $ka = 15$ , with Perpendicular Polarized Plane-Wave Illumination and Incremental Strips Parallel to x-Axis; ——— : Exact, - - - - - : PO + Approximate Nonuniform Current Field Obtained by Integrating IDC	53
16b.	Back Scatter Cross Section Pattern of Disk, $ka = 15$ , with Perpendicular Polarized Plane-Wave Illumination and Incremental Strips in Direction of Diffracted Rays; ——— : Exact, - - - - - : PO + Approximate Nonuniform Current Field Obtained by Integrating IDC	54
17a.	Back Scatter Cross Section Pattern of Disk, $ka = 15$ , with Parallel Polarized Plane-Wave Illumination and Incremental Strips Parallel to x-Axis; ——— : Exact, - - - - - : PO + Approximate Nonuniform Current Field Obtained by Integrating IDC	55
17b.	Back Scatter Cross Section Pattern of Disk, $ka = 15$ , with Parallel Polarized Plane-Wave Illumination and Incremental Strips in Direction of Diffracted Rays; ——— : Exact, - - - - - : PO + Approximate Nonuniform Current Field Obtained by Integrating IDC	56
18a.	Specular Scatter Cross Section Pattern of Disk, $ka = 15$ , with Perpendicular Polarized Plane-Wave Illumination and Incremental Strips Parallel to x-Axis; ——— : Exact, - - - - - : PO + Approximate Nonuniform Current Field Obtained by Integrating IDC	57
18b.	Specular Scatter Cross Section Pattern of Disk, $ka = 15$ , with Perpendicular Polarized Plane-Wave Illumination and Incremental Strips in Direction of Diffracted Rays; ——— : Exact, - - - - - : PO + Approximate Nonuniform Current Field Obtained by Integrating IDC	58
19a.	Specular Scatter Cross Section Pattern of Disk, $ka = 15$ , with Parallel Polarized Plane-Wave Illumination and Incremental Strips Parallel to x-Axis; ——— : Exact, - - - - - : PO + Approximate Nonuniform Current Field Obtained by Integrating IDC	59
19b.	Specular Scatter Cross Section Pattern of Disk, $ka = 15$ , with Parallel Polarized Plane-Wave Illumination and Incremental Strips in Direction of Diffracted Rays; ——— : Exact, - - - - - : PO + Approximate Nonuniform Current Field Obtained by Integrating IDC	60
20a.	Side Scatter Cross Section Pattern of Disk, $ka = 15$ , with Perpendicular Polarized Plane-Wave Illumination and Incremental Strips Parallel to x-Axis; ——— : Exact, - - - - - : PO + Approximate Nonuniform Current Field Obtained by Integrating IDC	61
20b.	Side Scatter Cross Section Pattern of Disk, $ka = 15$ , with Perpendicular Polarized Plane-Wave Illumination and Incremental Strips in Direction of Diffracted Rays; ——— : Exact, - - - - - : PO + Approximate Nonuniform Current Field Obtained by Integrating IDC	62

## Illustrations

21a.	Side Scatter Cross Section Pattern of Disk, $ka = 15$ , with Parallel Polarized Plane-Wave Illumination and Incremental Strips Parallel to x-Axis; ——— : Exact, - - - - - : PO + Approximate Nonuniform Current Field Obtained by Integrating IDC	63
21b.	Side Scatter Cross Section Pattern of Disk, $ka = 15$ , with Parallel Polarized Plane-Wave Illumination and Incremental Strips in Direction of Diffracted Rays; ——— : Exact, - - - - - : PO + Approximate Nonuniform Current Field Obtained by Integrating IDC	64
22a.	Co-Polarized Cross Section Pattern of Disk, $ka = 15$ , Illuminated by Perpendicular Polarized Plane Wave at $\theta_i = 45^\circ$ in Plane Defined by $\phi = 45^\circ$ and $\phi = 225^\circ$ , with Incremental Strips Parallel to x-Axis; ——— : Exact, - - - - - : PO + Approximate Nonuniform Current Field Obtained by Integrating IDC	65
22b.	Co-Polarized Cross Section Pattern of Disk, $ka = 15$ , Illuminated by Perpendicular Polarized Plane Wave at $\theta_i = 45^\circ$ in Plane Defined by $\phi = 45^\circ$ and $\phi = 225^\circ$ , with Incremental Strips in Direction of Diffracted Rays; ——— : Exact, - - - - - : PO + Approximate Nonuniform Current Field Obtained by Integrating IDC	66
23a.	Cross-Polarized Cross Section Pattern of Disk, $ka = 15$ , Illuminated by Perpendicular Polarized Plane Wave at $\theta_i = 45^\circ$ in Plane Defined by $\phi = 45^\circ$ and $\phi = 225^\circ$ , with Incremental Strips Parallel to x-Axis; ——— : Exact, - - - - - : PO + Approximate Nonuniform Current Field Obtained by Integrating IDC	67
23b.	Cross-Polarized Cross Section Pattern of Disk, $ka = 15$ , Illuminated by Perpendicular Polarized Plane Wave at $\theta_i = 45^\circ$ in Plane Defined by $\phi = 45^\circ$ and $\phi = 225^\circ$ , with Incremental Strips in Direction of Diffracted Rays; ——— : Exact, - - - - - : PO + Approximate Nonuniform Current Field Obtained by Integrating IDC	68
24a.	Co-Polarized Cross Section Pattern of Disk, $ka = 15$ , Illuminated by Parallel Polarized Plane Wave at $\theta_i = 45^\circ$ in Plane Defined by $\phi = 45^\circ$ and $\phi = 225^\circ$ , with Incremental Strips Parallel to x-Axis; ——— : Exact, - - - - - : PO + Approximate Nonuniform Current Field Obtained by Integrating IDC	69
24b.	Co-Polarized Cross Section Pattern of Disk, $ka = 15$ , Illuminated by Parallel Polarized Plane Wave at $\theta_i = 45^\circ$ in Plane Defined by $\phi = 45^\circ$ and $\phi = 225^\circ$ , with Incremental Strips in Direction of Diffracted Rays; ——— : Exact, - - - - - : PO + Approximate Nonuniform Current Field Obtained by Integrating IDC	70
25a.	Cross-Polarized Cross Section Pattern of Disk, $ka = 15$ , Illuminated by Parallel Polarized Plane Wave at $\theta_i = 45^\circ$ in Plane Defined by $\phi = 45^\circ$ and $\phi = 225^\circ$ , with Incremental Strips Parallel to x-Axis; ——— : Exact, - - - - - : PO + Approximate Nonuniform Current Field Obtained by Integrating IDC	71
25b.	Cross-Polarized Cross Section Pattern of Disk, $ka = 15$ , Illuminated by Parallel Polarized Plane Wave at $\theta_i = 45^\circ$ in Plane Defined by $\phi = 45^\circ$ and $\phi = 225^\circ$ , with Incremental Strips in Direction of Diffracted Rays; ——— : Exact, - - - - - : PO + Approximate Nonuniform Current Field Obtained by Integrating IDC	72
26a.	Back Scatter Cross Section Pattern of Disk, $ka = 15$ , with Perpendicular Polarized Plane-Wave Illumination; ——— : Exact, - - - - - : PO	74



## Illustrations

26b.	Back Scatter Cross Section Pattern of Disk, $ka = 15$ , with Parallel Polarized Plane-Wave Illumination; ——— : Exact, ——— : PO	75
27a.	Specular Scatter Cross Section Pattern of Disk, $ka = 15$ , with Perpendicular Polarized Plane-Wave Illumination; ——— : Exact, ——— : PO	76
27b.	Specular Scatter Cross Section Pattern of Disk, $ka = 15$ , with Parallel Polarized Plane-Wave Illumination; ——— : Exact, ——— : PO	77
28a.	Side Scatter Cross Section Pattern of Disk, $ka = 15$ , with Perpendicular Polarized Plane-Wave Illumination; ——— : Exact, ——— : PO	78
28b.	Side Scatter Cross Section Pattern of Disk, $ka = 15$ , with Parallel Polarized Plane-Wave Illumination; ——— : Exact, ——— : PO	79
29a.	Co-Polarized Cross Section Pattern of Disk, $ka = 15$ , Illuminated by Perpendicular Polarized Plane Wave at $\theta_i = 45^\circ$ in Plane Defined by $\phi = 45^\circ$ and $\phi = 225^\circ$ ; ——— : Exact, ——— : PO	80
29b.	Cross-Polarized Cross Section Pattern of Disk, $ka = 15$ , Illuminated by Perpendicular Polarized Plane Wave at $\theta_i = 45^\circ$ in Plane Defined by $\phi = 45^\circ$ and $\phi = 225^\circ$ ; ——— : Exact, ——— : PO	81
30a.	Co-Polarized Cross Section Pattern of Disk, $ka = 15$ , Illuminated by Parallel Polarized Plane Wave at $\theta_i = 45^\circ$ in Plane Defined by $\phi = 45^\circ$ and $\phi = 225^\circ$ ; ——— : Exact, ——— : PO	82
30b.	Cross-Polarized Cross Section Pattern of Disk, $ka = 15$ , Illuminated by Parallel Polarized Plane Wave at $\theta_i = 45^\circ$ in Plane Defined by $\phi = 45^\circ$ and $\phi = 225^\circ$ ; ——— : Exact, ——— : PO	83
31a.	Back Scatter Cross Section Pattern of Disk, $ka = 1.5$ , with Perpendicular Polarized Plane-Wave Illumination and Incremental Strips Parallel to x-Axis; ——— : Exact, ——— : PO + Approximate Nonuniform Current Field Obtained by Integrating IDC	84
31b.	Back Scatter Cross Section Pattern of Disk, $ka = 1.5$ , with Parallel Polarized Plane-Wave Illumination and Incremental Strips Parallel to x-Axis; ——— : Exact, ——— : PO + Approximate Nonuniform Current Field Obtained by Integrating IDC	85
32a.	Specular Scatter Cross Section Pattern of Disk, $ka = 1.5$ , with Perpendicular Polarized Plane-Wave Illumination and Incremental Strips Parallel to x-Axis; ——— : Exact, ——— : PO + Approximate Nonuniform Current Field Obtained by Integrating IDC	86
32b.	Specular Scatter Cross Section Pattern of Disk, $ka = 1.5$ , with Parallel Polarized Plane-Wave Illumination and Incremental Strips Parallel to x-Axis; ——— : Exact, ——— : PO + Approximate Nonuniform Current Field Obtained by Integrating IDC	87
33a.	Side Scatter Cross Section Pattern of Disk, $ka = 1.5$ , with Perpendicular Polarized Plane-Wave Illumination and Incremental Strips Parallel to x-Axis; ——— : Exact, ——— : PO + Approximate Nonuniform Current Field Obtained by Integrating IDC	88
33b.	Side Scatter Cross Section Pattern of Disk, $ka = 1.5$ , with Parallel Polarized Plane-Wave Illumination and Incremental Strips Parallel to x-Axis; ——— : Exact, ——— : PO + Approximate Nonuniform Current Field Obtained by Integrating IDC	89

## Illustrations

B1a. Geometry Of Disk with Incremental Strips Parallel to the x-Axis	96
B1b. Corresponding Strip Geometry	96

# Incremental Diffraction Coefficients for the Truncated Half-Plane and the Calculation of the Bistatic Radar Cross Section of the Disk

## 1. INTRODUCTION

Exact expressions for incremental diffraction coefficients (IDC's), also called equivalent edge currents, have been derived for the perfectly conducting wedge by integrating the wedge currents over an increment of the wedge<sup>1,2</sup> and more recently, for any planar current surface or combination of planar current surfaces by direct substitution of the two-dimensional (2-D) far fields of each planar surface into convenient general expressions.<sup>3,4,5</sup> Incremental diffraction coefficients obtained for the total current, the physical optics current, or the nonuniform current, that is, the difference between the total and physical optics currents, are referred to as the GTD (geometrical theory of diffraction), PO

---

(Received for Publication 14 November 1989)

1. Mitzner, K.M. (1974) *Incremental Length Diffraction Coefficients*, Tech. Rep. No. AFAL-TR-73-296, (available from National Technical Information Service, Springfield, VA 22161, AD918861).
2. Michaeli, A. (1984) Equivalent edge currents for arbitrary aspects of observation, *IEEE Trans. Antennas Propagat.* **AP-32**:252-258, (correction, (1985) **AP-33**:227).
3. Shore, R.A. and Yaghjian, A.D. (1988) Incremental diffraction coefficients for planar surfaces, *IEEE Trans. Antennas Propagat.* **36**:55-70, (correction, (1989) **AP-37**:1342), also, *Incremental Diffraction Coefficients for Planar Surfaces, Part I: Theory*, RADC-TR-87-35, ADA208595.
4. Shore, R.A. and Yaghjian, A.D. (1987) *Incremental Diffraction Coefficients for Planar Surfaces, Part II: Calculation of Nonuniform Current Correction to PO Reflector Antenna Patterns*, RADC-TR-87-213, ADA208596.
5. Shore, R.A. and Yaghjian, A.D. (1988) *Incremental Diffraction Coefficients for Planar Surfaces, Part III: Pattern Effects of Narrow Cracks in the Surface of a Paraboloid Antenna*, RADC-TR-88-119, ADA207796.

(physical optics) and PTD (physical theory of diffraction) incremental diffraction coefficients, respectively.<sup>3</sup> For the perfectly conducting wedge, Mitzner<sup>1</sup> concentrated on the PTD incremental diffraction coefficients, Michaeli derived the GTD coefficients initially<sup>2</sup> and later the PTD coefficients<sup>6</sup>, and Knott<sup>7</sup> determined the PO incremental diffraction coefficients from the difference between the GTD and PTD coefficients.

Assume incremental diffraction coefficients have been determined for a canonical 2-D scatterer of finite cross section. The integration of these finite incremental diffraction coefficients (multiplied by the incident field) along the bounding curves of three-dimensional (3-D) scatterers produces a uniform high-frequency solution even at and near caustics where conventional stationary-phase high-frequency techniques fail. As an example, Shore and Yaghjian obtained uniform IDC's for the narrow (electrically small) strip and slit and used them to calculate the effect of cracks between the panels of reflector antennas on the antennas' co-polarized and cross-polarized far fields.<sup>3,5</sup>

For canonical problems of infinite cross section, like the wedge, the incremental diffraction coefficients contain the same discontinuities and singularities as the far-field of the canonical 2-D problems. Specifically, the GTD incremental diffraction coefficients of the wedge contain the discontinuities in the diffracted H-wave fields at the face angles of the wedge, the singularities in the E- and H-wave far fields at a face angle of the wedge when an incident plane wave grazes that face from the outside, and the singularities in the total diffracted far fields at the shadow and reflection boundaries. Integrating the PO current separately and using PTD incremental diffraction coefficients, instead of GTD incremental coefficients, eliminates the singularities at the shadow and reflection boundaries, but retains the face-angle discontinuities and singularities.<sup>6</sup>

Figure 1 shows the specularly scattered fields of a perfectly conducting infinitely thin disk computed by numerically integrating the PTD incremental diffraction coefficients for the infinite half-plane around the rim of the disk, and adding the result to the PO fields. The comparison in Figure 1 of the PO plus IDC fields with the PO fields alone, and with the exact scattered fields obtained from the eigenfunction solution to the disk, shows that the integrated PTD incremental coefficients of the half-plane become divergent at grazing. (Interestingly, for specular scattering from the disk, the PO and integrated PTD-IDC far fields are identical for the two incidental plane-wave polarizations.) Thus, Figure 1 illustrates the limitations of infinite half-plane IDC's and motivates this report's primary objective: to determine accurate high-frequency incremental diffraction coefficients for the leading and trailing edges of the truncated half-plane in order to eliminate the singularities and discontinuities in the diffraction coefficients of the infinite half-plane. Of course, the 2-D truncated half-plane, that is the strip, has an exact eigenfunction solution that could be used to find the 3-D incremental coefficients by substituting the exact solution into the general expressions of Reference 3. However, the summation of eigenfunctions takes a considerable amount of computer time for

- 
6. Michaeli, A. (1986) Elimination of infinities in equivalent edge currents, Part I: fringe current components, *IEEE Trans. Antennas Propagat.* AP-34:912-918.
  7. Knott, E.F. (1985) The relationship between Mitzner's ILDC and Michaeli's equivalent currents, *IEEE Trans. Antennas Propagat.* AP-33:112-114.

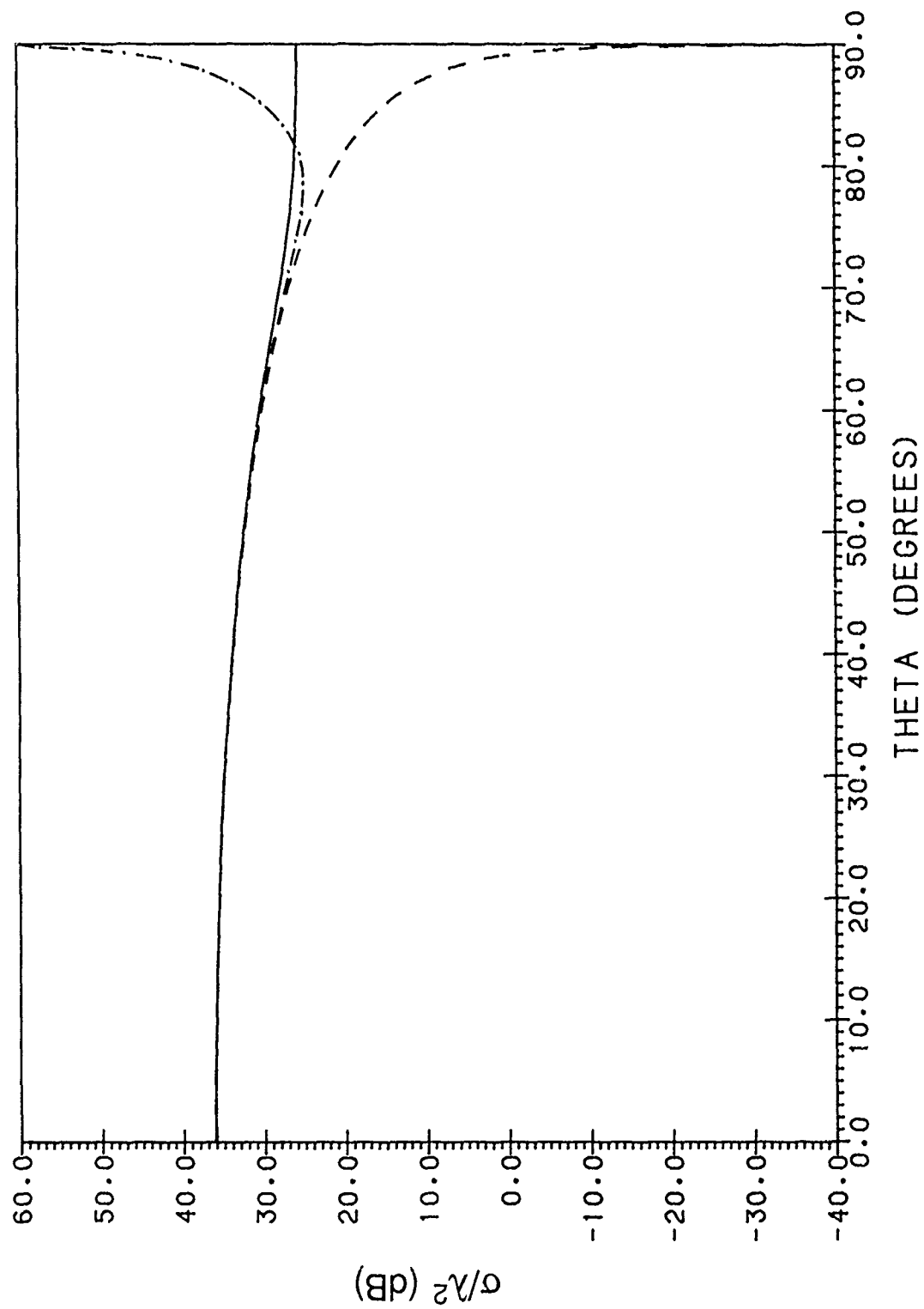


Figure 1a. Specular Scatter Cross Section Pattern of Disk,  $ka = 15$ , for Plane-Wave Illumination with the Electric Field Polarized Perpendicular to the Plane of Incidence: —: Exact, ----: PO, - . - . : PO + Half-Plane IDC

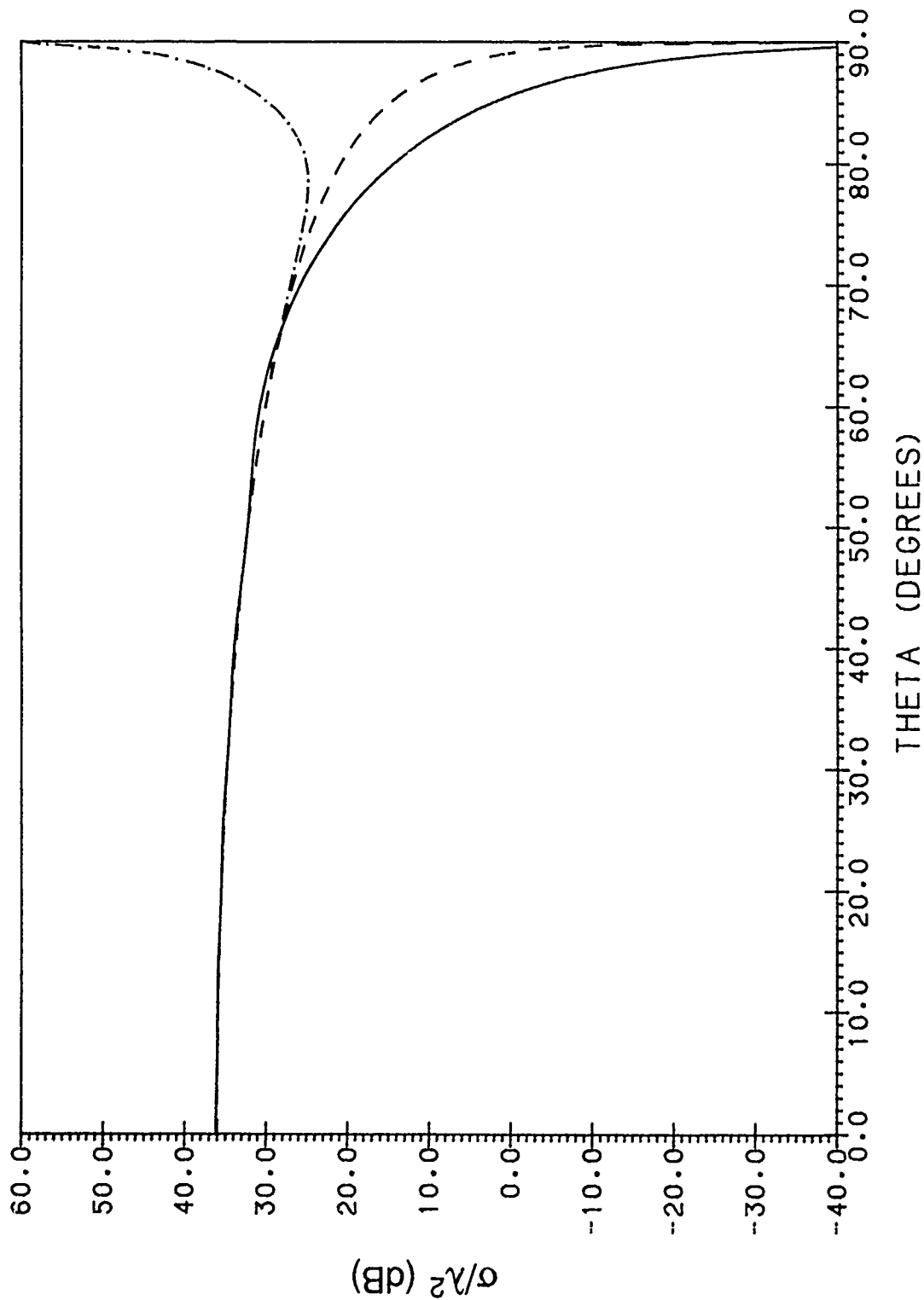


Figure 1b. Specular Scatter Cross Section Pattern of Disk,  $ka = 15$ , for Plane-Wave Illumination with the Electric Field Polarized Parallel to the Plane of Incidence; —: Exact, - - - - -: PO, - . - . - : PO + Half-Plane IDC

electrically large strips and the available computer codes encountered numerical difficulties evaluating the required Mathieu functions when the strips became wider than about 5 wavelengths. Moreover, the exact strip solution yields the incremental diffraction coefficients for rectangular incremental strips only, rather than for general trapezoidal strips that are able to conform to the rim of an arbitrarily shaped polygonal plate or disk. Thus, we found it desirable to determine an accurate, uniform high-frequency solution to the perfectly conducting truncated half-plane with the leading and trailing edges treated separately (though not necessarily independently) so that IDC's for trapezoidal strips could be found.

Previous IDC work has also involved high-frequency solutions to the strip.<sup>8,9,10</sup> Coleman et al<sup>8</sup> combined the use of rectangular incremental strips that do not conform to the rim of the general 3-D plates to which they are applied, with an early, relatively inaccurate, high-frequency 2-D strip solution of Ufimtsev.<sup>11</sup> Sikta et al<sup>9</sup> also used nonconformal rectangular incremental strips and obtained scattering in the plane of incidence only. Michaeli<sup>10</sup> used conformal incremental strips, but evaluated the current integrals of the incremental strips asymptotically so that singularities at grazing incidence arise. None of these previous strip solutions included diffraction of the nonuniform leading edge currents at the trailing edge of the strip. An essential feature of the high-frequency solution derived in this report is that the diffraction at the trailing edge of the H-wave nonuniform leading edge current, which becomes appreciable near grazing incidence, is taken into account even when the leading and trailing edges of the incremental strip are not parallel.

The analysis begins by finding convenient expressions for two-dimensional fields radiated by the truncated leading and trailing edge currents of a half-plane illuminated by a TM or TE plane wave. These 2-D leading and trailing edge diffracted fields are then used to compute the high-frequency bistatic radar cross section of an infinite strip. This high-frequency solution is then compared with the exact eigenfunction solution for the strip.

Next, the 2-D diffracted fields of the truncated half-plane are inserted into the general expressions of Reference 3 to obtain the PTD incremental diffraction coefficients for the leading and trailing edges of the truncated half-plane. Finally, these PTD incremental diffraction coefficients are applied to finding the approximate far fields scattered by a circular disk illuminated with a TM or TE plane wave. These approximate high-frequency scattered fields are compared with the exact far fields computed from the eigenfunction solution to the disk.

- 
8. Coleman, J.R. (1973) *Investigation of Radar Scattering by Simulated Aircraft Duct/Engine Combinations*, Air Force Avionics Laboratory, AFAL-TR-73-361.
  9. Sikta, F.A., Burnside, W.D., Chu, T.T., and Peters, L., Jr. (1983) First-order equivalent current and corner diffraction scattering from flat plate structures, *IEEE Trans. Antennas Propagat.* **AP-31**:584-589.
  10. Michaeli, A. (1987) Equivalent currents for second-order diffraction by the edges of perfectly conducting polygonal surfaces, *IEEE Trans. Antennas Propagat.* **AP-35**:183-190.
  11. Ufimtsev, P. Ya. (1958) Secondary diffraction of electromagnetic waves at a strip, *Journal of Technical Physics* **28** (No. 3).

## 2. THE FAR FIELDS RADIATED BY THE TRUNCATED CURRENTS OF A HALF-PLANE ILLUMINATED BY A PLANE WAVE

The general expressions in Reference 3 yield the 3-D incremental diffraction coefficients of a planar, perfectly conducting 2-D canonical scatterer through direct substitution of the 2-D far fields of this canonical scatterer. Thus we begin the derivation of IDC's for the truncated half-plane by deriving the far fields radiated by the currents on a truncated half-plane, or more precisely the far fields of the truncated currents of an infinite half-plane under plane-wave illumination. Figure 2 shows the truncated half-plane lying between  $x = 0$  and  $x = s$  and stretching from  $-\infty$  to  $\infty$  in the  $z$ -direction. The spherical angles  $(\phi, \theta)$  of the observation direction  $\hat{r}$ , and the spherical angles  $(\phi_0, \theta_0)$  of the propagation direction  $\hat{k}$  of the incident plane wave are also shown in Figure 2.

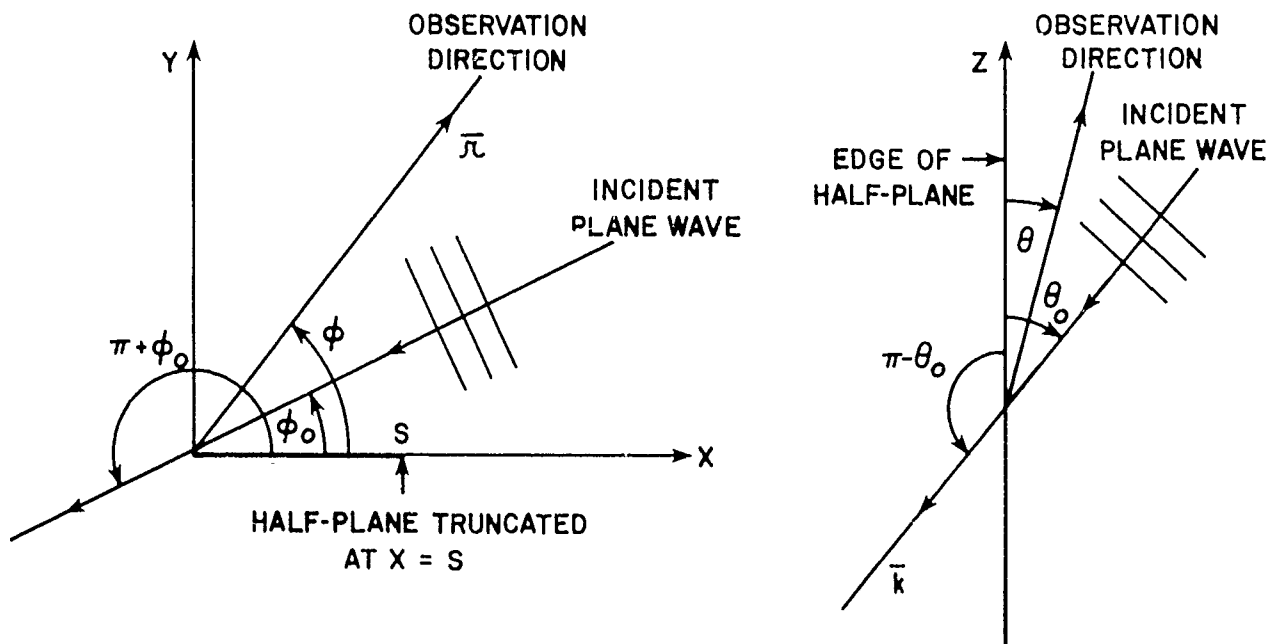


Figure 2. Geometry of the Truncated Half-Plane Illuminated by a Plane Wave

The far fields radiated by a current  $\bar{K}$  on the truncated half-plane are given by the integral<sup>3</sup>

$$\bar{H}(\bar{r}) \underset{r \rightarrow \infty}{\sim} \frac{e^{ik\hat{r}_0 \cdot \bar{r}} e^{i\pi/4}}{(8\pi k \rho \sin \theta_0)^{1/2}} i k \hat{r}_0 \times \int_0^S \bar{K}(x') e^{-ikx' \sin \theta_0 \cos \phi} dx' \quad (1a)$$

$$\bar{E}(\bar{r}) \sim -Z_0 \hat{r}_0 \times \bar{H}(\bar{r}), \quad r \rightarrow \infty, \quad (1b)$$

where the unit vector  $\hat{r}_0$  in Eq. (1) is defined as the unit vector  $\hat{r}$  evaluated at  $\phi$  and  $\theta = \pi - \theta_0$ , that is,  $\hat{r}_0 = \hat{\rho} \sin \theta_0 - \hat{z} \cos \theta_0$ . The  $\exp(-i\omega t)$  time dependence has been suppressed and  $Z_0$  is the plane-wave impedance of free space. For a normally incident plane wave ( $\theta_0 = 90^\circ$ ), Eq. (1) reduces to



$$\bar{H}(\bar{\rho}) \underset{\rho \rightarrow \infty}{\sim} \frac{e^{i(k\rho + \pi/4)}}{(8\pi k\rho)^{1/2}} i k \hat{\rho} \times \int_0^S \bar{K}(x') e^{-i k x' \cos \phi} dx', \quad (2a)$$

$$\bar{E}(\bar{\rho}) \sim -Z_0 \hat{\rho} \times \bar{H}(\bar{\rho}), \quad \rho \rightarrow \infty. \quad (2b)$$

The far-field expressions in Eq. (2) for normal incidence are especially important because once they are found, the far fields for an obliquely incident TM plane wave are determined immediately by substituting  $k \sin \theta_0$  for  $k$  and multiplying by  $\exp(-ikz \cos \theta_0)$ . The  $H_0$  (or  $E_0$ ) far-field for an obliquely incident TE plane wave is also determined by this simple substitution and multiplication. However, the  $H_\phi$  (or  $E_\phi$ ) far field, which occurs only at oblique incidence in the TE case, must be obtained by an alternative procedure; for example, by integrating the current in Eq. (1).<sup>3</sup>

## 2.1 The TM (Parallel Polarized) Fields: Normal Incidence

The total current on a perfectly electrically conducting infinite half-plane illuminated by a normally incident ( $\theta_0 = 90^\circ$ ) TM plane wave, given by

$$\bar{E}_i = \hat{z} E_i \exp[ik\rho \cos(\phi - \phi_0)], \quad (3)$$

may be found from Eq. (8.14) of Bowman, Senior and Uslenghi<sup>12</sup>:

$$\begin{aligned} \bar{K} = \hat{z} K_z = \hat{z} \frac{2}{Z_0} E_i \sin \frac{\phi_0}{2} e^{i\pi/4} \\ \cdot \left[ \left( \frac{2}{\pi k x} \right)^{1/2} e^{i k x} - 2i\sqrt{2} \left| \cos \frac{\phi_0}{2} \right| e^{-i k x \cos \frac{\phi_0}{2}} F\left( 2k \cos^2 \frac{\phi_0}{2} x \right) \right] \end{aligned} \quad (4)$$

where  $F$  is the Fresnel integral defined by

$$F(x) = \frac{1}{\sqrt{2\pi}} \int_0^x \frac{e^{it}}{\sqrt{t}} dt. \quad (5)$$

Substitute the total current  $\bar{K}$  from Eq. (4) into the integral of Eq. (2), and make use of the following integral of the Fresnel integral derived in Appendix A,

$$\int_0^x F(u) e^{ia u} du = \frac{1}{ia} \left[ e^{iax} F(x) - \frac{(F^o|a + 1|x)}{|a + 1|^{1/2}} \right] \quad (6)$$

12. Bowman, J.J., Senior, T.B.A., and Uslenghi, P.L.E. (1969) *Electromagnetic and Acoustic Scattering by Simple Shapes*, Amsterdam: North-Holland.

where  $F^o(t)$  denotes  $F(t)$  when  $t > 0$  and the complex conjugate of  $F(t)$  when  $t < 0$ , to obtain the TM far fields of the total current for normal incidence

$$\begin{aligned} \bar{E}_s^{TM}(\bar{\rho}) \rho \rightarrow \infty & \sim \hat{z} E_1 \frac{e^{ik\rho}}{(\pi k\rho)^{1/2}} \frac{\sin \frac{\phi_0}{2}}{\cos \phi_0 + \cos \phi} \\ & \cdot \left[ \frac{\sqrt{2}(1 - \cos \phi)}{\sqrt{|1 - \cos \phi|}} F^o(ks|1 - \cos \phi|) \right. \\ & \left. - 2 \left| \cos \frac{\phi_0}{2} \right| e^{-iks(\cos \phi_0 + \cos \phi)} F\left(2ks \cos^2 \frac{\phi_0}{2}\right) \right], \end{aligned} \quad (7a)$$

$$0 \leq \phi, \phi_0 < 2\pi,$$

$$\bar{H}_s^{TM}(\bar{\rho}) \sim \hat{\rho} \times \bar{E}_s^{TM}(\bar{\rho}), \rho \rightarrow \infty. \quad (7b)$$

(We retain the absolute value signs in  $|1 - \cos \phi|$  because when the IDC's are found by substitution of Eq. (7) into the general expression of Reference 3,  $\cos \phi$  is replaced by a variable that may become greater than one; see Section 3.)

Eqs. (7) give the far fields of the total current emanating from either a leading or trailing edge of the truncated half-plane. To obtain the TM far fields of the truncated nonuniform current, simply subtract the TM, PO far fields,

$$\bar{E}^{PO(TM)}(\bar{\rho}) \rho \rightarrow \infty \sim \hat{z} E_1 \sqrt{2} \frac{e^{i(k\rho + \pi/4)}}{(\pi k\rho)^{1/2}} \frac{\sin \frac{\phi_0}{2} \left| \cos \frac{\phi_0}{2} \right|}{\cos \phi_0 + \cos \phi} \left[ 1 - e^{iks(\cos \phi_0 + \cos \phi)} \right] \quad (8a)$$

$$\bar{H}^{PO(TM)}(\bar{\rho}) \sim \hat{\rho} \times \bar{E}^{PO(TM)}/Z_0, \rho \rightarrow \infty, \quad (8b)$$

from Eq. (7) to get

$$\begin{aligned} \bar{E}^{nu(TM)}(\bar{\rho}) \rho \rightarrow \infty & \sim \hat{z} E_1 \frac{e^{ik\rho}}{(\pi k\rho)^{1/2}} \frac{\sin \frac{\phi_0}{2}}{\cos \phi_0 + \cos \phi} \left\{ \frac{\sqrt{2}(1 - \cos \phi)}{\sqrt{|1 - \cos \phi|}} F^o(ks|1 - \cos \phi|) \right. \\ & - \left| \cos \frac{\phi_0}{2} \right| \left[ 2e^{-iks(\cos \phi_0 + \cos \phi)} F\left(2ks \cos^2 \frac{\phi_0}{2}\right) \right. \\ & \left. \left. + \sqrt{2} e^{i\pi/4} (1 - e^{-iks(\cos \phi_0 + \cos \phi)}) \right] \right\}, \end{aligned} \quad (9a)$$

$$0 \leq \phi, \phi_0 < 2\pi,$$

$$\bar{H}^{nu(TM)}(\bar{\rho}) \sim \hat{\rho} \times \bar{E}^{nu(TM)}(\bar{\rho})/Z_0, \rho \rightarrow \infty. \quad (9b)$$

Depending on whether the incident plane wave makes an angle  $\phi_0$  greater than or less than  $90^\circ$  (or less than or greater than  $270^\circ$ ), Eq. (9) gives the far fields of the nonuniform half-plane current of the leading or trailing edge, respectively, truncated at the trailing or leading edge, respectively. Of course, in reality, there will exist multiple interactions between the leading and trailing edges dominated by the nonuniform current from the leading edge diffracting at the trailing edge. However, for the TM incident fields the nonuniform current decays as the inverse of the square root of the distance from the edge, and thus Eq. (9) is a good approximation for the nonuniform far fields of the trailing as well as the leading edges of electrically large strips ( $s \geq \lambda$ ).

## 2.2 The TM Fields: Oblique Incidence

As mentioned in Section 2, the far fields radiated by the total, PO, and nonuniform currents can be determined for an obliquely incident TM plane wave essentially by replacing  $k$  with  $k \sin \theta_0$  in the far fields for normal incidence and multiplying by  $\exp(-ikz \cos \theta_0)$ . In particular, Eqs. (7) generalize for oblique incidence to

$$\begin{aligned} \bar{E}^{\text{nu(TM)}}(\bar{r}) \underset{r \rightarrow \infty}{\sim} & -\hat{\theta}_0^\pi E_1 \frac{C_0 2\sqrt{2} e^{-i\pi/4}}{ik} \frac{\sin \frac{\phi_0}{2}}{\cos \phi_0 + \cos \phi} \\ & \cdot \left\{ \frac{\sqrt{2} (1 - \cos \phi)}{\sqrt{|1 - \cos \phi|}} F^o(ks \sin \theta_0 | 1 - \cos \phi |) \right. \\ & - \left| \cos \frac{\phi_0}{2} \right| \left[ 2e^{-i ks \sin \theta_0 (\cos \phi_0 + \cos \phi)} \cdot F\left(2ks \sin \theta_0 \cos^2 \frac{\phi_0}{2}\right) \right. \\ & \left. \left. + \sqrt{2} e^{i\pi/4} \left( 1 - e^{-i ks \sin \theta_0 (\cos \phi_0 + \cos \phi)} \right) \right] \right\}. \end{aligned} \quad (10a)$$

$$0 \leq \phi, \phi_0 < 2\pi,$$

$$0 \leq \theta_0 < \pi,$$

$$\bar{H}^{\text{nu(TM)}}(\bar{r}) \sim \hat{r}_0 \times \bar{E}^{\text{nu(TM)}}(\bar{r}) / Z_0, \quad r \rightarrow \infty \quad (10b)$$

where  $\hat{\theta}_0^\pi$  is the unit vector  $\hat{\theta}$  evaluated at  $\theta = \pi - \theta_0$ , and

$$C_0 = \frac{e^{ik(\rho \sin \theta_0 - z \cos \theta_0)} e^{i\pi/4} ik}{(8\pi k \rho \sin \theta_0)^{1/2}}. \quad (11)$$

In Section 3, the 2-D TM fields [Eqs. (10)] are substituted into Eqs. (23) and (24) of Reference 3 to obtain the 3-D incremental diffraction coefficients for TM plane wave incidence on the leading and trailing edges of the truncated half-plane.

### 2.3 The TE (Perpendicular Polarized) Fields: Normal Incidence

The 2-D far fields of a perfectly conducting truncated half-plane for a normally incident ( $\theta_0 = 90^\circ$ ) TE plane wave, given by

$$\bar{H}_1 = \hat{z} H_1 \exp[-ik\rho \cos(\phi - \phi_0)] \quad (12)$$

begins, as in the TM case, with the total current on the infinite half-plane:

$$\bar{K} = K_x \hat{x} = \hat{x} H_1 \operatorname{sign}(\pi - \phi_0) 2\sqrt{2} e^{-i\pi/4} e^{-ik \cos \phi_0 x} F\left(2k \cos^2 \frac{\phi_0}{2} x\right) \quad (13)$$

which can be found from Eq. (8.31) of Bowman, Senior and Uslenghi.<sup>12</sup> The  $\operatorname{sign}(\pi - \phi_0)$  function in Eq. (13) is +1 or -1 for  $\phi_0$  less than or greater than  $\pi$ , respectively. Substituting  $\bar{K}$  from Eq. (13) into Eq. (2), and making use of Eq. (6) to perform the integration of the Fresnel integral, yields the TE far fields of the total current for normal incidence

$$\begin{aligned} \bar{H}_s^{\text{TE}}(\bar{\rho}) \underset{\rho \rightarrow \infty}{\sim} \hat{z} H_1 \operatorname{sign}(\pi - \phi_0) \frac{e^{ik\rho}}{(\pi k\rho)^{1/2}} \frac{\sin \phi}{\cos \phi_0 + \cos \phi} \\ \cdot \left[ e^{-iks(\cos \phi_0 + \cos \phi)} F\left(2ks \cos^2 \frac{\phi_0}{2}\right) - \frac{\sqrt{2} \left| \cos \frac{\phi_0}{2} \right|}{|1 - \cos \phi|^{1/2}} F_0(ks|1 - \cos \phi|) \right], \end{aligned} \quad (14a)$$

$$0 \leq \phi, \phi_0 < 2\pi,$$

$$\bar{E}_s^{\text{TE}}(\bar{\rho}) \sim -Z_0 \hat{\rho} \times \bar{H}_s^{\text{TE}}(\bar{\rho}), \rho \rightarrow \infty \quad (14b)$$

(Again, we retain the absolute value signs in  $|1 - \cos \phi|$  because when the IDC's are found by substitution of Eq. (14) into the general expressions of Reference 3,  $\cos \phi$  is replaced by a variable that may become greater than one; see Section 3 below.)

The TE far fields of the truncated nonuniform current are determined by subtracting the TE, PO far fields,

$$\begin{aligned} \bar{H}^{\text{PO(TE)}}(\bar{\rho}) \underset{\rho \rightarrow \infty}{\sim} -\hat{z} H_1 \operatorname{sign}(\pi - \phi_0) \frac{e^{i(k\rho + \pi/4)}}{(2\pi k\rho)^{1/2}} \frac{\sin \phi}{\cos \phi_0 + \cos \phi} \\ \cdot \left[ 1 - e^{-iks(\cos \phi_0 + \cos \phi)} \right], \end{aligned} \quad (15a)$$

$$\bar{E}^{\text{PO(TE)}}(\bar{\rho}) \sim -Z_0 \hat{\rho} \times \bar{H}^{\text{PO(TE)}}(\bar{\rho}), \rho \rightarrow \infty \quad (15b)$$

from Eq. (14) to get

$$\begin{aligned} \bar{H}^{nu(TE)}(\bar{\rho}) \quad \rho \rightarrow \infty \quad \hat{z} H_1 \text{sign}(\pi - \phi_0) \frac{e^{ik\rho}}{(\pi k \rho)^{1/2}} \frac{\sin \phi}{\cos \phi_0 + \cos \phi} \\ \cdot \left\{ e^{-iks(\cos \phi_0 + \cos \phi)} F\left(2ks \cos^2 \frac{\phi_0}{2}\right) - \frac{\sqrt{2} \left| \cos \frac{\phi_0}{2} \right|}{|1 - \cos \phi|^{1/2}} F^o(ks|1 - \cos \phi|) \right. \\ \left. + \frac{e^{i\pi/4}}{\sqrt{2}} \left[ 1 - e^{-iks(\cos \phi_0 + \cos \phi)} \right] \right\}, \quad 0 \leq \phi, \phi_0 < 2\pi, \end{aligned} \quad (16a)$$

$$\bar{E}^{nu(TE)}(\bar{\rho}) \sim -Z_0 \hat{\rho} \times \bar{H}^{nu(TE)}(\bar{\rho}), \quad \rho \rightarrow \infty. \quad (16b)$$

Eqs (16) present a good high frequency approximation to the fields radiated by truncated TE nonuniform current emanating from the leading edge for all angles of incidence. However, unlike the analogous TM Eqs. (9), Eqs. (16) need to be modified for the trailing edge, when the incident angle is near grazing ( $\phi_0 \approx 0^\circ$ ), to take into account the nonuniform current that emanates from the leading edge and diffracts at the trailing edge. Fortunately, this modification required for the trailing edge under TE illumination is accomplished through a simple multiplicative factor that will be derived in Section 2.5.

## 2.4 The TE Fields: Oblique Incidence

As mentioned in Section 2, the  $H_\phi$  or  $E_\phi$  far fields radiated by the nonuniform current can be determined for an obliquely incident TE plane wave essentially by replacing  $k$  with  $k \sin \theta_0$  in the far fields for normal incidence and multiplying by  $\exp(-ikz \cos \theta_0)$ . In particular, Eqs. (14) and (16) generalize respectively for oblique incidence to

$$\begin{aligned} H_{S\phi}^{(TE)}(\bar{r}) \quad \hat{\theta}_0^\pi \quad r \rightarrow \infty \sim \hat{\theta}_0^\pi H_1 \text{sign}(\pi - \phi_0) \frac{C_0 2\sqrt{2} e^{-i\pi/4}}{ik} \frac{\sin \phi}{\cos \phi_0 + \cos \phi} \\ \cdot \left[ e^{-iks \sin \theta_0 (\cos \phi_0 + \cos \phi)} F\left(2ks \sin \theta_0 \cos^2 \frac{\phi_0}{2}\right) - \frac{\sqrt{2} \left| \cos \frac{\phi_0}{2} \right|}{|1 - \cos \phi|^{1/2}} F^o(ks \sin \theta_0 |1 - \cos \phi|) \right], \end{aligned} \quad (17a)$$

$$0 \leq \phi, \phi_0 < 2\pi,$$

$$0 \leq \theta_0 < \pi,$$

$$E_{S\phi}^{TE}(\bar{r}) \quad \hat{\phi} \quad r \rightarrow \infty \sim -Z_0 \hat{r}_0 \times \bar{H}_{S\phi}^{TE}(\bar{r}) \hat{\theta}_0^\pi, \quad r \rightarrow \infty, \quad (17b)$$

and

$$\begin{aligned}
\bar{H}_0^{nu(TE)}(\bar{r}) \hat{\theta}_0^\pi r \rightarrow \infty &= \hat{\theta}_0^\pi H_1 \operatorname{sign}(\pi - \phi_0) \frac{2C_0}{1k} \frac{\sin \phi}{\cos \phi_0 + \cos \phi} \\
&\cdot \left\{ \sqrt{2} e^{-i\pi/4} \left[ e^{-1ks \sin \theta_0 (\cos \phi_0 + \cos \phi)} F\left(2ks \sin \theta_0 \cos^2 \frac{\phi_0}{2}\right) \right. \right. \\
&\quad \left. \left. - \frac{\sqrt{2} \left| \cos \frac{\phi_0}{2} \right|}{|1 - \cos \phi|^{1/2}} F^0(ks \sin \theta_0 |1 - \cos \phi|) \right] \right. \\
&\quad \left. - \left[ 1 - e^{-1ks \sin \theta_0 (\cos \phi_0 + \cos \phi)} \right] \right\},
\end{aligned} \tag{18a}$$

$$0 \leq \phi, \phi_0 < 2\pi,$$

$$0 \leq \theta_0 < \pi,$$

$$\bar{E}_\phi^{nu(TE)}(\bar{r}) \hat{\phi} \sim -Z_0 \hat{\theta}_0 \times \bar{H}_\theta^{nu(TE)}(\bar{r}) \hat{\theta}_0^\pi, r \rightarrow \infty. \tag{18b}$$

For the TE case, there may also exist  $H_\phi$  and  $E_\theta$  far fields when the plane wave is obliquely incident. These  $H_\phi$  and  $E_\theta$  far fields can be found by integrating the TE current that exists on the half-plane for oblique incidence. In particular, the nonuniform far fields,  $H_\phi^{nu(TE)}$  or  $E_\theta^{nu(TE)}$ , can be found for the truncated half-plane by subtracting the PO far fields,  $H_\phi^{PO(TE)}$  or  $E_\theta^{PO(TE)}$ , of the truncated half-plane from the TE far fields,  $H_{s\phi}^{TE}$  or  $E_{s\theta}^{TE}$ , obtained by integrating the total current over the truncated half-plane. Before we do these integrations to determine the  $H_\phi$  or  $E_\theta$  fields, however, let us address an objection that may arise at this point in the analysis.

If the total TE current that we are integrating were the exact total current of the 2-D perfectly conducting strip, then the basic theory of 2-D scattering from perfect conductors (see Chapter 1 of Reference 12), tells us that these total currents, when integrated will not produce an  $H_\phi$  and  $E_\theta$  component in the far fields. Of course, we are not integrating the total currents of the strip, but the truncated currents of the infinite half-plane. Thus, we cannot expect the  $H_\phi$  or  $E_\theta$  far fields to be zero. Still, one could argue that when we eventually apply these far fields to both the leading and trailing edges of incremental strips, the combined truncated currents from both the leading and trailing edges should closely approximate the exact total currents of the strip; and thus, we should ignore the  $H_\phi$  and  $E_\theta$  components of TE far fields at all points in the analysis. This argument is valid provided the leading and trailing edges of the incremental strip are parallel. Only for these rectangular strips is the incremental strip part of an infinite 2-D strip for which the above-mentioned theory in Chapter 1 of Reference 12 holds. For trapezoidal incremental strips, that is, strips with nonparallel leading and trailing edges, we must include, in general, the TE  $H_\phi$  and  $E_\theta$  far fields radiated by the truncated half-plane currents for oblique incidence.

To obtain the total scattered TE  $H_\phi$  or  $E_\theta$  far fields it suffices to obtain the z-component of the total current on the half-plane since then Eqs. (9b) and (14b) of Reference 3 combined with Eq. (17a) already derived for  $H_{s\theta}$  yield  $H_{s\phi}$ . Since  $K_z$  on the surfaces of the half-plane is equal to  $H_x$  within a sign, we seek an expression for  $H_x$  on the half-plane surfaces.

For the normally incident TE plane wave given by Eq. (11), Eq. (8.28) of Reference 12 gives the total  $H_z$  everywhere in space. A general procedure for generating the solution for oblique incidence is given in Reference 12. For H-polarization let  $V$  be obtained from the normal incidence (two-dimensional) solution by substituting  $k \rightarrow k \sin \theta_0$  and multiplying by  $\exp(-ikz \cos \theta_0)$ . Then Eq. (1.6) of Reference 12 adapted to the form of the obliquely incident plane wave

$$\vec{H}_{inc} = -H_1 (\cos \phi_0 \cos \theta_0 \hat{x} + \sin \phi_0 \cos \theta_0 \hat{y} - \sin \theta_0 \hat{z}) \cdot \exp \left[ -ik (x \cos \phi_0 \sin \theta_0 + y \sin \phi_0 \sin \theta_0 + z \cos \theta_0) \right] \quad (19)$$

gives the total magnetic field

$$\vec{H} = -\frac{1}{k} \frac{\cos \theta_0}{\sin \theta_0} \left( \frac{\partial V}{\partial x} \hat{x} + \frac{\partial V}{\partial y} \hat{y} \right) + \sin \theta_0 V \hat{z} \quad (20)$$

with, from Eq. (8.28) of Reference 12,

$$V = H_1 \frac{e^{-i\pi/4}}{\sqrt{\pi}} e^{-ikz \cos \theta_0} \left\{ \exp \left[ -ik \sin \theta_0 \rho \cos (\phi - \phi_0) \right] \mathcal{F} \left[ -\sqrt{2k \sin \theta_0 \rho} \cos \frac{1}{2} (\phi - \phi_0) \right] + \exp \left[ -ik \sin \theta_0 \rho \cos (\phi + \phi_0) \right] \mathcal{F} \left[ -\sqrt{2k \sin \theta_0 \rho} \cos \frac{1}{2} (\phi + \phi_0) \right] \right\} \quad (21)$$

and

$$\mathcal{F}(\omega) = \int_{-\infty}^{\infty} e^{it^2} dt. \quad (22)$$

Then  $H_x$  on the surfaces of the half-plane is given by

$$H_x = -\frac{1}{k} \frac{\cos \theta_0}{\sin \theta_0} \frac{\partial V}{\partial x} \quad (23)$$

with

$$V = 2H_1 \frac{e^{-i\pi/4}}{\sqrt{\pi}} e^{-ikz \cos \theta_0} \exp(-ik \sin \theta_0 \cos \phi_0 x) \mathcal{F} \left( \mp \sqrt{2k \sin \theta_0 x} \cos \frac{\phi_0}{2} \right) \quad (24)$$

where the - or + sign applies on the top and bottom half-plane faces respectively. The current on the top and bottom faces of the half-plane is then given by

$$K_z^{(\pm)} = \mp H_x = \pm \cos \theta_0 \cos \phi_0 V + H_1 e^{i\pi/4} e^{-ikz \cos \theta_0} \left( \frac{2}{\pi k \sin \theta_0} \right)^{1/2} \cos \theta_0 \cos \frac{\phi_0}{2} \frac{e^{ik \sin \theta_0 x}}{x^{1/2}}. \quad (25)$$

The total current is obtained by adding the currents on the two faces:

$$\begin{aligned}
K_z = & \text{sign}(\pi - \phi_0) H_1 2\sqrt{2} \cos \theta_0 e^{-ikz \cos \theta_0} \\
& \cdot \left[ e^{-i\pi/4} e^{-ik \sin \theta_0 \cos \phi_0 x} \cos \phi_0 F\left(2k \sin \theta_0 \cos^2 \frac{\phi_0}{2} x\right) \right. \\
& \left. + \frac{e^{i\pi/4}}{\sqrt{\pi k \sin \theta_0}} \left| \cos \frac{\phi_0}{2} \right| \frac{e^{ik \sin \theta_0 x}}{x^{1/2}} \right]
\end{aligned} \quad (26)$$

with  $F(x)$  given by Eq. (5). Integrating  $K_z^{\text{tot}}$  over the half-plane from 0 to  $s$  and making use of Eq. (6) yields [see Eq. (9b), Reference 3].

$$\begin{aligned}
A_{0z} = & \int_0^s K_z^{\text{tot}}(x) e^{-ikx \sin \theta_0 \cos \phi} dx \\
= & \text{sign}(\pi - \phi_0) H_1 2\sqrt{2} e^{i\pi/4} \frac{\cos \theta_0}{k \sin \theta_0} \frac{1}{\cos \phi_0 + \cos \phi} \\
& \cdot \left[ \cos \phi_0 e^{-iks \sin \theta_0 (\cos \phi_0 + \cos \phi)} F\left(2ks \sin \theta_0 \cos^2 \frac{\phi_0}{2}\right) \right. \\
& \left. + \sqrt{2} \frac{\left| \cos \frac{\phi_0}{2} \right| \cos \phi}{|1 - \cos \phi|^{1/2}} F\left(ks \sin \theta_0 |1 - \cos \phi|\right) \right].
\end{aligned} \quad (27)$$

From Eq. (14b) of Reference 3 we then obtain

$$H_{s\phi}^{(\text{TE})} = -\sin \theta_0 (C_0 A_{0z} + \cot \theta_0 \cot \phi H_{s0}) \quad (28)$$

from which, with Eq. (17a),

$$\begin{aligned}
H_{s\phi}^{(\text{TE})}(\vec{r}) \hat{\phi} \xrightarrow{r \rightarrow \infty} & \text{sign}(\pi - \phi_0) H_1 2\sqrt{2} e^{-i\pi/4} \frac{C_0}{ik} \cos \theta_0 \\
& \cdot e^{-iks \sin \theta_0 (\cos \phi_0 + \cos \phi)} F\left(2k \sin \theta_0 \cos^2 \frac{\phi_0}{2}\right),
\end{aligned} \quad (29a)$$

$$0 \leq \phi, \phi_0 < 2\pi, 0 \leq \theta_0 < \pi,$$

$$E_{s0}^{(\text{TE})}(\vec{r}) \hat{\theta}_0 = -\hat{r}_0 \times H_{s\phi}^{(\text{TE})}(\vec{r}) \hat{\phi}, r \rightarrow \infty. \quad (29b)$$

The corresponding PO fields are readily obtained from the expressions for  $H_{\phi}^{\text{PO}}$  for the faces of the infinite wedge given on pp. 32-33 of the technical report version of Reference 3 by multiplying by the factor  $\left\{ 1 - \exp[-iks \sin \theta_0 (\cos \phi_0 + \cos \phi)] \right\}$ :

$$\begin{aligned}
H_{\phi}^{\text{PO(TE)}}(\vec{r}) \hat{\phi} \xrightarrow{r \rightarrow \infty} & \text{sign}(\pi - \phi_0) H_1 \frac{2C_0}{ik} \cos \theta_0 \left[ 1 - e^{-iks \sin \theta_0 (\cos \phi_0 + \cos \phi)} \right], \\
0 \leq \phi, \phi_0 < 2\pi, 0 \leq \theta_0 < \pi,
\end{aligned} \quad (30a)$$



$$E_{\theta}^{PO(TE)}(\vec{r}) \hat{\theta} \sim -\hat{r}_0 \times H_{\phi}^{PO(TE)}(\vec{r}) \hat{\phi}, r \rightarrow \infty, \quad (30b)$$

and hence, subtracting Eq. (30) from Eq. (29),

$$H_{\phi}^{nu(TE)}(\vec{r}) \hat{\phi} \sim -\text{sign}(\pi - \phi_0) H_1 \frac{2C_0}{1k} \cos \theta_0 \cdot \left\{ \sqrt{2} e^{-i\pi/4} e^{-1ks \sin \theta_0 (\cos \phi_0 + \cos \phi)} F\left(2ks \sin \theta_0 \cos^2 \frac{\phi_0}{2}\right) + \left[ 1 - e^{-1ks \sin \theta_0 (\cos \phi_0 + \cos \phi)} \right] \right\}, \quad (31a)$$

$$0 \leq \phi, \phi_0 < 2\pi, 0 \leq \theta_0 < \pi,$$

$$E_{\theta}^{nu(TE)}(\vec{r}) \hat{\theta} \sim -\hat{r}_0 \times H_{\phi}^{nu(TE)}(\vec{r}) \hat{\phi}, r \rightarrow \infty. \quad (31b)$$

## 2.5 Modification of the TE Fields for the Trailing Edge

Consider the truncated half-plane in Figure 2 with a TE plane wave incident near  $\phi_0 = 180^\circ$ . The nonuniform current, defined as the difference between the total and PO currents, emanating from the leading edge decays very slowly (unlike in the TM case) toward the trailing edge. This appreciable nonuniform TE current impinging upon the trailing edge produces diffracted fields from the trailing edge that modify the diffracted TE fields, Eq. (18), applied to the trailing edge. We can determine this modification approximately by first deriving from Eqs. (20) and (21) that the total TE current for oblique incidence on the half-plane is given, for all angles of incidence, by

$$\begin{aligned} \vec{K} = & -\text{sign}(\pi - \phi_0) 2\hat{y} \times \hat{\theta}_0 H_1 e^{-1k(x \sin \theta_0 \cos \phi_0 + z \cos \theta_0)} \sqrt{2} e^{-i\pi/4} F\left(2kx \sin \theta_0 \cos^2 \frac{\phi_0}{2}\right) \\ & + 2\hat{z} H_1 e^{i\pi/4} \frac{\sqrt{2}}{\sqrt{\pi}} \frac{\cos \theta_0 \frac{\phi_0}{2}}{\sqrt{kx \sin \theta_0}} e^{1k(x \sin \theta_0 - z \cos \theta_0)} \end{aligned} \quad (32a)$$

where  $\hat{\theta}_0$  is the unit vector  $\hat{\theta}$  at  $\theta = \theta_0$ . For  $2kx \sin \theta_0 \gg 1$ , the second term in Eq. (32a) is small compared to the first term, and Eq. (32a) can be written approximately as

$$\begin{aligned} \vec{K} = & -\text{sign}(\pi - \phi_0) 2\hat{y} \times \hat{\theta}_0 H_1 e^{-1k(x \sin \theta_0 \cos \phi_0 + z \cos \theta_0)} \\ & \cdot \sqrt{2} e^{-i\pi/4} F\left(2kx \sin \theta_0 \cos^2 \frac{\phi_0}{2}\right), \quad 2kx \sin \theta_0 \gg 1. \end{aligned} \quad (32b)$$

The TE H-field corresponding to this current, Eq. (32b), impinging on the trailing edge ( $x = s$ ) of the truncated half-plane is

$$\bar{H}_{\text{imp}} = -\hat{\theta}_0 H_i e^{-ik(x \sin \theta_0 \cos \phi_0 + z \cos \theta_0)} \cdot 2\sqrt{2} e^{-i\pi/4} F\left(2kx \sin \theta_0 \cos^2 \frac{\phi_0}{2}\right), \quad (33)$$

$$2kx \sin \theta_0 \gg 1.$$

Now, the obliquely incident TE plane-wave field alone along the half-plane is given by

$$\bar{H}_i = -\hat{\theta}_0 H_i e^{-ik(x \sin \theta_0 \cos \phi_0 + z \cos \theta_0)}. \quad (34)$$

Comparing Eqs. (33) and (34), we see that the impinging field, that is the effective incident field on the trailing edge ( $x = s$ ), is approximately the actual incident field multiplied by the factor

$$2\sqrt{2} e^{-i\pi/4} F\left(2ks \sin \theta_0^L \cos^2 \frac{\phi_0^L}{2}\right), \quad (35)$$

where the superscripts L on  $\phi_0^L$  and  $\theta_0^L$  in (35) emphasize that they are the  $\theta_0$  and  $\phi_0$  angles defined with respect to the leading edge — even though (35) is used as a factor multiplying Eqs. (18) and (31) when and only when Eqs. (18) and (31) are applied to the trailing edge. If the leading edge makes an angle  $\psi$  with the incremental strip, so that  $s$  is given in terms of the length  $L$  of the incremental strip by

$$s = L \sin \psi, \quad (36)$$

(35) becomes

$$\sqrt{2} e^{-i\pi/4} F\left(2kL \sin \psi \sin \theta_0^L \cos^2 \frac{\phi_0^L}{2}\right). \quad (37)$$

If in addition  $\psi$  is taken as the direction of propagation in the half-plane of the PO current or, equivalently, of the total and nonuniform current near grazing ( $\phi_0^L = 180^\circ$ ) then  $\sin \psi$  equals  $-\sin \theta_0^L \phi_0^L \sqrt{1 - \sin^2 \theta_0^L \sin^2 \phi_0^L}$  and (37) becomes

$$\sqrt{2} e^{-i\pi/4} F\left(\frac{-2kL \sin^2 \theta_0^L \cos^2 \frac{\phi_0^L}{2} \cos \theta_0^L}{\sqrt{1 - \sin^2 \theta_0^L \sin^2 \phi_0^L}}\right). \quad (38)$$

In summary, then, for incremental strips chosen along the direction of propagation in the half-plane of the PO current, the factor (38) should multiply the fields in Eq. (18) when Eq. (18) is applied to the trailing edge of the truncated half-plane.

Of course, a more accurate method of accounting for the diffraction at the trailing edge of the nonuniform TE current emanating from the leading edge of an arbitrary scatterer, would be to first determine the path of the diffracted ray from the leading edge to the trailing edge, and then calculate the diffraction at the trailing edge of this leading-edge ray. We did not use this more accurate

technique in the present report, not only because it would require an extra calculation, but because the TE nonuniform current decays fairly rapidly away from the leading edge except near grazing where the diffracted ray path nearly coincides with the direction of propagation of the PO current in the corresponding half-plane [and thus (38) applies].

In general, Appendix C shows that whenever the significant nonuniform current of integration for a given observation point extends a distance from the edge larger than a small fraction (say 1/4) of the distance to the focal point of the diffracted rays, the incremental strips of nonuniform current will not closely approximate the actual nonuniform current, and thus the fields computed from the incremental diffraction coefficients at the given observation point may contain significant error. (For example, see the discussion of Figures 22 - 25 in Section 4.4.) Near grazing, the focal length approaches infinity and the incremental strips of nonuniform current accurately approximate the actual nonuniform current across the whole distance from leading to trailing edges.

## 2.6 Calculations of the Two-Dimensional Bistatic Radar Cross Section of a Strip

In this section we show the results of calculations made of the two-dimensional bistatic cross section of an infinitely long strip. The bistatic cross section,  $\sigma(\phi)$ , per unit length, for normal incidence (that is, the direction vector of the incident plane wave normal to the edges of the strip) of an infinitely long strip is defined by Eq. (I.34) of Reference 12:

$$\sigma(\phi) = \lim_{\rho \rightarrow \infty} 2\pi\rho \left| \frac{V^s}{V^i} \right|^2 \quad (39)$$

where  $V^{s,i} = E_z^{s,i}$  if the electric field is parallel to the z-axis (TM) and  $V^{s,i} = H_z^{s,i}$  if the magnetic field is parallel to the z-axis (TE), with the superscripts s,i denoting the scattered and incident field, respectively. In our results we normalize  $\sigma$  by dividing by the wavelength  $\lambda$ .

In Figures 3a and b we compare the TM and TE back scatter cross sections obtained using the approximations of Sections 2.1, 2.3, and 2.5, with the corresponding bistatic cross sections obtained using a computer program to calculate the exact two-dimensional fields scattered from an infinite strip.<sup>13</sup> The width of the strip is  $s/\lambda = 30/2\pi = 4.77$ . In these plots  $\theta$  is the angle between the direction vector of the incident plane wave (or the observation direction) and the normal to the plane of the strip. For calculating the contribution of the leading edge of the strip from Eq. (7a) or Eq. (14a),  $\phi_0 = \phi = \pi/2 + \theta$ , while for calculating the contribution of the trailing edge from Eq. (7a) or Eq. (14a) with Eq. (35),  $\phi_0 = \phi = \pi/2 - \theta$ ,  $0 \leq \theta \leq \pi/2$ . The cross sections are, of course, symmetrical with respect to  $\theta = \pi/2$ . The total field scattered from the strip is obtained by summing the contributions of the leading and trailing edges. Note that the direction of z in Eqs. (7a) and (14a) must be reversed for the trailing edge from what it is for the leading edge of the strip. As can be seen from Figures 3a and 3b, the exact back scatter cross sections (——) are virtually indistinguishable from the approximate back scatter cross sections (-----).

In Figures 4a and b we compare the approximate TM and TE specular (or, equivalently, forward)

---

13. Dominek, A.K. (1988) Personal Communication, Ohio State University ElectroScience Laboratory.

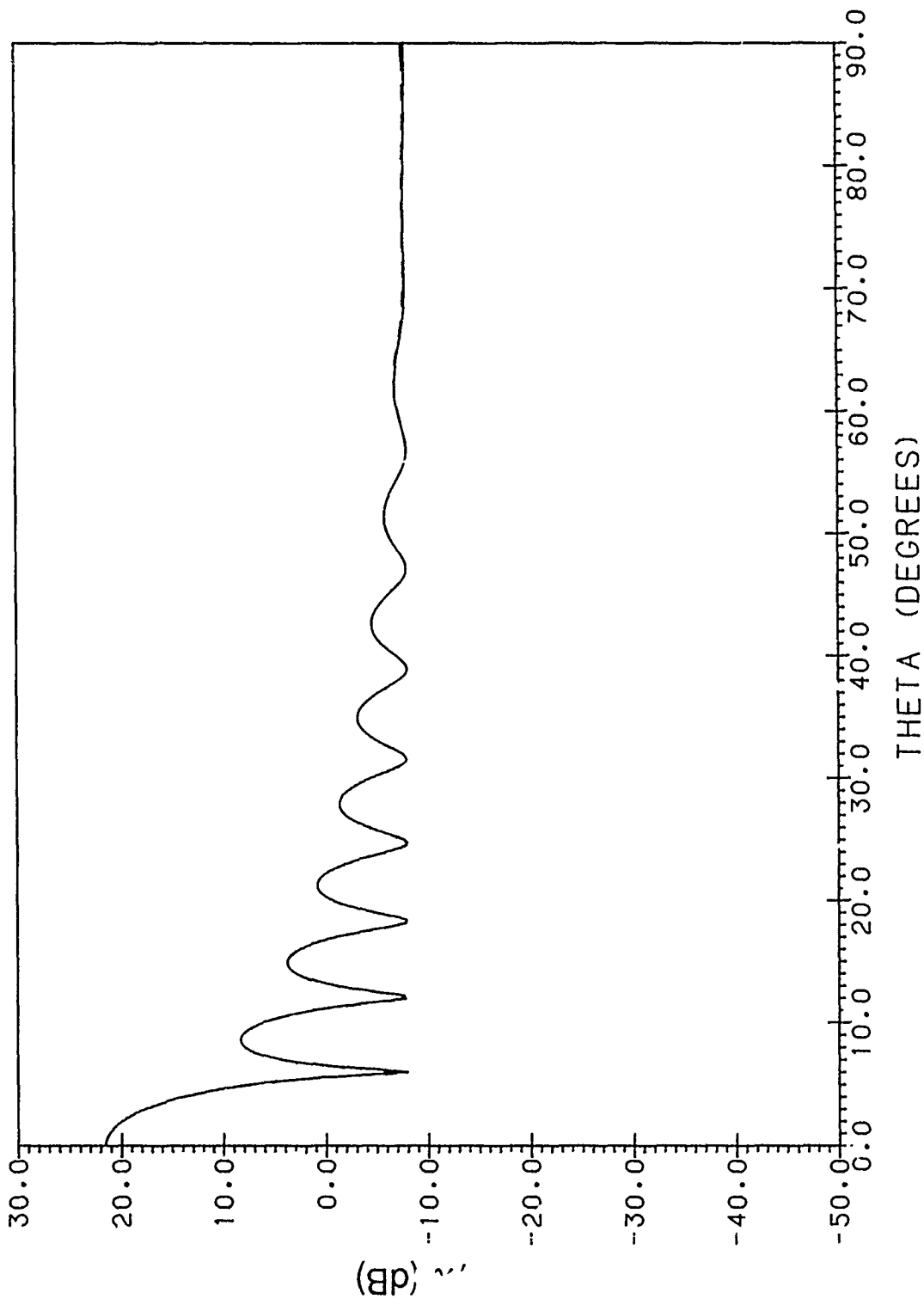


Figure 3a. Back Scatter Cross Section Pattern of Strip,  $k_s = 30$ , with TM (Perpendicular Polarized) Plane-Wave Illumination:  
 —: Exact, ----: PO + Approximate Nonuniform Current Field

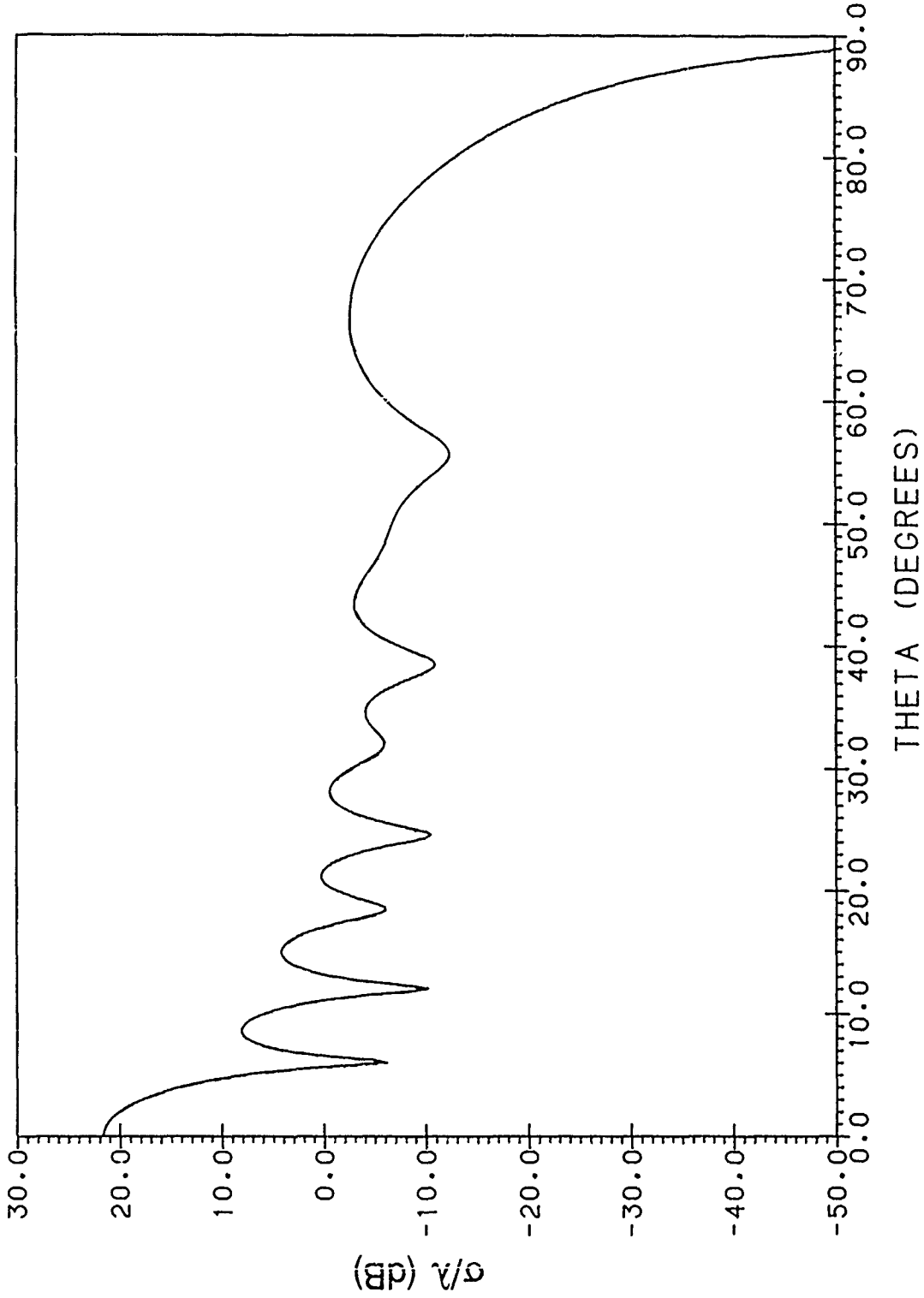


Figure 3b. Back Scatter Cross Section Pattern of Strip,  $ks = 30$ , with TE (Parallel Polarized) Plane-Wave Illumination:  
 —: Exact, ----: PO + Approximate Nonuniform Current Field

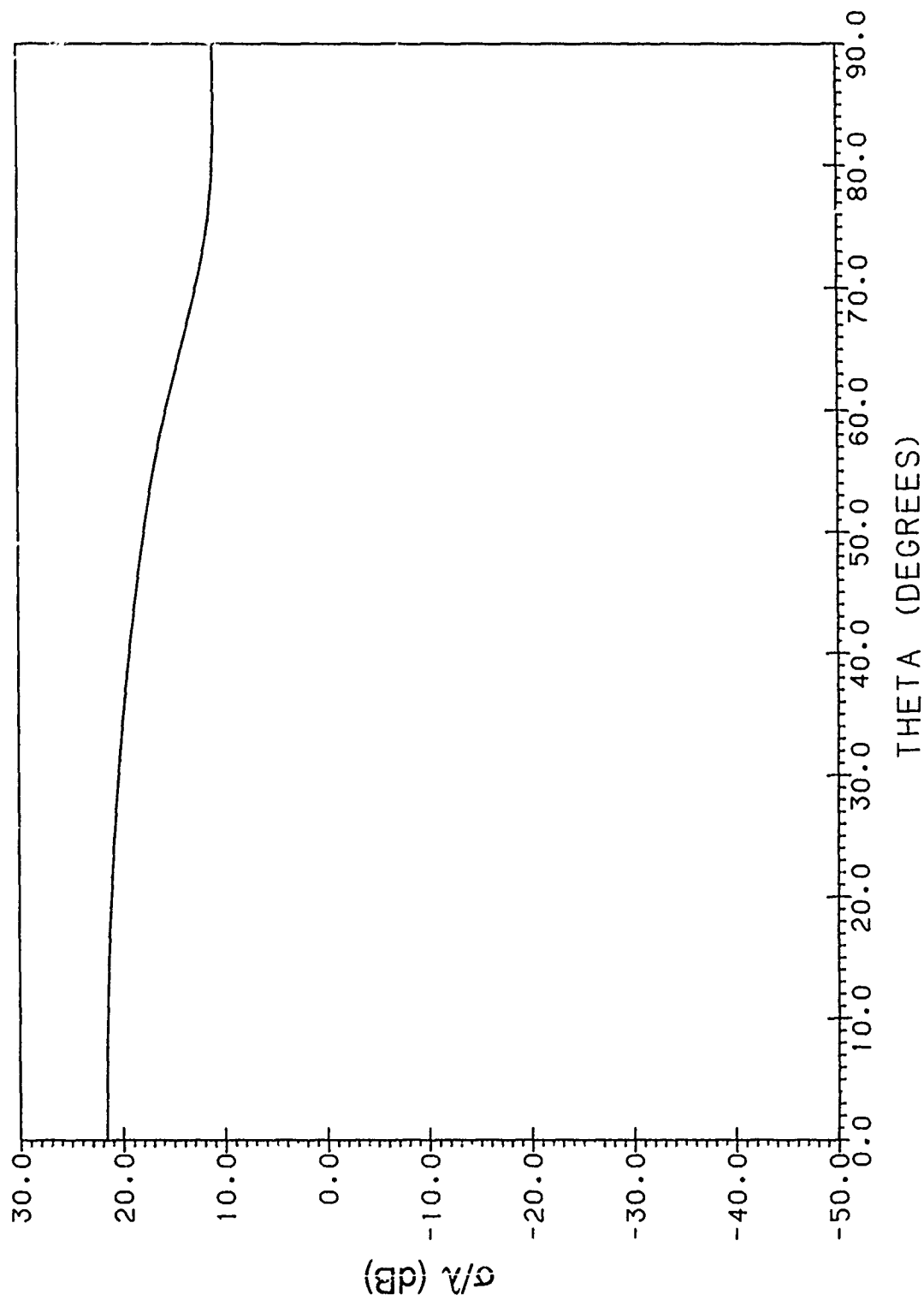


Figure 4a. Specular Scatter Cross Section Pattern of Strip,  $k_s = 30$ , with TM (Perpendicular Polarized) Plane-Wave Illumination:  
 —: Exact, ----: PO + Approximate Nonuniform Current Field

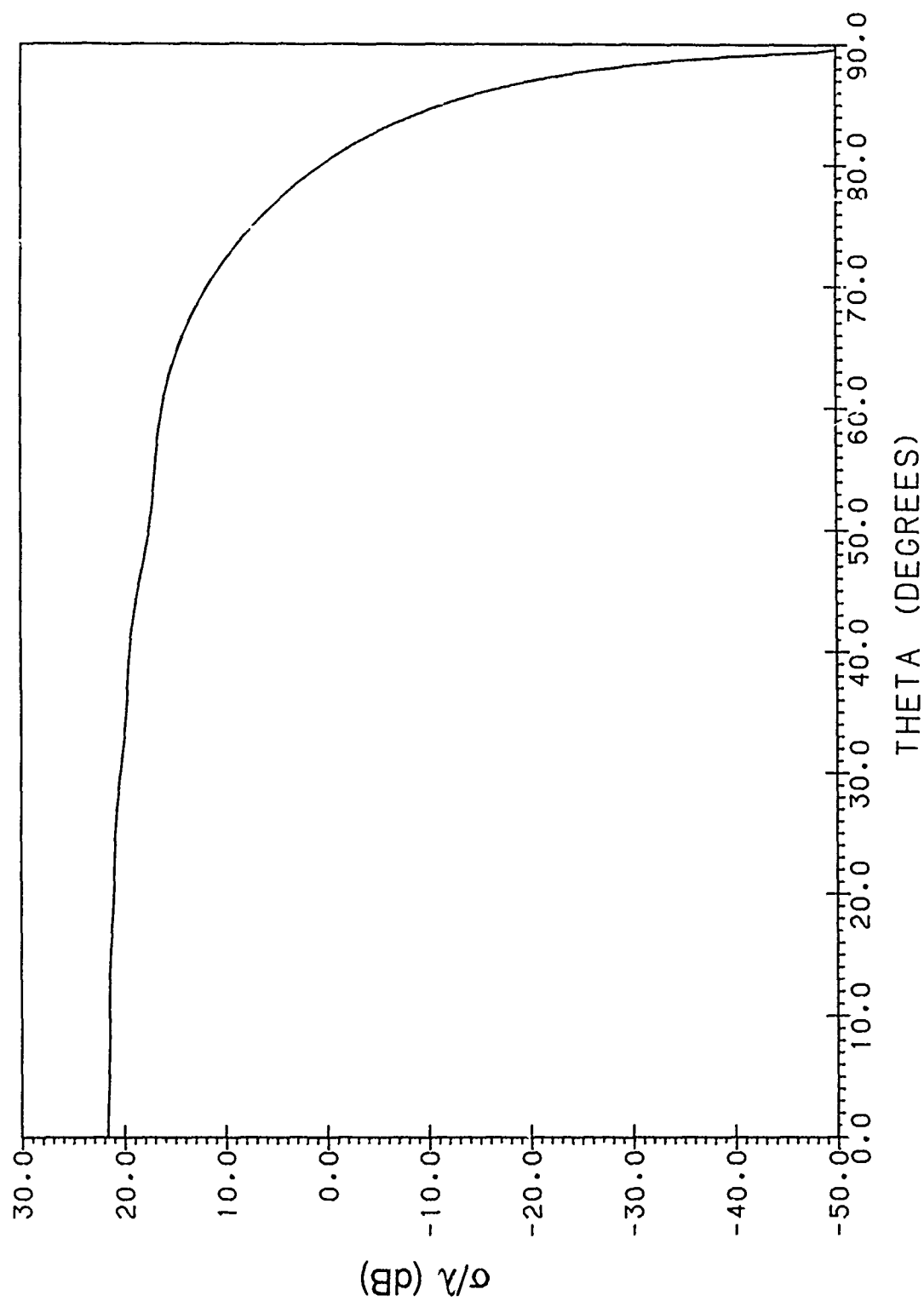


Figure 4b. Specular Scatter Cross Section Pattern of Strip,  $ks = 30$ , with TE (Parallel Polarized) Plane-Wave Illumination; —: Exact, ---: PO + Approximate Nonuniform Current Field

scatter cross sections with the corresponding exact cross sections. As with the back scatter plots, here  $\theta$  is the angle between the direction vector of the incident plane wave (or the observation direction) and the normal to the plane of the strip, so that  $\phi_0 = \pi/2 + \theta$  and  $\phi = \pi/2 - \theta$  for obtaining the contribution of the leading edge of the strip, while  $\phi_0 = \pi/2 - \theta$  and  $\phi = \pi/2 + \theta$  for the trailing edge. Again, there is hardly any difference between the exact and the approximate curves.

In Figures 5a and b, we compare the approximate TM and TE "side scatter" cross sections with the corresponding exact cross sections. By "side scatter", we mean that the observation direction and the incidence direction are at right angles to each other. In these plots  $\theta_1$  is the angle between the direction vector of the incident plane wave and the normal to the plane of the strip, so that  $\phi_0 = \pi/2 + \theta_1$  and  $\phi = \theta_1$  for calculating the contribution of the strip leading edge from Eq. (7a) or Eq. (14a), while  $\phi_0 = \pi/2 - \theta_1$  and  $\phi = \pi - \theta_1$  for calculating the contribution of the strip trailing edge from Eq. (7a) or from Eqs. (14a) and (35). There is again very close agreement between the exact and the approximate side scatter cross section curves.

In Figures 6a, b, and c we compare respectively the TE back scatter, specular (forward) scatter, and side scatter cross section plots obtained without the use of the trailing edge correction factor Eq. (35), with the corresponding exact cross section plots. Comparing these figures with Figures 3b, 4b, and 5b, respectively, we see that the trailing edge correction factor plays a significant role in improving the accuracy of the approximation in the back scatter and side scatter cases.

It is of considerable interest to see the limitations of the PO approximation for the strip bistatic cross sections. In Figures 7a and b, 8a and b, and 9a and b, we compare the TM and TE back scatter, specular scatter, and side scatter cross section curves obtained with the PO approximation (-----), with the exact curves (——). It is apparent that the PO approximation is, in general, of rather limited value in giving an accurate picture of the scattering cross section patterns apart from the portion of the patterns in the vicinity of specular scatter.

Figures 10a and b compare the E- and H-wave back scatter cross sections of the strip computed from the high-frequency solution of Michaeli's 1984 Radio Science paper<sup>14</sup>, with the exact E- and H-wave cross sections. Agreement between the exact E-wave solution and Michaeli's E-wave solution is excellent. However, Figure 10b shows a significant discrepancy between the H-wave solutions. Comparison of Figure 10b with Figure 6a reveals that this discrepancy is caused by the neglect in Michaeli's solution of the diffraction of the H-wave, leading-edge nonuniform current at the trailing edge. That is, Michaeli's high-frequency solution does not include the trailing edge factor in Eq. (35), and thus, shows poor agreement with the exact solution of the strip illuminated by an H-polarized plane wave.

Ufimtsev's first order H-wave back scatter radar cross section from his 1969 paper<sup>15</sup> is compared to the exact solution in Figure 11. Except in the vicinity of the main lobe, this first order H-wave solution which is more accurate (according to Ufimtsev<sup>15</sup>) than his solution in Reference 11 used by Coleman et al<sup>8</sup>, shows poor agreement with the exact H-wave solution.

14. Michaeli, A. (1984) A closed form physical theory of diffraction solution for electromagnetic scattering by strips and 90° dihedrals, *Radio Science* 19:609-616.

15. Ufimtsev, P. Ya. (1969) Asymptotic investigation of the problem of diffraction on a strip, *Radio Engineering and Electronic Physics* 14:1014-1025.



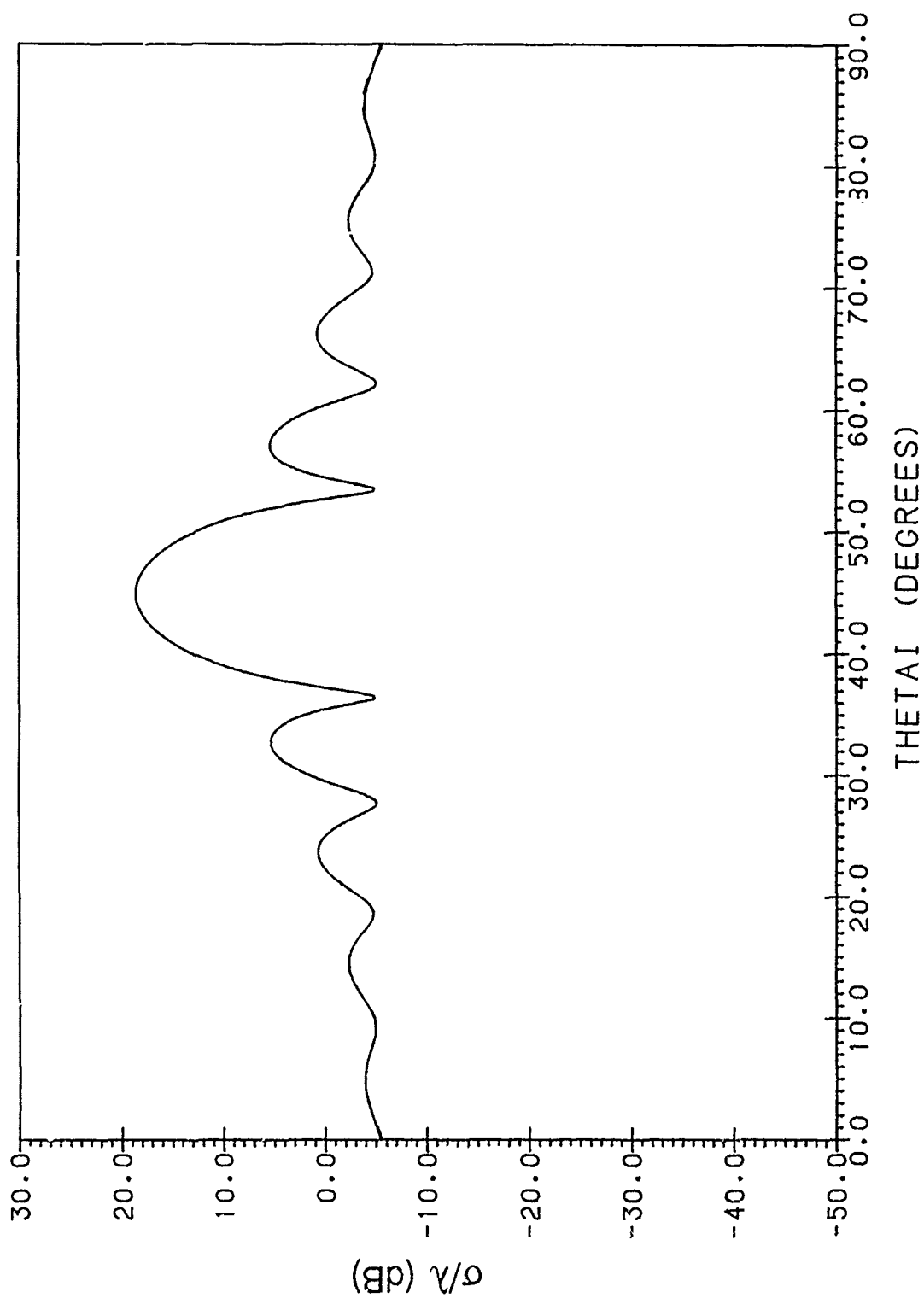


Figure 5a. Side Scatter Cross Section Pattern of Strip,  $k_s = 30$ , with TM (Perpendicular Polarized) Plane-Wave Illumination:  
 —: Exact, - - - - : PO + Approximate Nonuniform Current Field

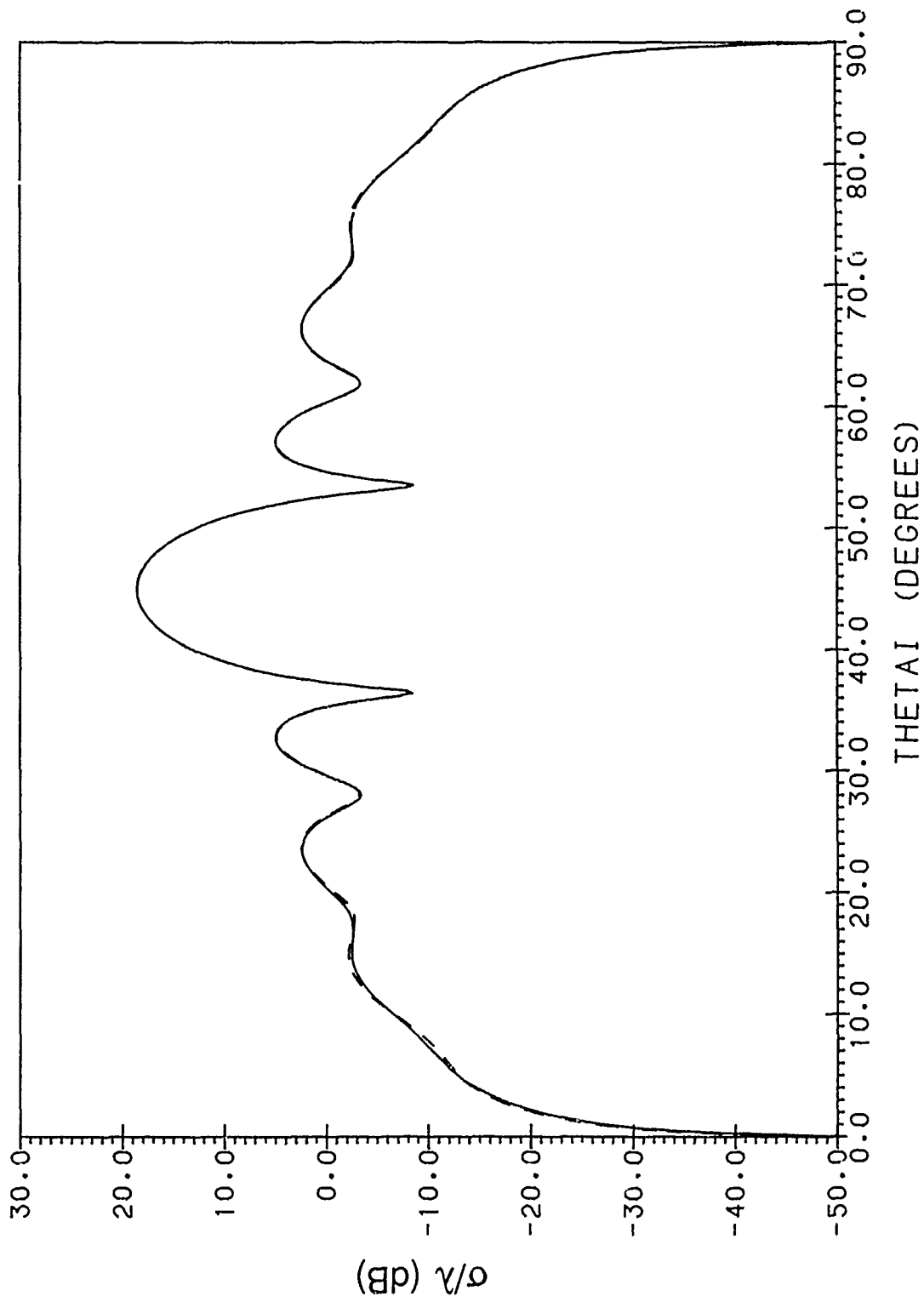


Figure 5b. Side Scatter Cross Section Pattern of Strip,  $k_s = 30$ , with TE (Parallel Polarized) Plane-Wave Illumination;  
 —: Exact, ----: PO + Approximate Nonuniform Current Field

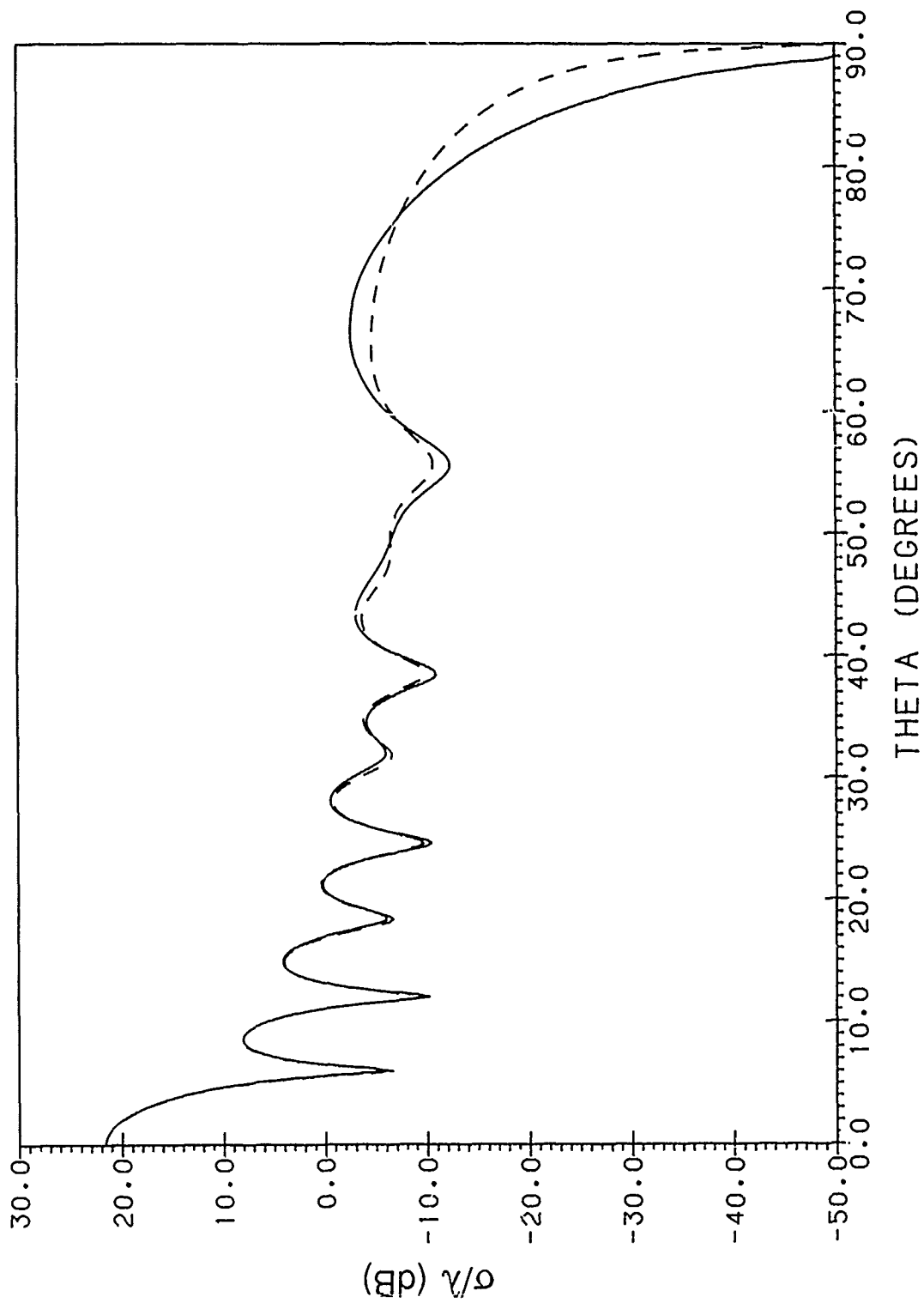


Figure 6a. Back Scatter Cross Section Pattern of Strip,  $ks = 30$ , with TE (Parallel Polarized) Plane-Wave Illumination;  
 —: Exact, ----: PO + Approximate Nonuniform Current Field (No Trailing Edge Correction)

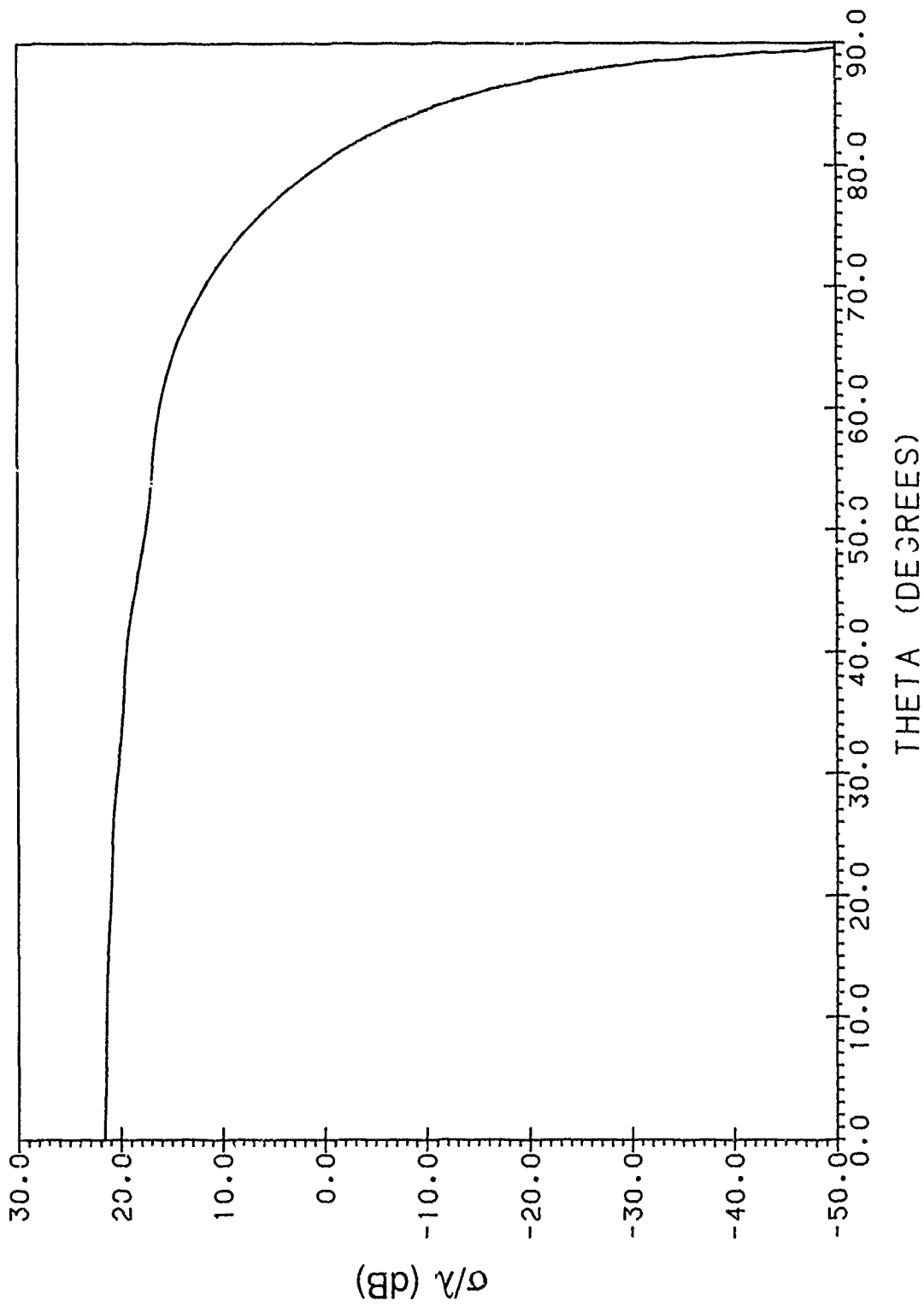


Figure 8b. Specular Scatter Cross Section Pattern of Strip,  $ks = 30$ , with TE (Parallel Polarized) Plane-Wave Illumination;  
 -----: Exact, - - - - -: PO + Approximate Nonuniform Current Field (No Trailing Edge Correction)

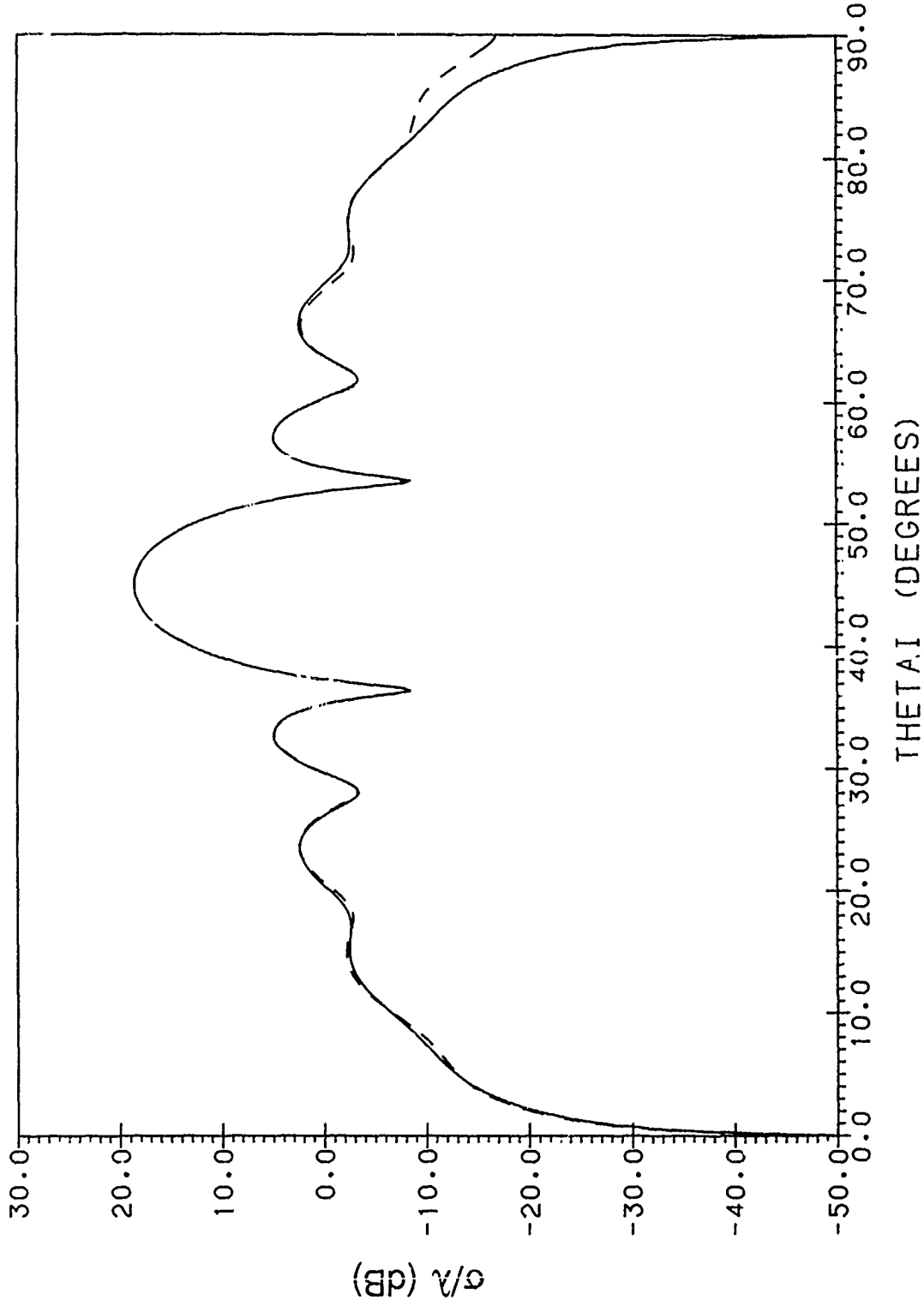


Figure 6c. Side Scatter Cross Section Pattern of Strip,  $ks = 30$ , with TE (Parallel Polarized) Plane-Wave Illumination:  
 —: Exact, ----: PO + Approximate Nonuniform Current Field (No Trailing Edge Correction)

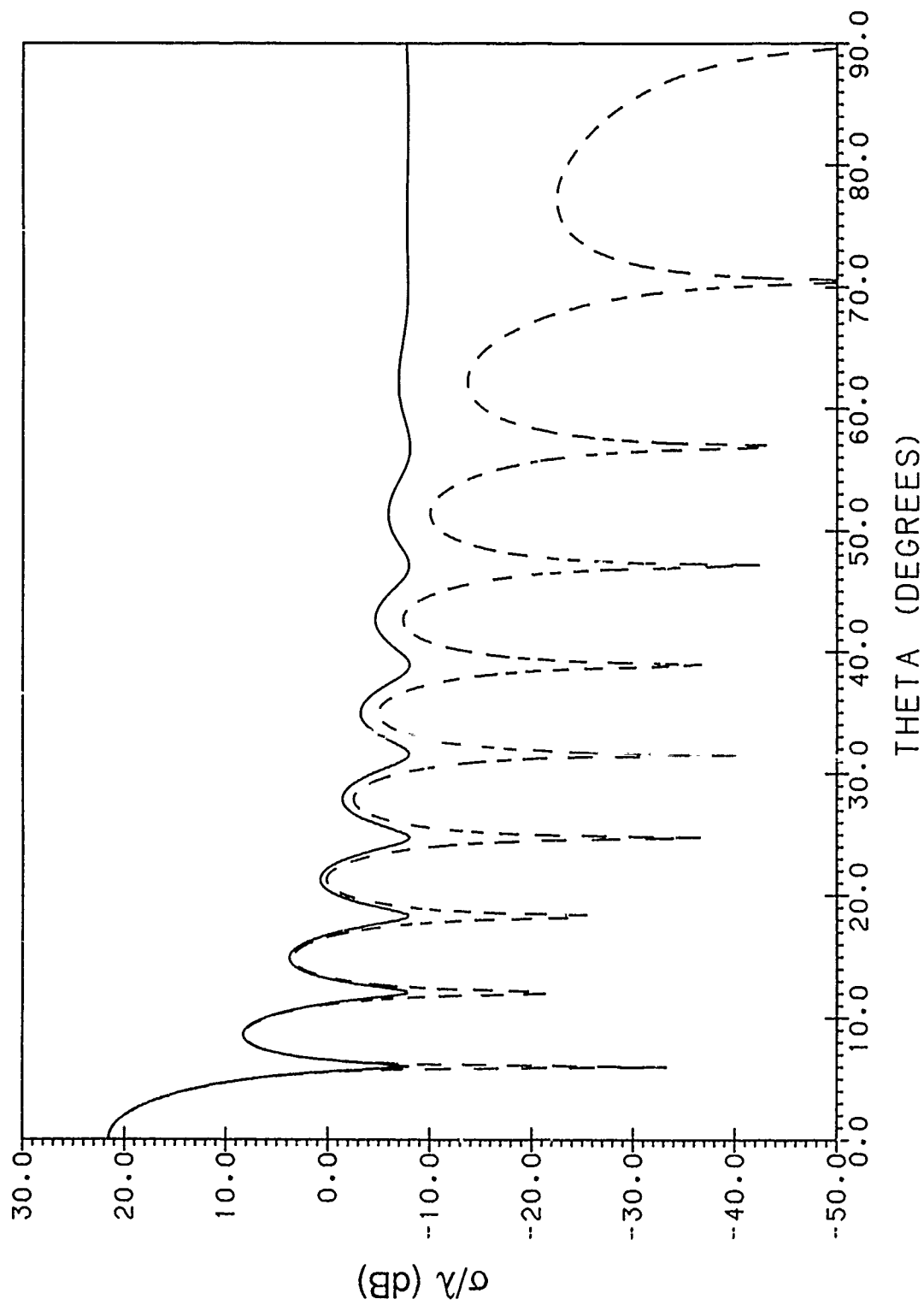


Figure 7a. Back Scatter Cross Section Pattern of Strip,  $ks = 30$ , with TM (Perpendicular Polarized) Plane-Wave Illumination; — : Exact, - - - - : PO

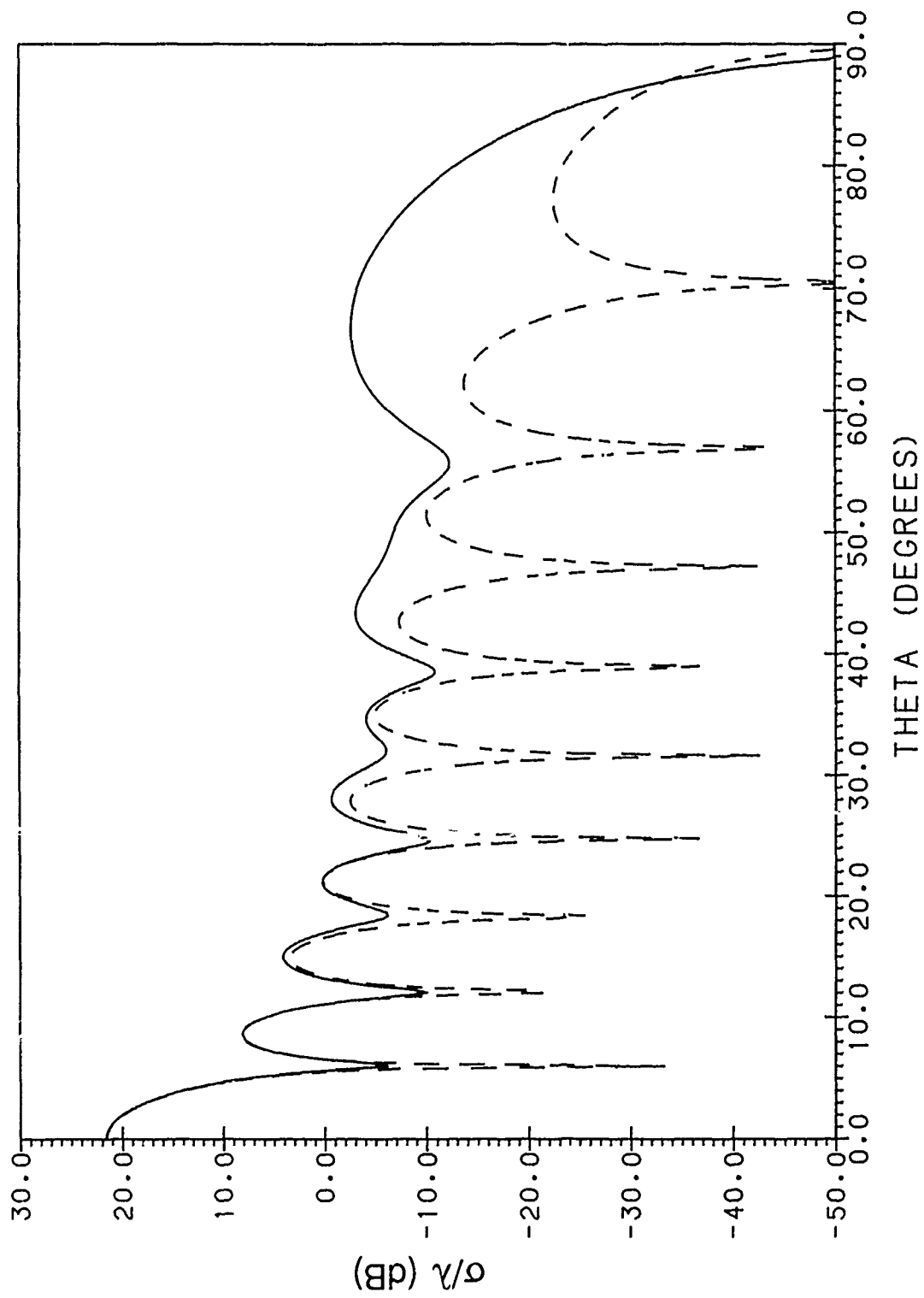


Figure 7b. Back Scatter Cross Section Pattern of Strip,  $ks = 30$ , with TE (Parallel Polarized) Plane-Wave Illumination: —: Exact, ----: PO

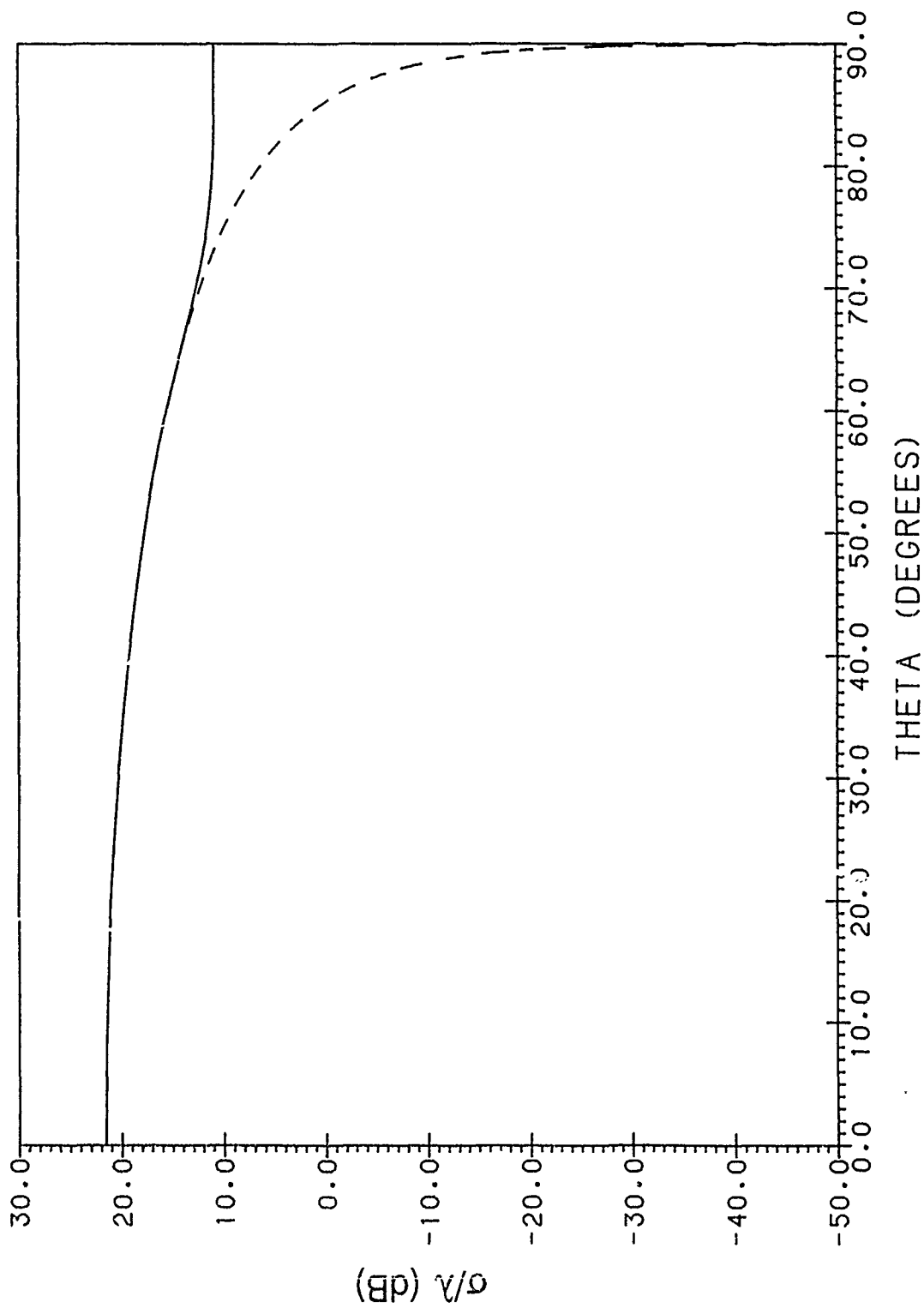


Figure 8a. Specular Scatter Cross Section Pattern of Strip,  $k_s = 30$ , with TM (Perpendicular Polarized) Plane-Wave Illumination; —: Exact, ----: PO



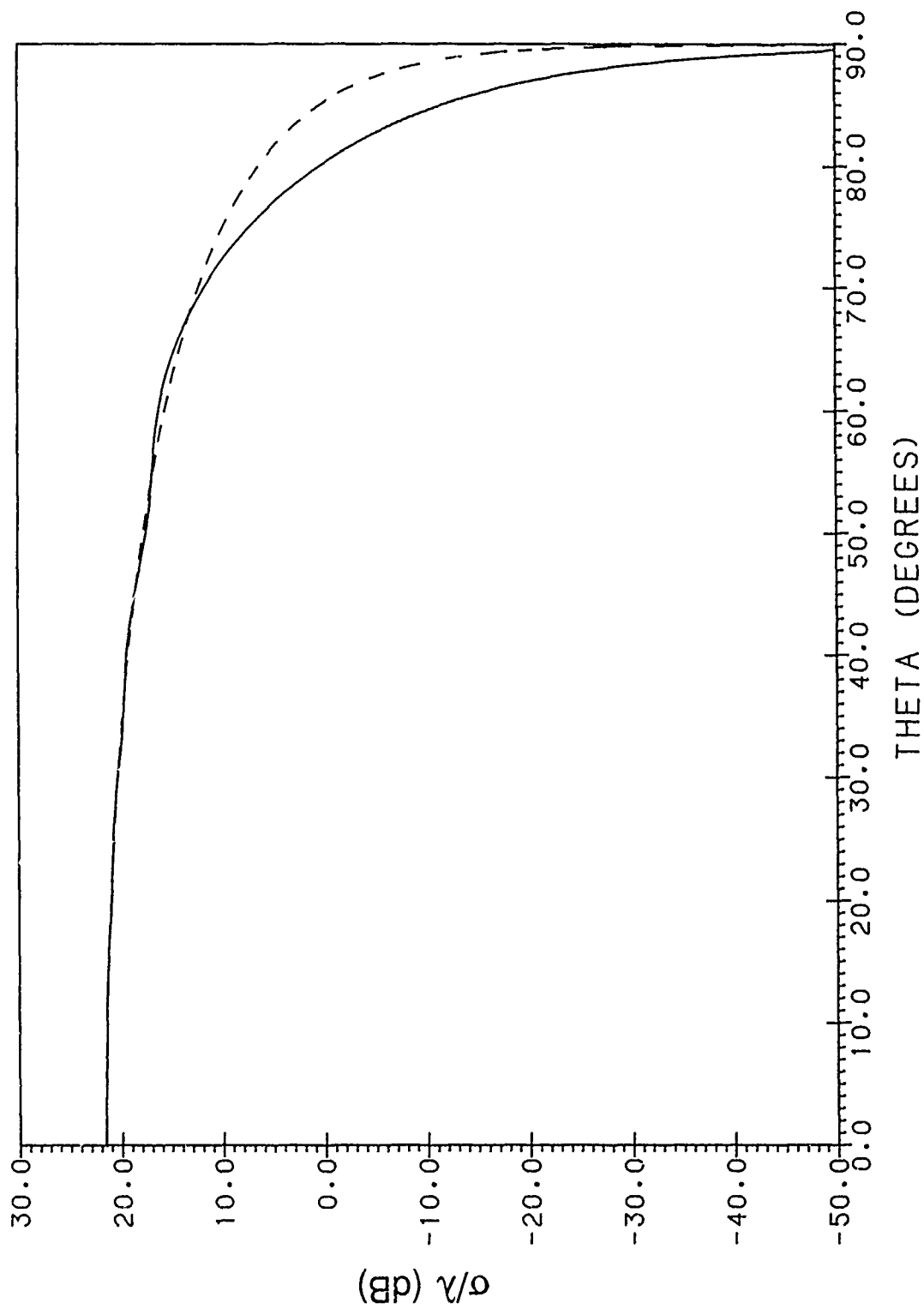


Figure 8b. Specular Scatter Cross Section Pattern of Strip,  $k_s = 30$ , with TE (Perpendicular Polarized) Plane-Wave Illumination:  
 — : Exact, ---- : PO

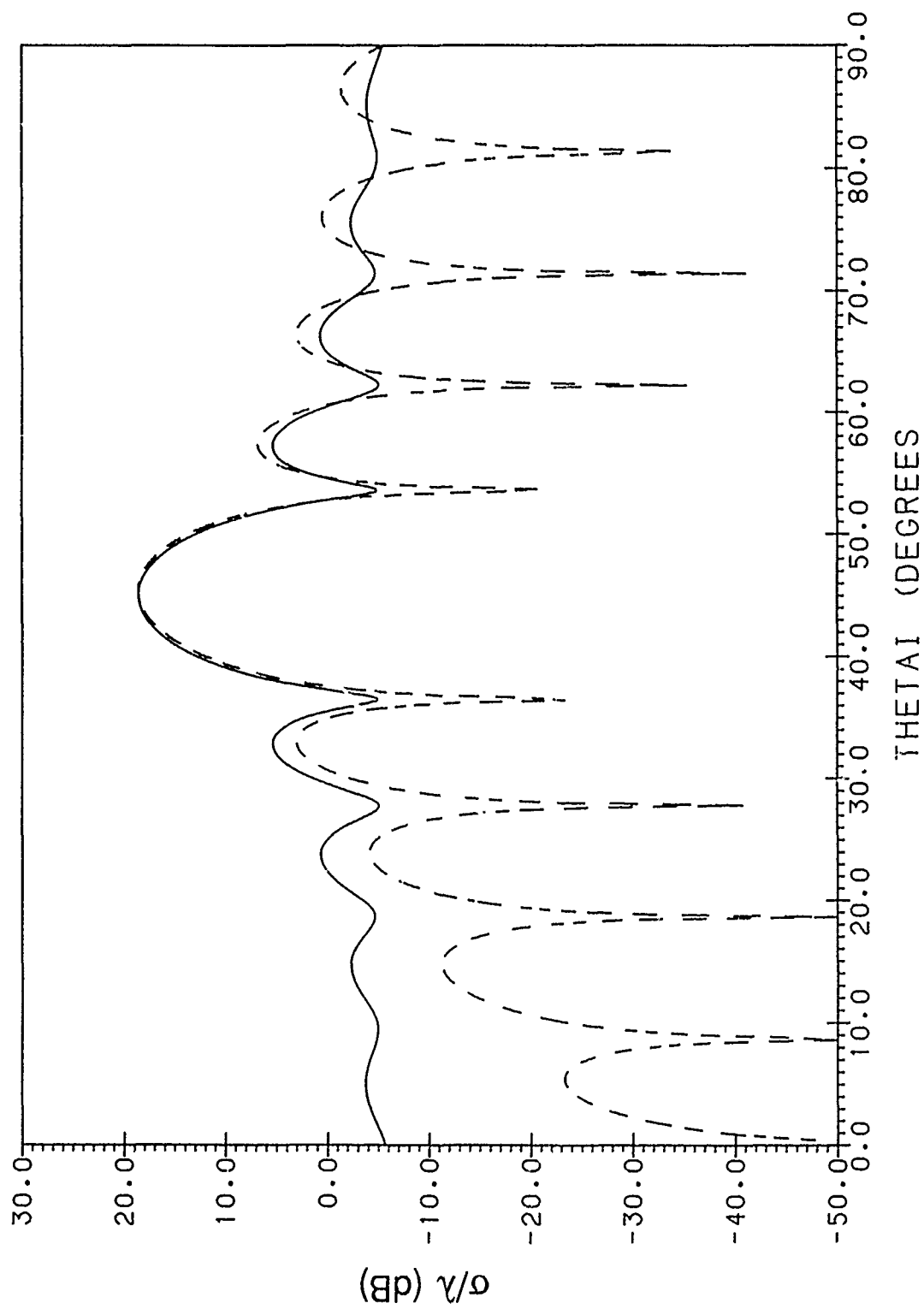


Figure 9a. Side Scatter Cross Section Pattern of Strip,  $ks = 30$ , with TM (Perpendicular Polarized) Plane-Wave Illumination;  
 —: Exact, ----: PO

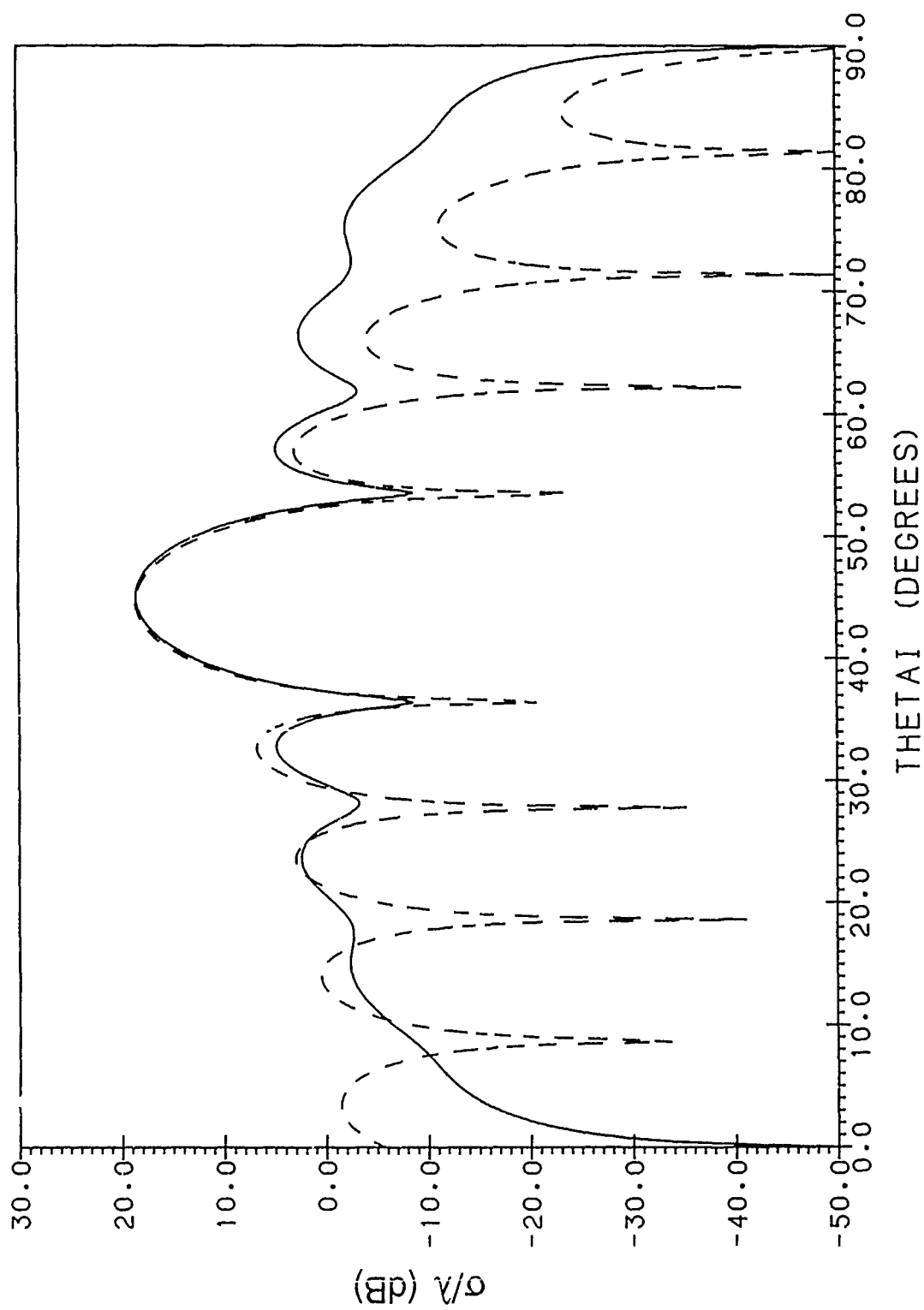


Figure 9b. Side Scatter Cross Section Pattern of Strip,  $ks = 30$ , with TE (Parallel Polarized) Plane-Wave Illumination;  
 —: Exact, ----: PO

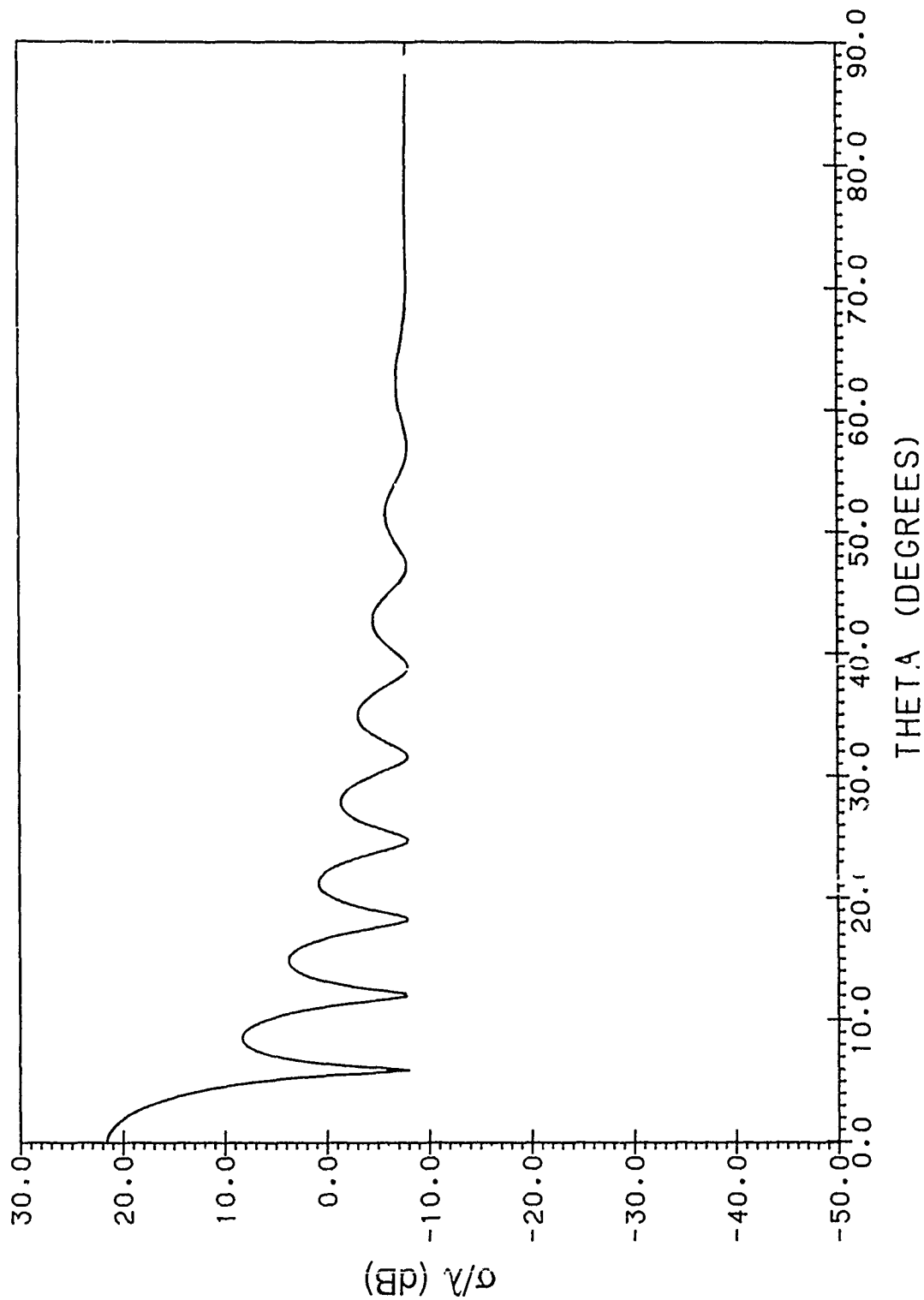


Figure 10a. Back Scatter Cross Section Pattern of Strip,  $ks = \pi/2$ , with TM (Perpendicular Polarized) Plane-Wave Illumination;  
 ----- : Exact, ----- : Michaeli (1984)

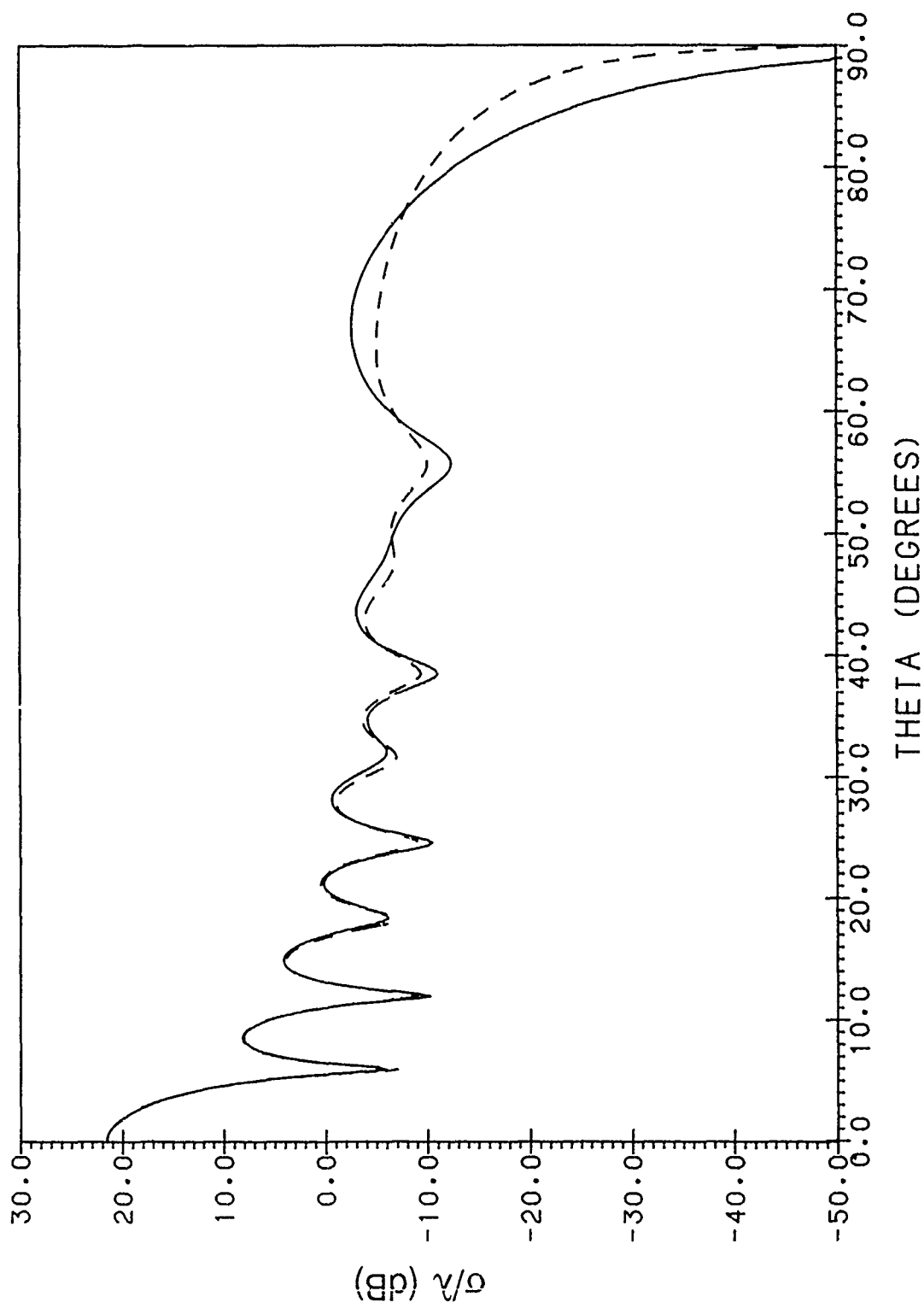


Figure 10b. Back Scatter Cross Section Pattern of Strip,  $k \cdot s = 30$ , with TE (Parallel Polarized) Plane-Wave Illumination;  
 — : Exact, ---- : Michaeli (1984)

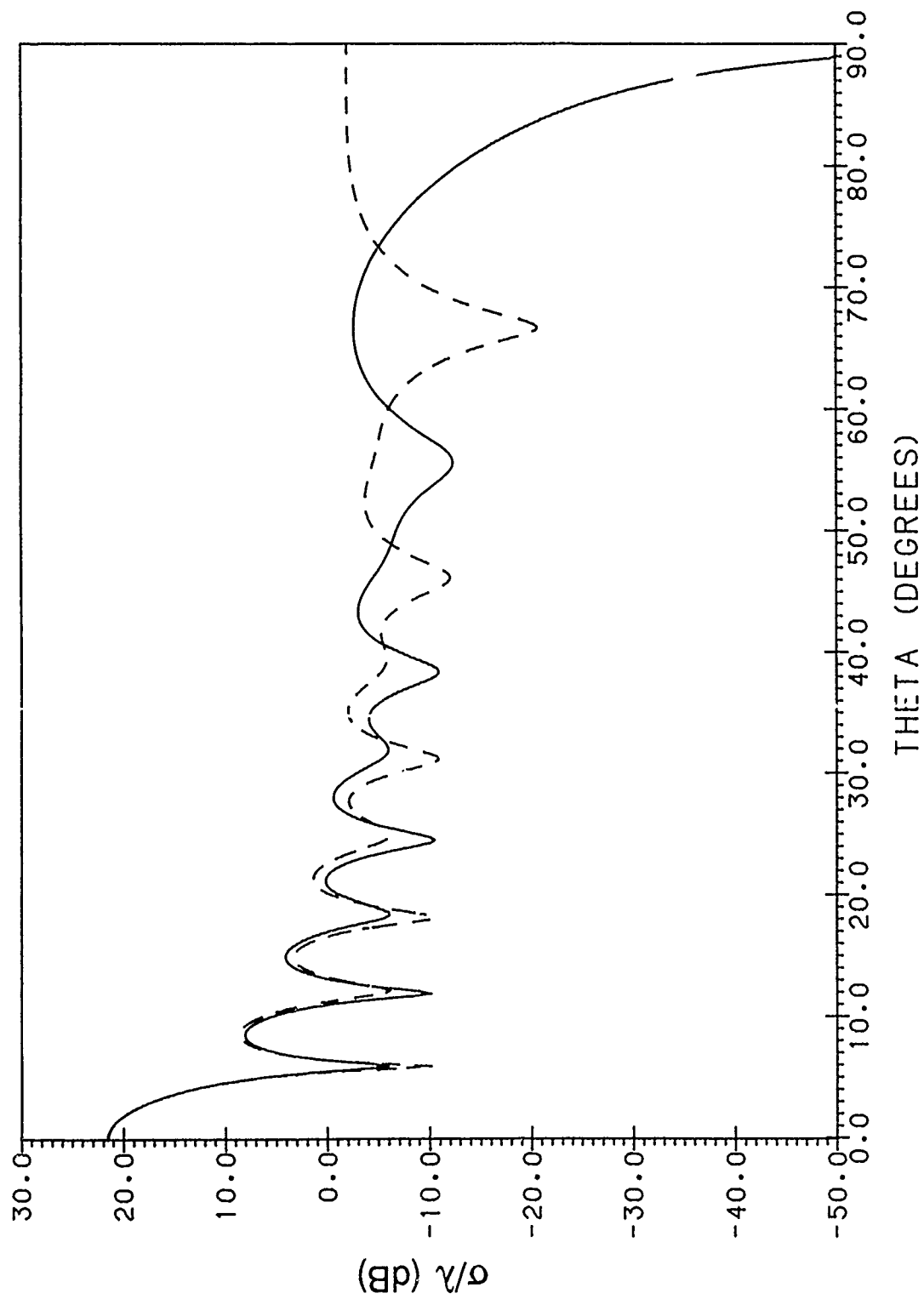


Figure 11. Back Scatter Cross Section Pattern of Strip,  $ks = 30$ , with TE (Parallel Polarized) Plane-Wave Illumination;  
 — Exact, ---- : Ufimtsev (1969)

To show how the accuracy of the approximations derived in Sections 2.1 through 2.5 depends on the strip width, in Figures 12a and b, 13a and b, and 14a and b, we show the TM and TE back scatter, specular scatter, and side scatter cross section plots obtained for a strip of width  $s/\lambda = 3/2\pi = 0.48$ . Although the approximations are not quite as accurate as they are for the strip of width  $s/\lambda = 30/2\pi$ , nevertheless the approximate cross sections differ at most by only 1.5 dB from the exact cross sections.

### 3. NONUNIFORM (PTD) INCREMENTAL DIFFRACTION COEFFICIENTS FOR THE TRUNCATED HALF-PLANE

In this section we obtain the TM and TE nonuniform or PTD IDC's for the leading and trailing edges of a truncated half-plane. The TM nonuniform IDC for either the leading or trailing edge of a truncated half-plane is obtained by substituting  $E_\theta^{\text{nu(TM)}}$  in Eq. (24b) of Reference 3 with  $E_\theta^{\text{nu(TM)}}$  given by the coefficient of  $\theta_0^2$  in Eq. (10a). Thus,

$$\begin{aligned} \overline{dE}^{\text{nu(TM)}}(\vec{r}_l) \quad r_l \rightarrow \infty \sim & dz_l E_{iz_l} \frac{e^{ikr_l}}{4\pi r_l} 2\sqrt{2} \sin \frac{\phi_{0l}}{2} \frac{\sin \theta_l}{\sin^2 \theta_{0l}} \frac{1}{\cos \phi_{0l} + \cos \alpha} \\ & \cdot \left\{ e^{-i\pi/4} \left[ \frac{\sqrt{2} (1 - \cos \alpha)}{|1 - \cos \alpha|^{1/2}} F_0(ks \sin \theta_{0l} | 1 - \cos \alpha |) \right. \right. \\ & - 2 \left| \cos \frac{\phi_{0l}}{2} \right| e^{-i ks \sin \theta_{0l} (\cos \phi_{0l} + \cos \alpha)} F \left( 2ks \sin \theta_{0l} \cos^2 \frac{\phi_{0l}}{2} \right) \Big] \\ & \left. - \sqrt{2} \left| \cos \frac{\phi_{0l}}{2} \right| \left[ 1 - e^{-i ks \sin \theta_{0l} (\cos \phi_{0l} + \cos \alpha)} \right] \right\} \hat{\theta}_{0l} \end{aligned} \quad (40)$$

where

$$\cos \alpha = \frac{\sin \theta_l \cos \phi_l + \cot \psi_l (\cos \theta_l + \cos \theta_{0l})}{\sin \theta_{0l}} \quad (41)$$

with  $\psi_l$  the angle between the axis of the incremental strip and the positive local  $z$ -axis. We have inserted the subscript "l" in Eqs. (40) and (41) to indicate that the subscripted quantities are defined with reference to a local coordinate system with origin at the incremental length  $dz_l$ .

The TE nonuniform IDC for the leading edge of a truncated half-plane is obtained by substituting  $H_\theta^{\text{nu(TE)}}$  and  $H_\phi^{\text{nu(TE)}}$  in Eq. (17) of Reference 3 followed by Eq. (18) of Reference 3, with  $H_\theta^{\text{nu(TE)}}$  and  $H_\phi^{\text{nu(TE)}}$  given by Eq. (18a) and Eq. (31a) respectively. Thus,

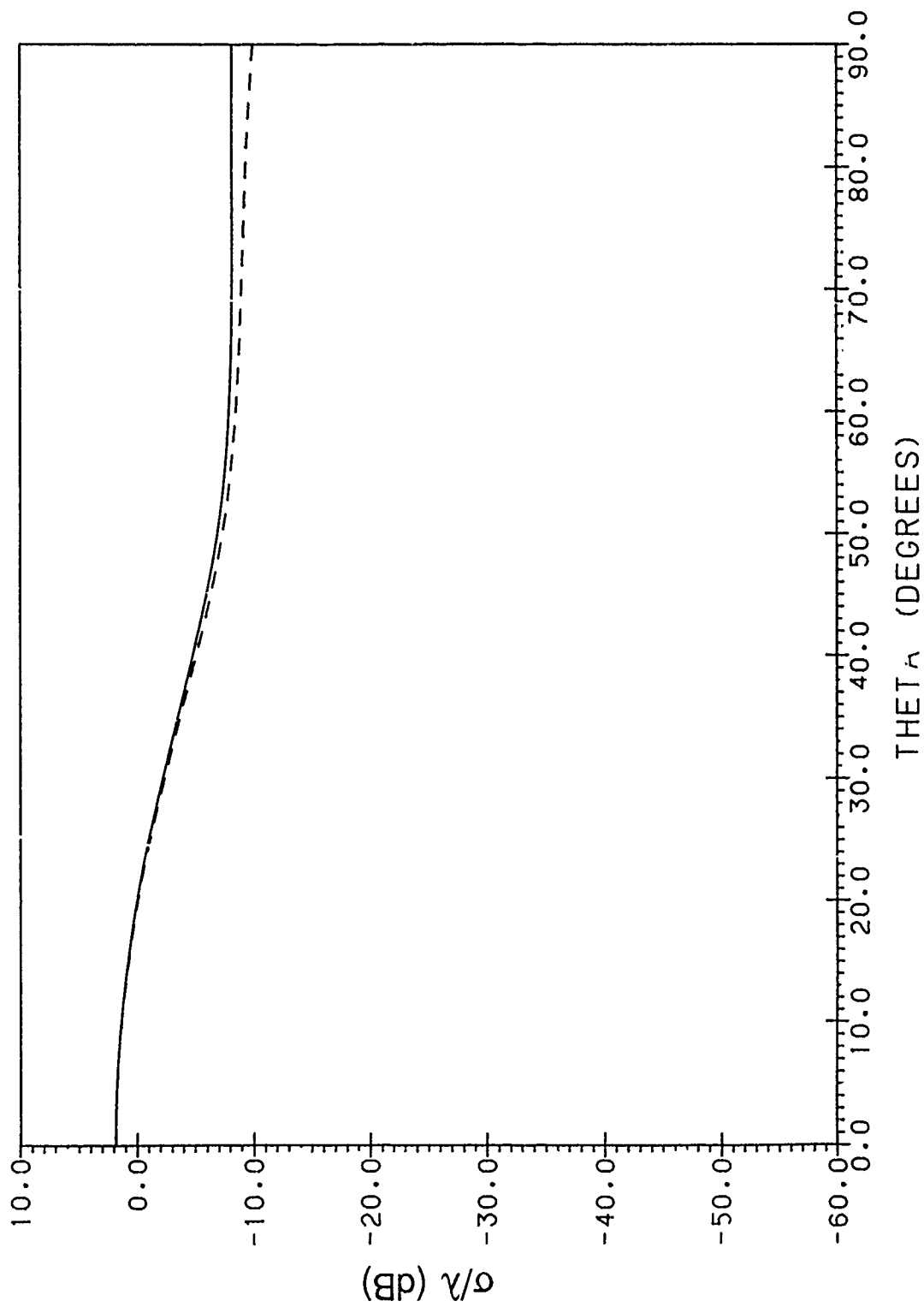


Figure 12a. Back Scatter Cross Section Pattern of Strip,  $ks = 3$ , with TM (Perpendicular Polarized) Plane-Wave Illumination; —: Exact, ---: PO + Approximate Nonuniform Current Field



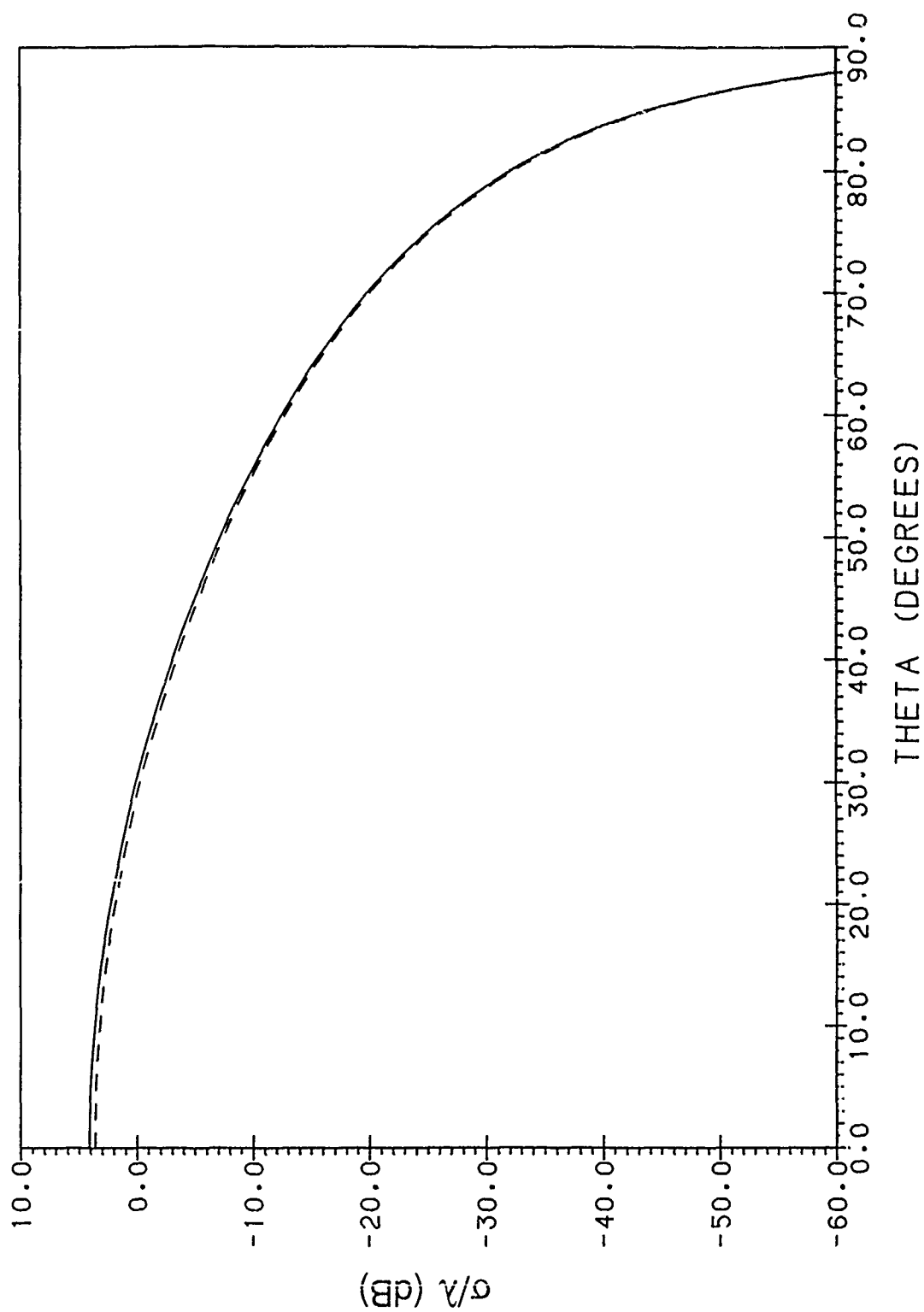


Figure 12b. Back Scatter Cross Section Pattern of Strip,  $ks = 3$ , with TE (Parallel Polarized) Plane-Wave Illumination;  
 — : Exact, - - - - : PO + Approximate Nonuniform Current Field

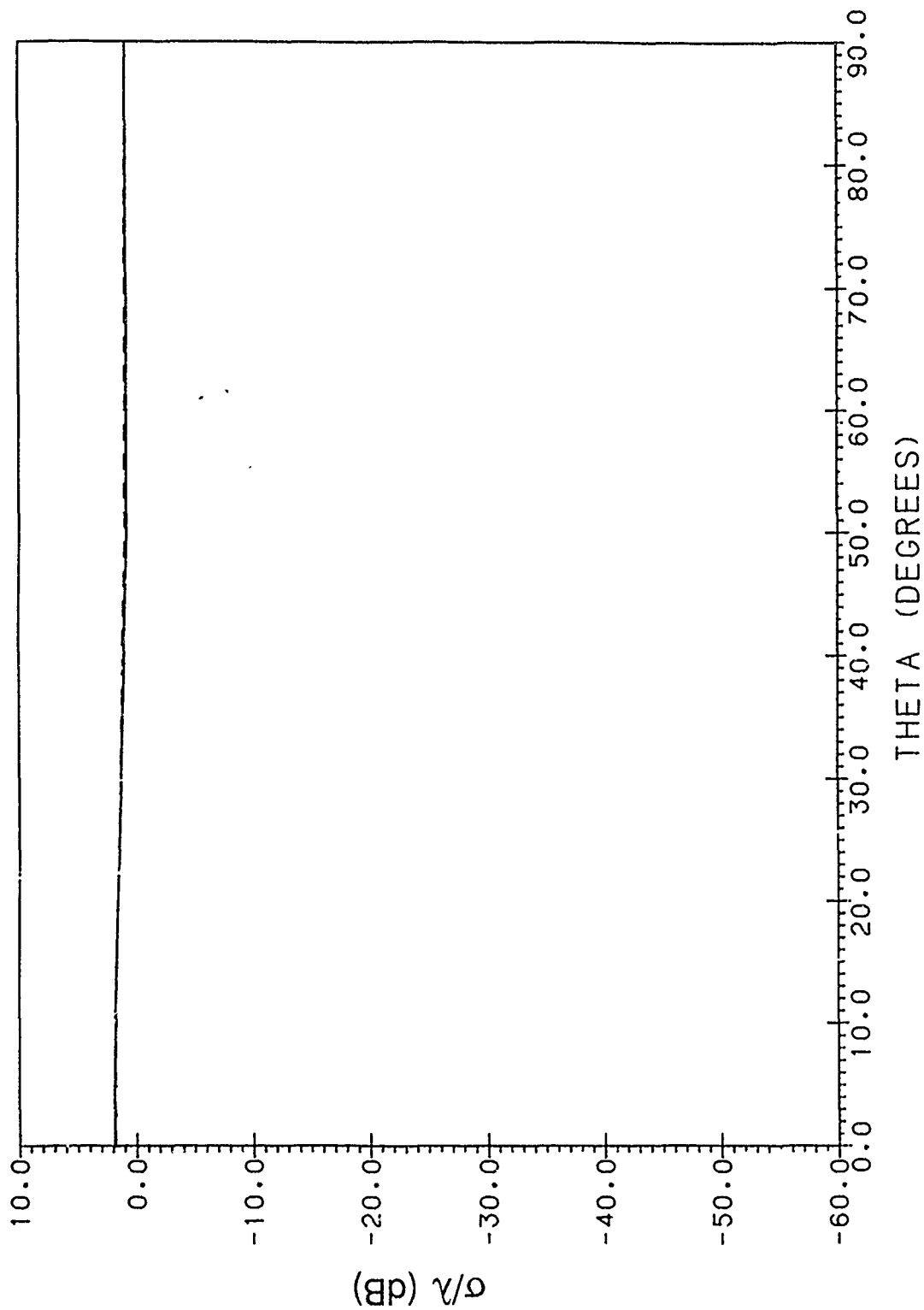


Figure 13a. Specular Scatter Cross Section Pattern of Strip,  $ks = 3$ , with TM (Perpendicular Polarized) Plane-Wave Illumination;  
 ----- : Exact, - - - - - : PO + Approximate Nonuniform Current Field

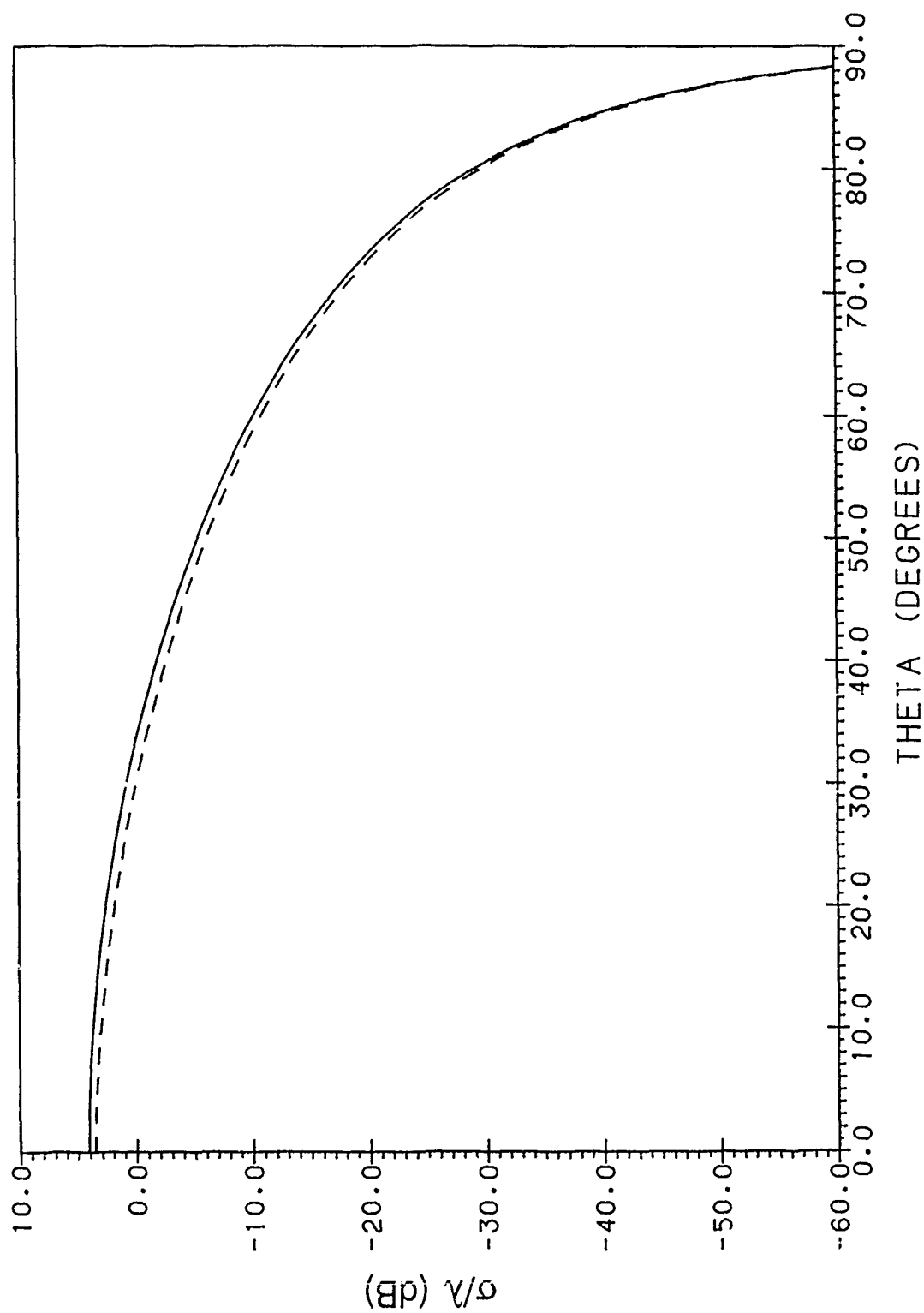


Figure 13b. Specular Scatter Cross Section Pattern of Strip,  $k_s = 3$ , with TE (Parallel Polarized) Plane-Wave Illumination; — : Exact, - - - - : PO + Approximate Nonuniform Current Field

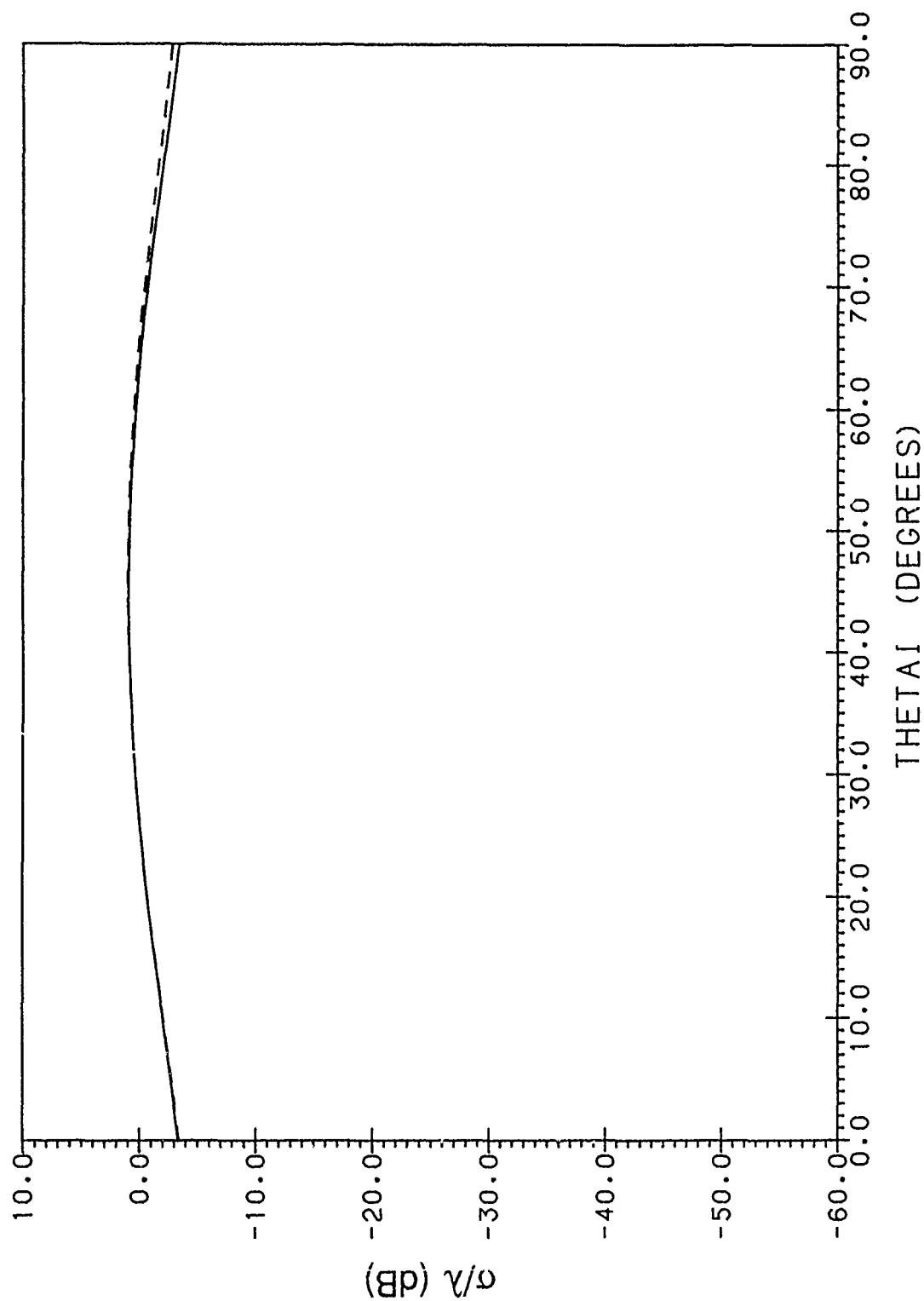


Figure 14a. Side Scatter Cross Section Pattern of Strip,  $k_s = 3$ , with TM (Perpendicular Polarized) Plane-Wave Illumination;  
 — : Exact, - - - : PO + Approximate Nonuniform Current Field

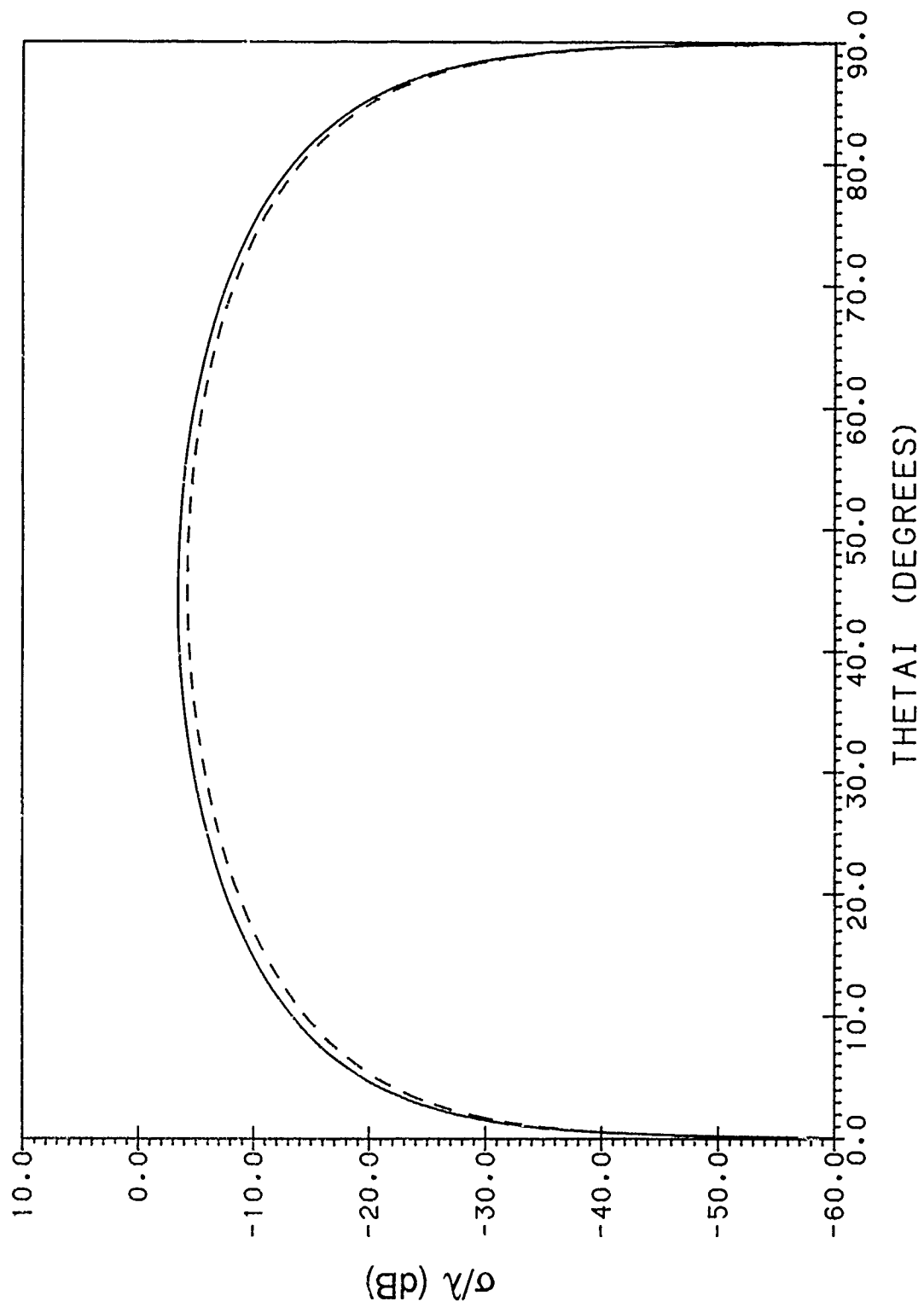


Figure 14b. Side Scatter Cross Section Pattern of Strip,  $ks = 3$ , with TE (Parallel Polarized) Plane-Wave Illumination; — : Exact, ---- : PO + Approximate Nonuniform Current Field

$$\begin{aligned}
\overline{dE}^{\text{nu(TE)}}(\vec{r}_l) \quad r_l \gtrsim \infty \quad -dz_l \text{sign}(\pi - \phi_{0l}) Z_0 H_{1z_l} \frac{e^{ikr_l}}{4\pi r_l} \frac{2}{\sin \theta_{0l}} \\
\cdot \left\{ \left[ \left( \sqrt{2} e^{-i\pi/4} \left[ e^{-iks \sin \theta_{0l} (\cos \phi_{0l} + \cos \alpha)} F \left( 2ks \sin \theta_{0l} \cos^2 \frac{\phi_{0l}}{2} \right) \right. \right. \right. \right. \\
- \frac{\sqrt{2} \left| \cos \frac{\phi_{0l}}{2} \right|}{|1 - \cos \alpha|^{1/2}} F_0(ks \sin \theta_{0l} |1 - \cos \alpha|) \left. \right] \\
+ \left[ 1 - e^{-iks \sin \theta_{0l} (\cos \phi_{0l} + \cos \alpha)} \right] \frac{\cos \phi_l \cos \theta_l + \cos \alpha \cot \theta_{0l} \sin \theta_l}{\cos \phi_{0l} + \cos \alpha} \\
- \left( \sqrt{2} e^{-i\pi/4} e^{-iks \sin \theta_{0l} (\cos \phi_{0l} + \cos \alpha)} F \left( 2ks \sin \theta_{0l} \cos^2 \frac{\phi_{0l}}{2} \right) \right. \\
+ \left. \left[ 1 - e^{-iks \sin \theta_{0l} (\cos \phi_{0l} + \cos \alpha)} \right] \cot \theta_{0l} \sin \theta_l \right] \hat{\theta}_l \\
- \frac{\sin \phi_l}{\cos \phi_{0l} + \cos \alpha} \left[ \sqrt{2} e^{-i\pi/4} \left( e^{-iks \sin \theta_{0l} (\cos \phi_{0l} + \cos \alpha)} F \left( 2ks \sin \theta_{0l} \cos^2 \frac{\phi_{0l}}{2} \right) \right. \right. \\
- \frac{\sqrt{2} \left| \cos \frac{\phi_{0l}}{2} \right|}{|1 - \cos \alpha|^{1/2}} F_0(ks \sin \theta_{0l} |1 - \cos \alpha|) \left. \right) + \left. \left[ 1 - e^{-iks \sin \theta_{0l} (\cos \phi_{0l} + \cos \alpha)} \right] \right] \hat{\phi}_l \left. \right\}
\end{aligned} \quad (42)$$

with  $\cos \alpha$  given by Eq. (41). The TE nonuniform IDC for the trailing edge of a truncated half-plane is obtained by multiplying the edge expression in Eq. (42) by the factor given in Eq. (35) or (37), as explained previously in Section 2.5.

#### 4. SCATTERING OF A PLANE WAVE BY A PERFECTLY CONDUCTING DISK

In this section we apply the IDC's derived in Section 3 to calculate the far fields scattered from a perfectly electrically conducting disk of radius  $a$ . The geometry is shown in Figure 15. The primary source is a plane wave whose direction of propagation lies in the  $xz$ -plane and makes an angle of  $\theta_l$  with the  $z$ -axis. The observation direction is given in spherical polar coordinates  $(R, \theta, \phi)$ . Two polarizations of the incident plane wave are considered:

1) perpendicular (TE) or

$$\vec{E}_{\text{inc}} = E_l e^{i\vec{k}_l \cdot \vec{r}} \hat{y}, \quad (43a)$$

$$\vec{H}_{\text{inc}} = Y_0 E_l e^{i\vec{k}_l \cdot \vec{r}} (\cos \theta_l \hat{x} - \sin \theta_l \hat{z}), \quad (43b)$$

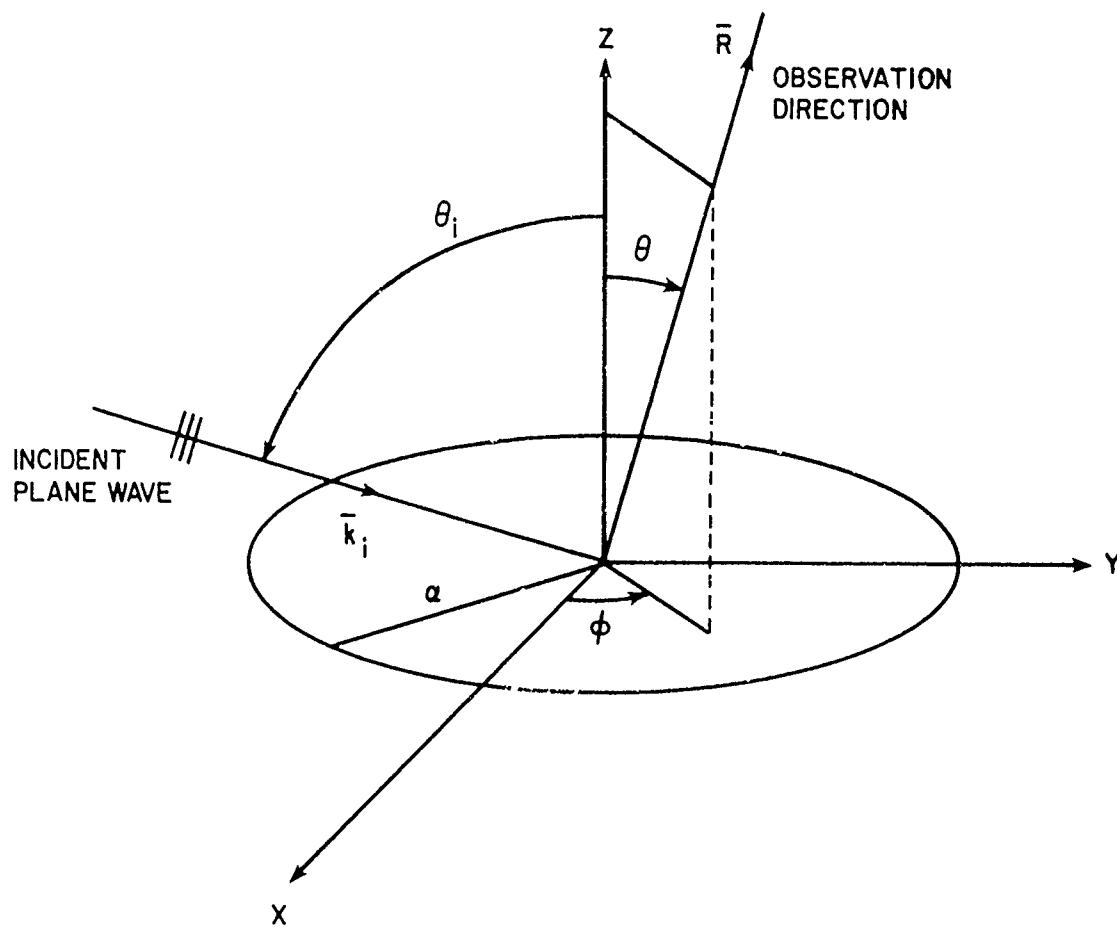


Figure 15. Geometry of Disk Illuminated by a Plane Wave

and

2) parallel (TM) or

$$\vec{E}_{\text{inc}} = E_1 e^{i\vec{k}_1 \cdot \vec{r}} (\cos \theta_1 \hat{x} - \sin \theta_1 \hat{z}), \quad (44a)$$

$$\vec{H}_{\text{inc}} = -Y_0 E_1 e^{i\vec{k}_1 \cdot \vec{r}} \hat{y}, \quad (44b)$$

with

$$\vec{k}_1 = -k\hat{r}_1 = -k(\sin \theta_1 \hat{x} + \cos \theta_1 \hat{z}), \quad (45)$$

and

$$\vec{r} = x\hat{x} + y\hat{y} + z\hat{z}. \quad (46)$$

The far field scattered from the disk is obtained by adding the integrals of the strip nonuniform IDC's around the edge of the disk to the PO far field. The nonuniform high-frequency solution presented here for scattering from the disk remains valid for all angles of incidence and scattering, and thus, is distinguished from the previous high-frequency solutions that concentrated on back scattering.<sup>16,17</sup>

#### 4.1 Physical Optics Field

The PO scattered field is derived in Reference 18 and we give only the results here. For perpendicular polarization of the incident plane wave

$$\vec{E}_s^{\text{PO}}(P) = iE_1 a \frac{e^{ikR}}{R} \frac{J_1(ka\beta)}{\beta} \cos \theta_1 (\cos \theta \sin \phi \hat{\theta} + \cos \phi \hat{\phi}) \quad (47)$$

while for parallel polarization

$$\vec{E}_s^{\text{PO}}(P) = iE_1 a \frac{e^{ikR}}{R} \frac{J_1(ka\beta)}{\beta} \cos \theta_1 (\cos \theta \cos \phi \hat{\theta} - \sin \phi \hat{\phi}) \quad (48)$$

with

$$\beta = \left[ \sin^2 \theta \sin^2 \phi + (\sin \theta_1 + \sin \theta \cos \phi)^2 \right]^{1/2} \quad (49)$$

and  $J_1$  the Bessel function of order one.

- 
- 16 DeVore, R., Hodge, D.B., and Kouyoumjian, R.C. (1971) Backscattering cross sections of circular disks for arbitrary incidence, *J. Applied Physics* **42**:3075-3083.
  - 17 Marsland, D.P., Balanis, C.A., and Brunley, S.A. (1987) Higher order diffractions from a circular disk, *IEEE Trans. Antennas Propagat.* **AP-35**:1436-1444.
  - 18 Trott, K. (1988) *The Disk: A Comparison of Electromagnetic Scattering Solutions and Its Use as a Calibration Standard for Bistatic RCS Measurements*, RADC-TR-88-16, ADA200327.



## 4.2 Transformation of the Local Coordinates of the Strip IDC's to the Global Coordinate System of the Disk

The correction to the PO electric far field of the disk is obtained as indicated above by integrating the nonuniform strip IDC's, Eqs. (40) and (42), around the edge of the disk. Since all quantities in Eqs. (40) and (42) are defined with respect to a local coordinate system with origin at the differential element of the disk edge, it is first necessary to transform Eqs. (40) and (42) to the global coordinate system of Figure 15. It is also necessary to define the local coordinate system. Since we are modelling the edge locally by the truncated half-plane defined as in Figure 2, we want the local x-axis to be in the plane of the disk, normal to the edge, and directed inward from the edge; the local y-axis to be the normal to the disk at the edge directed toward the half-space from which the illuminating plane wave is incident; and the local z-axis to be tangent to the edge of the disk. Hence,

$$\hat{x}_l = -\hat{\rho}' = -\cos \phi' \hat{x} - \sin \phi' \hat{y}, \quad (50a)$$

$$\hat{y}_l = \hat{z}, \quad (50b)$$

and

$$\hat{z}_l = \hat{x}_l \times \hat{y}_l = \hat{\phi}' = \cos \phi' \hat{x} - \sin \phi' \hat{y}, \quad (50c)$$

where we use primes to denote the point of integration.

We now systematically express the locally defined quantities of Eqs. (40) and (42) in the global coordinate system. Starting with  $\theta_{0l}$ , the angle between the local unit z-vector,  $\hat{\phi}'$ , and the vector  $\hat{r}_l$  given by Eq. (45),

$$\begin{aligned} \cos \theta_{0l} &= \hat{r}_l \cdot \hat{z}_l \\ &= -\sin \theta_l \sin \phi' \end{aligned} \quad (51a)$$

and

$$\sin \theta_{0l} = + (1 - \sin^2 \theta_l \sin^2 \phi')^{1/2} \quad (51b)$$

where the positive root must be taken since  $0 \leq \theta_{0l} \leq \pi$ .

Next, since  $\phi_{0l}$  is the angle between  $\hat{x}_l$  and the projection of  $\hat{r}_l$  on the  $x_l y_l$ -plane,

$$\begin{aligned} \cos \phi_{0l} &= \hat{r}_l \cdot \hat{x}_l / \sin \theta_{0l} \\ &= -\sin \theta_l \cos \phi' / \sin \theta_{0l} \end{aligned} \quad (52a)$$

and

$$\begin{aligned} \sin \phi_{0l} &= \hat{r}_l \cdot \hat{y}_l / \sin \theta_{0l} \\ &= \cos \theta_l / \sin \theta_{0l} \end{aligned} \quad (52b)$$

from which

$$\cos \frac{\phi_{0l}}{2} = + \left( \frac{1 - \frac{\sin \theta_l \cos \phi'}{\sin \theta_{0l}}}{2} \right)^{1/2} . \quad (53)$$

where the positive root must be taken since for a plane wave incident from the upper half-space,  $z > 0$ ,  $0 \leq \phi_{0l} \leq \pi$ .

Proceeding to  $\theta_l$ , the angle between  $\hat{z}_l$  and the ray from the edge point to the far-field observation point,

$$\begin{aligned} \cos \theta_l &= \hat{z}_l \cdot \hat{r}_l = \hat{\phi}' \cdot \hat{R} \\ &= -\sin \theta \sin(\phi' - \phi) \end{aligned} \quad (54a)$$

and

$$\sin \theta_l = + \left[ 1 - \sin^2 \theta \sin^2(\phi' - \phi) \right]^{1/2} \quad (54b)$$

where the positive root must be taken since  $0 \leq \theta_l \leq \pi$ . The cosine and sine of  $\phi_l$  are given by

$$\begin{aligned} \cos \phi_l &= \hat{r}_l \cdot \hat{x}_l / \sin \theta_l = \hat{R} \cdot \hat{x}_l / \sin \theta_l \\ &= -\sin \theta \cos(\phi' - \phi) / \sin \theta_l \end{aligned} \quad (55a)$$

and

$$\begin{aligned} \sin \phi_l &= \hat{r}_l \cdot \hat{y}_l / \sin \theta_l = \hat{R} \cdot \hat{y}_l / \sin \theta_l \\ &= \cos \theta / \sin \theta_l . \end{aligned} \quad (55b)$$

The unit vector  $\hat{\theta}_l$  is transformed to global coordinates by starting with

$$\hat{\theta}_l = \cos \theta_l \cos \phi_l \hat{x}_l + \cos \theta_l \sin \phi_l \hat{y}_l - \sin \theta_l \hat{z}_l ,$$

substituting global Cartesian component expressions for  $\hat{x}_l$ ,  $\hat{y}_l$ , and  $\hat{z}_l$ , and simplifying trigonometrically, thereby obtaining

$$\begin{aligned} \hat{\theta}_l &= (-\cos \theta_l \cos \phi_l \cos \phi' + \sin \theta_l \sin \phi') \hat{x} \\ &\quad - (\cos \theta_l \cos \phi_l \sin \phi' + \sin \theta_l \cos \phi') \hat{y} \\ &\quad + \cos \theta_l \sin \phi_l \hat{z} , \end{aligned} \quad (56)$$

with  $\cos \theta_l$ ,  $\sin \theta_l$ ,  $\cos \phi_l$ , and  $\sin \phi_l$ , given by Eqs. (54a), (54b), (55a), and (55b) respectively. A similar procedure gives

$$\hat{\phi}_l = \sin \phi_l \cos \phi' \hat{x} + \sin \phi_l \sin \phi' \hat{y} + \cos \phi_l \hat{z} . \quad (57)$$

When the IDC's, Eqs. (40) and (42), are integrated around the edge of the disk to obtain the nonuniform current correction to the PO far field, it is the  $\theta$ - and  $\phi$ - components of the electric far field

that are required (the radial component, is of course, zero). Hence, it is desirable to have expressions for the  $\theta$ - and  $\phi$ - components of  $\hat{\theta}_l$  and  $\hat{\phi}_l$ . Letting

$$\sigma = \hat{\theta}_l \cdot \hat{\theta}, \quad \tau = \hat{\theta}_l \cdot \hat{\phi}, \quad \mu = \hat{\phi}_l \cdot \hat{\theta}, \quad \nu = \hat{\phi}_l \cdot \hat{\phi}, \quad (58)$$

we have

$$\sigma = a \cos \theta \cos \phi + b \cos \theta \sin \phi - c \sin \theta, \quad (59a)$$

$$\tau = -a \sin \phi + b \cos \phi, \quad (59b)$$

$$\mu = d \cos \theta \cos \phi + e \cos \theta \sin \phi - f \sin \theta, \quad (59c)$$

$$\nu = -d \sin \phi + e \cos \phi, \quad (59d)$$

where  $a$ ,  $b$ , and  $c$  are the coefficients of  $\hat{x}$ ,  $\hat{y}$ , and  $\hat{z}$ , respectively, in Eq. (56) and  $d$ ,  $e$ , and  $f$  are the coefficients of  $\hat{x}$ ,  $\hat{y}$ , and  $\hat{z}$  in Eq. (57). Substituting explicit expressions for  $a$ ,  $b$ , and  $c$ , and  $d$ ,  $e$ , and  $f$  from Eqs (56) and (57) in (59) followed by substitution of the expressions Eqs. (54) and (55) for  $\cos \theta_l$ ,  $\sin \theta_l$ ,  $\cos \phi_l$ , and  $\sin \phi_l$ , yields after algebraic and trigonometric simplification

$$\sigma = \frac{\cos \theta \sin u}{(1 - \sin^2 \theta \sin^2 u)^{1/2}}, \quad (60a)$$

$$\tau = -\frac{\cos u}{(1 - \sin^2 \theta \sin^2 u)^{1/2}}, \quad (60b)$$

$$\mu = \frac{\cos u}{(1 - \sin^2 \theta \sin^2 u)^{1/2}}, \quad (60c)$$

$$\nu = \frac{\cos \theta \sin u}{(1 - \sin^2 \theta \sin^2 u)^{1/2}} \quad (60d)$$

where

$$u = \phi' - \phi. \quad (61)$$

Next, proceeding to  $e^{ikr_l/r_l}$  and replacing  $r_l$  by  $r$

$$\frac{e^{ikr_l}}{r_l} = \frac{e^{ikr}}{r} \underset{r \rightarrow \infty}{\sim} \frac{e^{ik(R - \hat{r}' \cdot \hat{R})}}{R}. \quad (62)$$

It is then simple to find that

$$\hat{r}' \cdot \hat{R} = a \sin \theta \cos(\phi' - \phi). \quad (63)$$

The differential length  $dz'_l$  is given by

$$dz'_l = a d\phi' \quad (64)$$

Finally, the components of the illuminating field in the local  $z$ -direction,  $E_{z'l}$  and  $H_{z'l}$ , are given by

$$E_{1z_l} = E_{1\phi'}, \quad (65a)$$

$$H_{1z_l} = H_{1\phi'}, \quad (65b)$$

where, from Eqs. (43) and (44),

$$E_{1\phi'} = E_1 \cos \phi' e^{i \bar{k}_1 \cdot \bar{r}'}, \quad (66a)$$

$$H_{1\phi'} = -Y_0 E_1 \cos \theta_1 \sin \phi' e^{i \bar{k}_1 \cdot \bar{r}'}, \quad (66b)$$

for perpendicular polarization of the incident plane wave, and

$$E_{1\phi'} = -E_1 \cos \theta_1 \sin \phi' e^{i \bar{k}_1 \cdot \bar{r}'}, \quad (67a)$$

$$H_{1\phi'} = -Y_0 E_1 \cos \phi' e^{i \bar{k}_1 \cdot \bar{r}'}, \quad (67b)$$

for parallel polarization of the incident plane wave.

### 4.3 Choice of Incremental Strips

In integrating the nonuniform current IDC's around the edge of the disk to obtain the correction to the PO far field, a choice must be made of the orientation of the incremental strips, since the strips can be chosen to cut across the disk in any direction. Thus, for example, the strips can be taken straight across the disk parallel to the x-axis, the projection of the direction vector of the incident plane wave on the disk, or they can be chosen to lie in the directions of the diffracted rays on the disk, or they can be chosen to be diameters, normal to the edge at the points of integration. In general, if the nonuniform current dies away rapidly from the edge, the choice of the orientation of the incremental strips plays little role in determining the nonuniform current field. However, if the nonuniform current does not decrease rapidly away from the edge as it does not here, for parallel polarization close to grazing incidence, the choice of the incremental strips can significantly affect the calculated nonuniform current field.

In the calculations performed, two choices of incremental strips were made: 1) straight across the disk parallel to the x-axis; and 2) in the directions of the diffracted rays on the disk. (The choice of diameter incremental strips was ruled out because it would lead to serious overlapping, and hence overweighting, of the nonuniform currents close to the center of the disk.) The choice of the incremental strip orientations enters into the calculations analytically through 1) the value of  $s$ , the width of the strip, in the IDC's given by Eqs. (40) and (42); and 2)  $\cot \psi_l$  in Eq. (41) where  $\psi_l$  is the angle between the axis of the incremental strip and the positive local z-axis. The derivation of these quantities is given in Appendix B and we state the results here. For incremental strips taken straight across the disk parallel to the x-axis

$$s = 2a \cos^2 \phi', \quad (68)$$

$$\cot \psi_l = \tan \phi', \quad (69)$$

while for strips taken along the diffracted rays on the disk

$$s = 2a(1 - \sin^2 \theta_i \sin^2 \phi') , \quad (70)$$

$$\cot \psi_l = -\cos \theta_{ol} / \sin \theta_{ol} . \quad (71)$$

with  $\cos \theta_{ol}$  and  $\sin \theta_{ol}$  given by Eq. (51). For both choices, the parameter  $L$  in the factors, (37) or (38), used to multiply the TE trailing edge field, is taken as the value for strips straight across the disk; that is,

$$L = 2a |\cos \phi'| \quad (72)$$

because the use of (37) as a simple multiplicative factor applied to the incident field assumes that the direction of propagation of the field impinging upon the trailing edge is in the direction of the incident field. Near grazing, where the multiplicative factor, (37), differs significantly from unity, all the diffracted rays approach the direction straight across the disk and thus, the value of  $L$  in Eq. (72) is valid for the diffracted ray directions as well as the direction across the disk. Away from grazing, where the diffracted rays do not all lie in the direction across the disk, the multiplicative factor approaches unity, and thus its effect becomes insignificant for large disks.

#### 4.4 Calculations of the Bistatic Radar Cross Section of a Disk

In this section we show the results of calculations of the bistatic section of a perfectly conducting disk. The bistatic cross section,  $\sigma(\theta, \phi)$ , is defined by Eq. (I.30) of Reference 12:

$$\sigma(\theta, \phi) = \lim_{R \rightarrow \infty} 4\pi R^2 \frac{|\bar{E}^s|^2}{|\bar{E}_{inc}|^2} \quad (73)$$

where  $\bar{E}^s$  is the scattered electric field at the observation point  $(R, \theta, \phi)$ . In our calculations we normalize the bistatic cross section by dividing it by the square of the wavelength. We present plots of the bistatic cross section for perpendicular and parallel polarization of the incident plane wave, and for both co- and cross-polarized scattered fields defined according to Ludwig's third definition<sup>19</sup> as

$$E_{co} = E_\theta \cos \phi + E_\phi \sin \phi , \quad (74a)$$

$$E_{cr} = E_\theta \cos \phi - E_\phi \sin \phi . \quad (74b)$$

Cross sections were calculated for the two choices of incremental strip orientations discussed in the previous section: strips taken straight across the disk parallel to the  $x$ -axis, the projection of the direction vector of the incident plane wave on the disk; and strips taken in the direction of the diffracted rays on the disk. The approximate cross sections obtained by adding the integrals of the nonuniform current IDC's around the edge of the disk to the PO fields are compared with the exact

---

19. Ludwig, A.C. (1973) The definition of cross polarization, *IEEE Trans. Antennas Propagat.* AP-21:116-119.

cross sections obtained from an eigenfunction solution.<sup>20</sup> A modification of a computer code implementation<sup>20</sup> of the eigenfunction solution, made by Dominek<sup>21</sup> to allow for the use of larger  $ka$  values, was used to calculate the exact cross sections.

In Figures 16a and b, we show the back scatter ( $\theta = \theta_i$ ,  $\phi = \phi_i = 0$ ) cross section patterns for a disk of size  $ka = 15$  for perpendicular polarization of the incident plane wave, with the incremental strips taken straight across the disk and in the direction of the diffracted rays, respectively. Figures 17a and b show the corresponding back scatter patterns for parallel polarization of the incident plane wave. Both strip orientations yield similar satisfactory approximations over the entire range of  $\theta$ .

In Figures 18a and b we show the specular scatter ( $\theta = \theta_i$ ,  $\phi = \pi$ ) cross sections for perpendicular polarization of the incident plane wave, with the strips oriented parallel to the x-axis and in the direction of the diffracted rays, respectively. Figures 19a and b show the corresponding plots for parallel incident plane wave polarization. Both choices of incremental strips yield excellent approximations over the entire range of  $\theta$  that could be used as an accurate calibration standard for bistatic RCS measurements.

The side scatter (observation direction normal to the incidence direction:  $\theta = \pi/2 - \theta_i$ ,  $\phi = \pi$ ) cross section patterns for perpendicular polarization of the incident plane wave, with the incremental strips parallel to the x-axis and in the directions of the diffracted rays, are shown in Figures 20a and b, respectively. The corresponding patterns for parallel incident plane wave polarization are shown in Figures 21a and b. The patterns obtained with the strips taken parallel to the x-axis give a slightly better approximation to the exact cross sections than do the patterns obtained with the strips in the direction of the diffracted rays.

A significant feature seen in Figures 17, 19, and 21 is that the scattered fields of the high-frequency solution approach zero like the exact scattered fields as the parallel polarized plane wave approaches grazing incidence. This high accuracy near grazing for the parallel polarized plane wave further confirms the validity of the trailing edge factor in (37).

In Figures 22 - 25 we show the cut through the cross section pattern in the plane defined by  $\phi = 45^\circ$  and  $\phi = 225^\circ$ , for a plane wave incident on the disk at angle of  $\theta_i = 45^\circ$ . In these plots we have let  $\beta\gamma = 90^\circ - \theta$  for  $\phi = 45^\circ$ ,  $90^\circ \geq \theta \geq 0^\circ$ , and  $\gamma = 90^\circ + \theta$  for  $\phi = 225^\circ$ ,  $0 \leq \theta \leq 90^\circ$ . We show both the co- and cross-polarization patterns in this cut. (For the back, specular, and side scatter patterns, the cross-polarized field equals zero.) Figures 22a and b display the co-polarized pattern for perpendicular polarization of the incident plane wave, with the incremental strips parallel to the x-axis, and in the diffracted ray directions respectively. Figures 23a and b show the corresponding cross-polarized patterns. In Figures 24a and b we show the co-polarized patterns for parallel polarization of the incident plane wave, and in Figures 25a and b the corresponding cross-polarized patterns are shown.

We see from Figures 22 - 25 that again there is not a large difference in accuracy between the high-frequency solution calculated from strips parallel to the x-axis and in the directions of the diffracted rays. The larger discrepancy between the high-frequency solution and the exact solution for

---

20. Hodge, D.B. (1979) *The Calculation of Far Field Scattering by a Circular Metal Disk*, Ohio State University ElectroScience Laboratory Report 710816-2.

21. Dominek, A.K. (1988) Personal Communication, Ohio State University ElectroScience Laboratory.

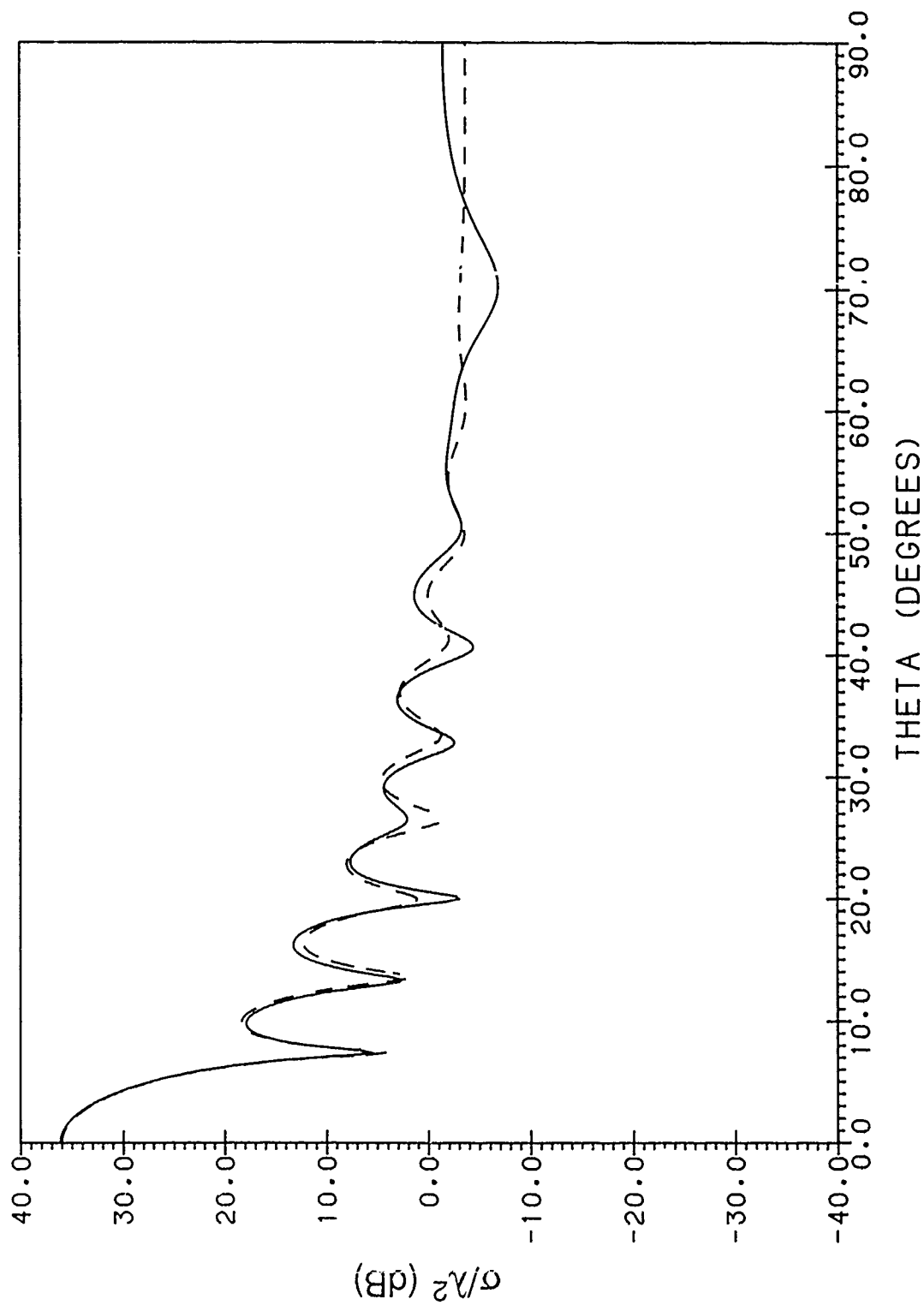


Figure 16a. Back Scatter Cross Section Pattern of Disk,  $ka = 15$ , with Perpendicular Polarized Plane-Wave Illumination and Incremental Strips Parallel to x-Axis; — : Exact, - - - : PO + Approximate Nonuniform Current Field Obtained by Integrating IDC

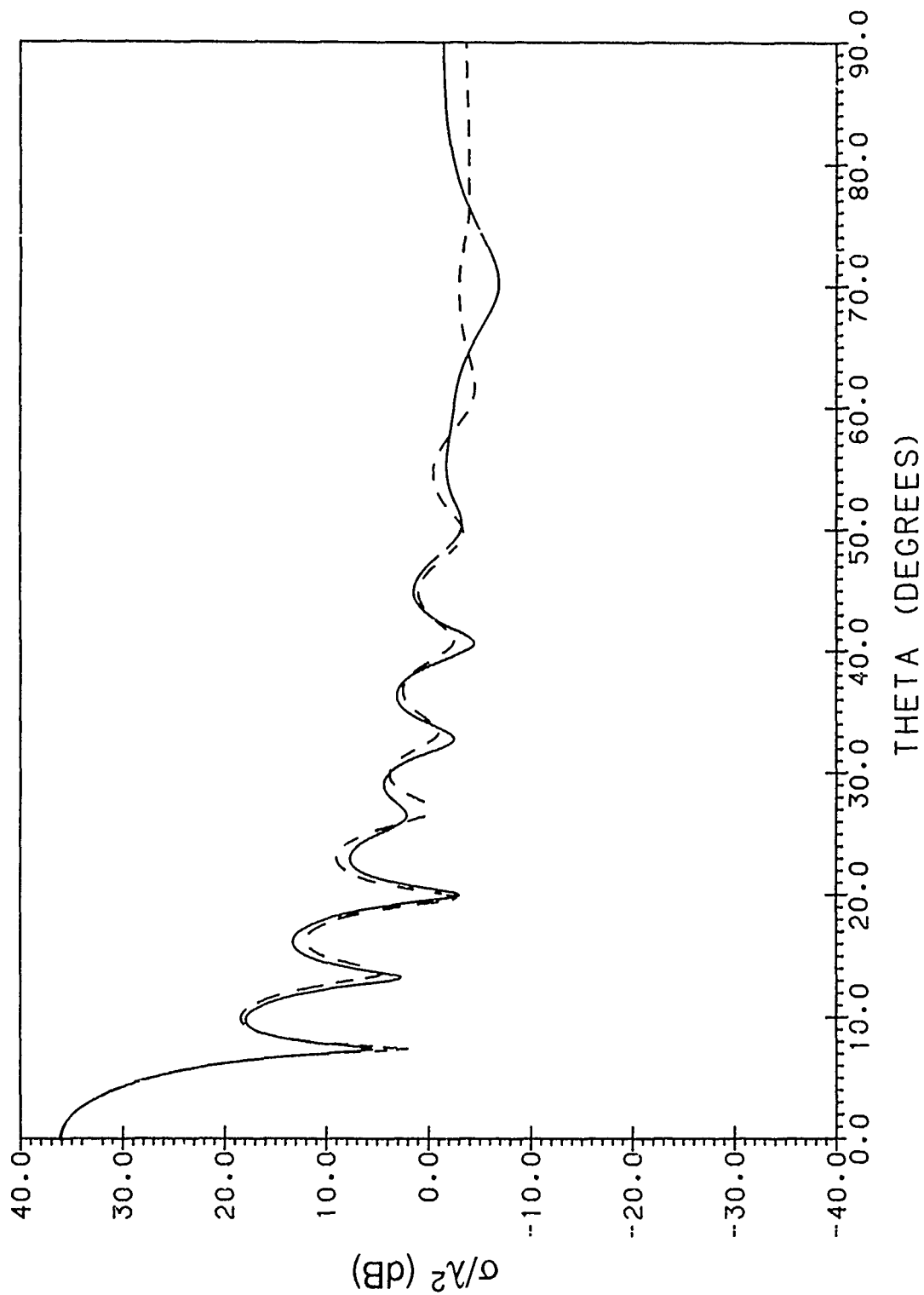


Figure 16b. Back Scatter Cross Section Pattern of Disk,  $ka = 15$ , with Perpendicular Polarized Plane-Wave Illumination and Incremental Strips in Direction of Diffracted Rays; — : Exact, - - - : PO + Approximate Nonuniform Current Field Obtained by Integrating IDC



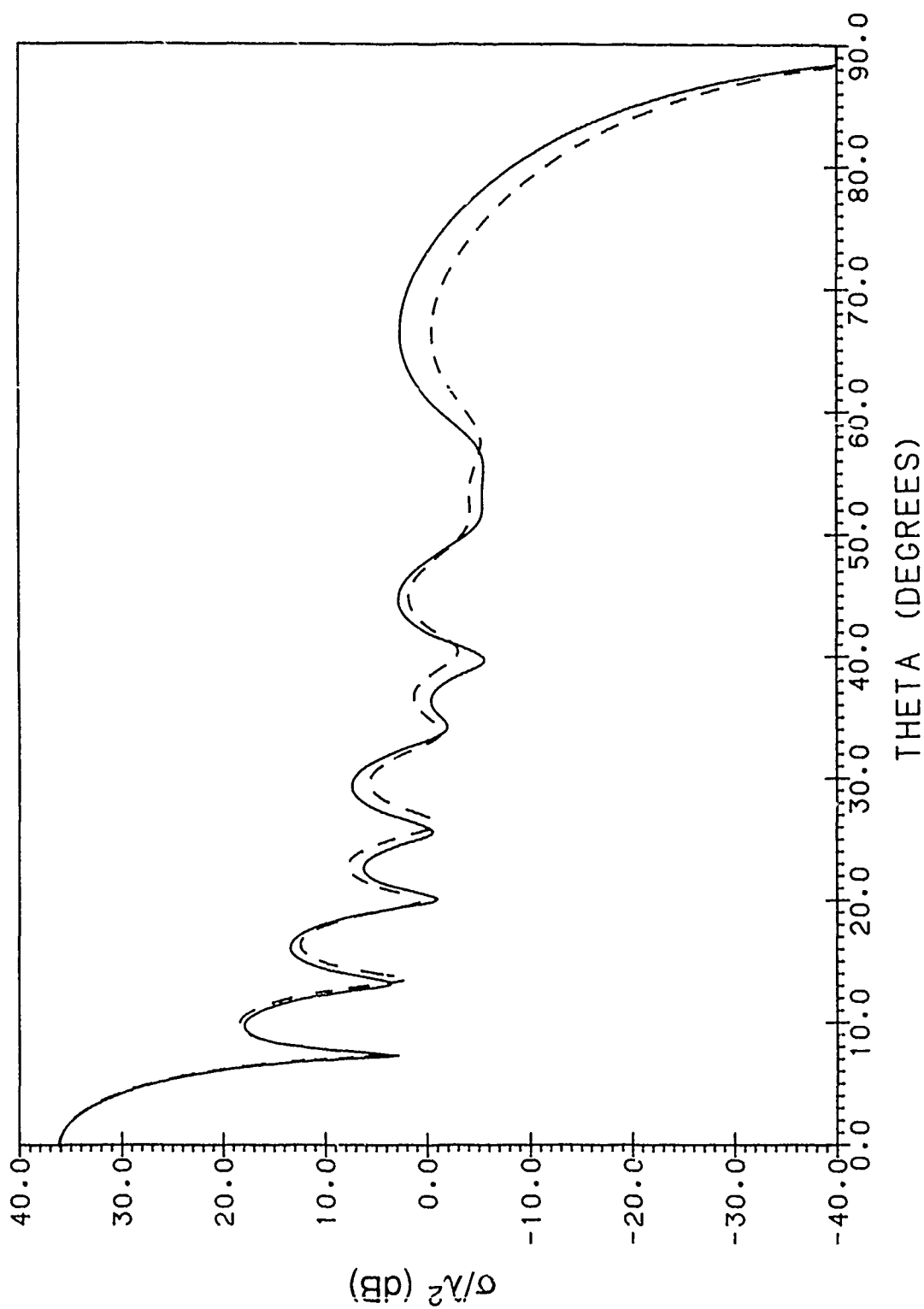


Figure 17a. Back Scatter Cross Section Pattern of Disk,  $ka = 15$ , with Parallel Polarized Plane-Wave Illumination and Incremental Strips Parallel to x-Axis; ———: Exact, - - - - - : PO + Approximate Nonuniform Current Field Obtained by Integrating IDC

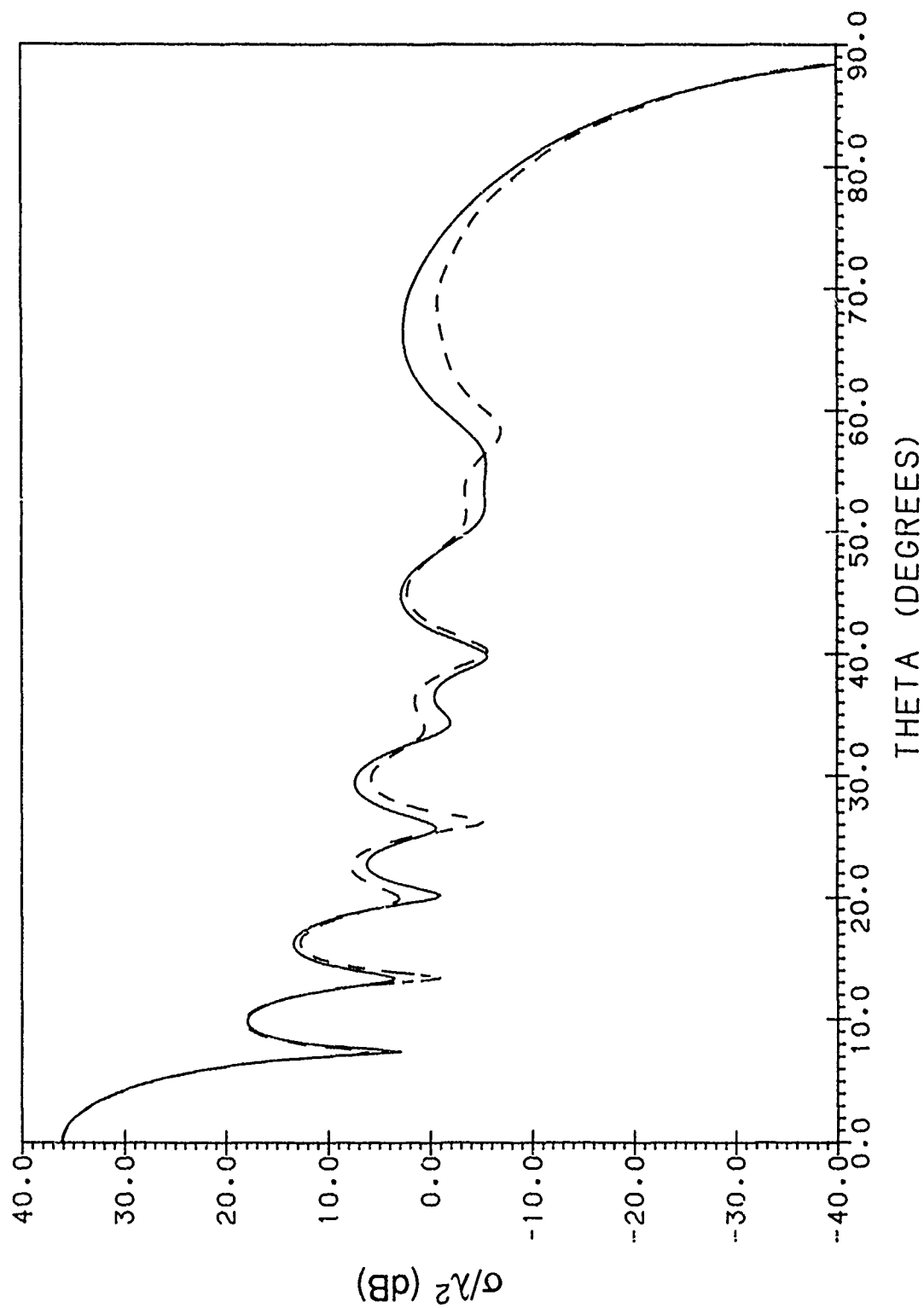


Figure 17b. Back Scatter Cross Section Pattern of Disk,  $ka = 15$ , with Parallel Polarized Plane-Wave Illumination and Incremental Strips in Direction of Diffracted Rays; —: Exact, ----: PO + Approximate Nonuniform Current Field Obtained by Integrating IDC

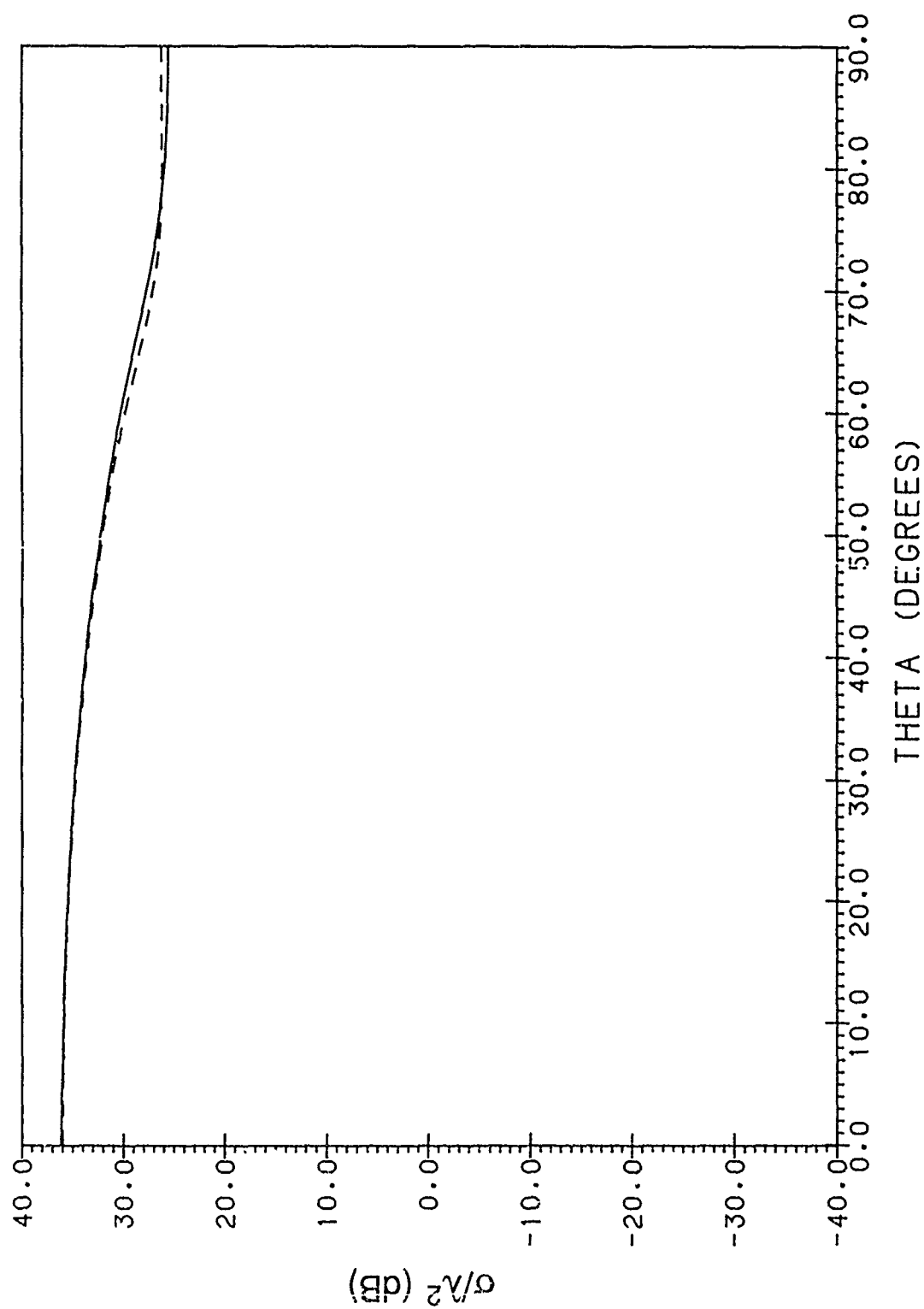


Figure 18a. Specular Scatter Cross Section Pattern of Disk,  $ka = 15$ , with Perpendicular Polarized Plane-Wave Illumination and Incremental Strips Parallel to x-Axis; —: Exact, ----: PO + Approximate Nonuniform Current Field Obtained by Integrating IDC

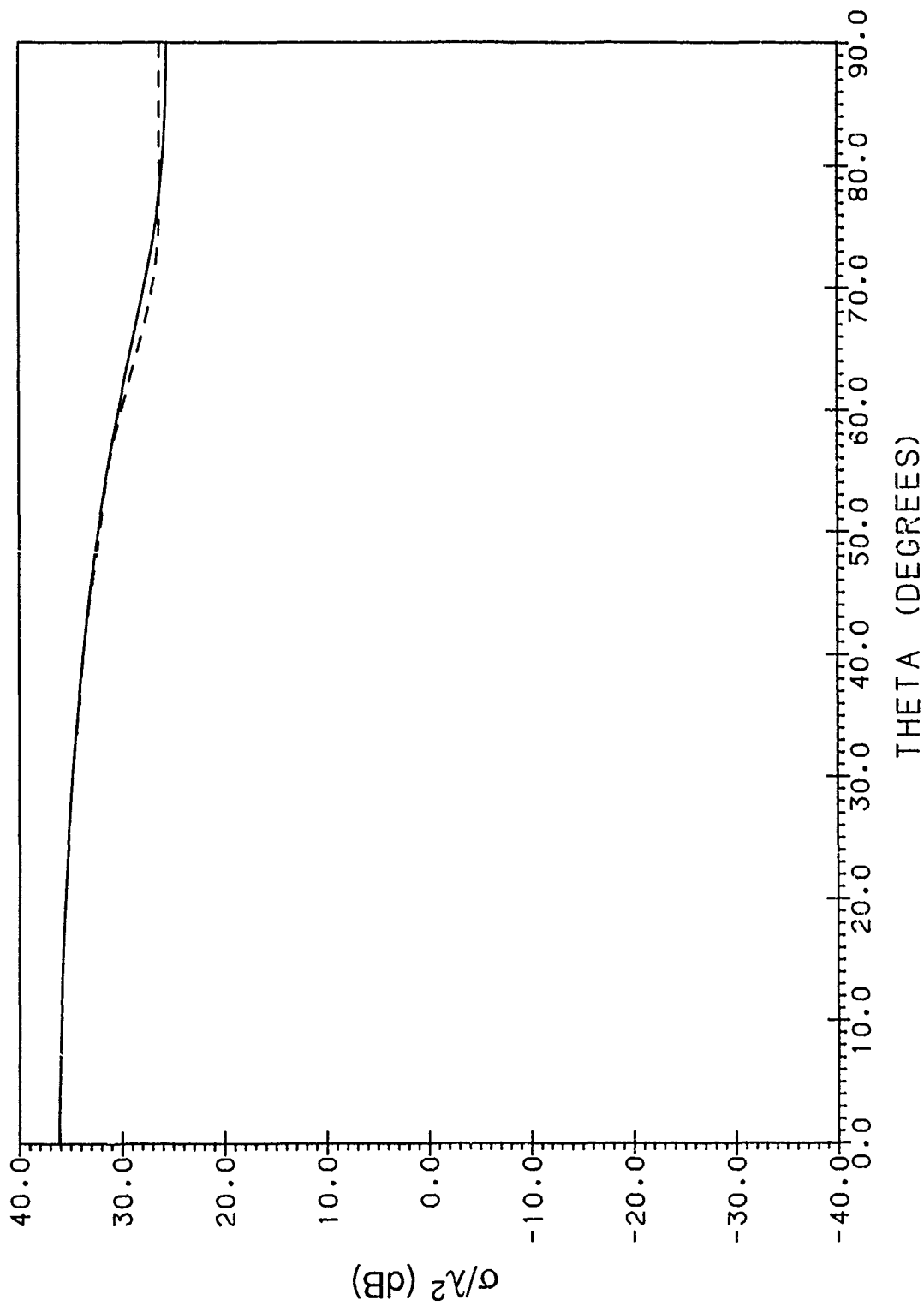


Figure 18b. Specular Scatter Cross Section Pattern of Disk,  $ka = 15$ , with Perpendicular Polarized Plane-Wave Illumination and Incremental Strips in Direction of Diffracted Rays; —: Exact, - - - - : PO + Approximate Nonuniform Current Field Obtained by Integrating IDC

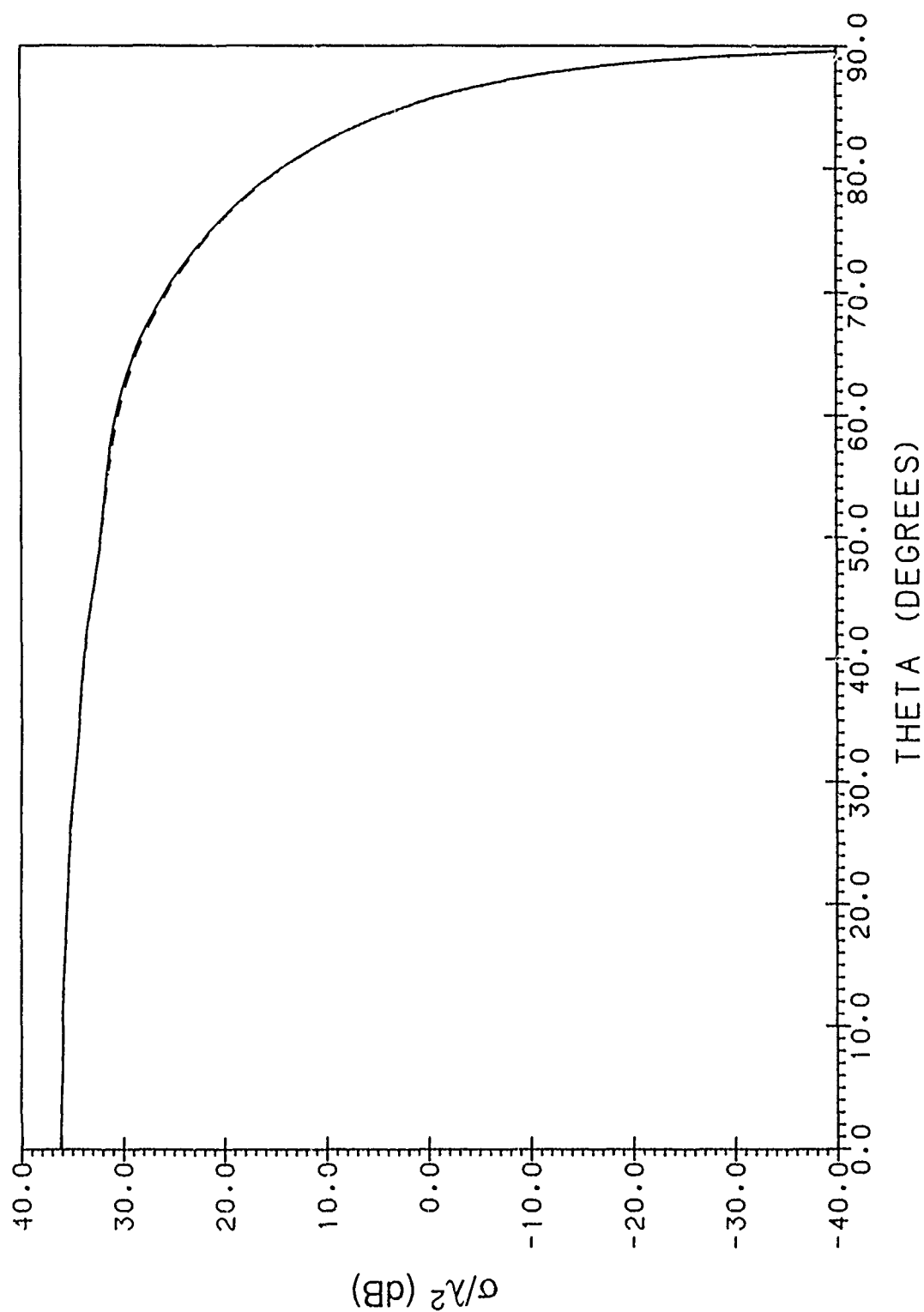


Figure 19a. Specular Scatter Cross Section Pattern of Disk,  $ka = 15$ , with Parallel Polarized Plane-Wave Illumination and Incremental Strips Parallel to x-Axis; — : Exact, - - - : PO + Approximate Nonuniform Current Field Obtained by Integrating IDC

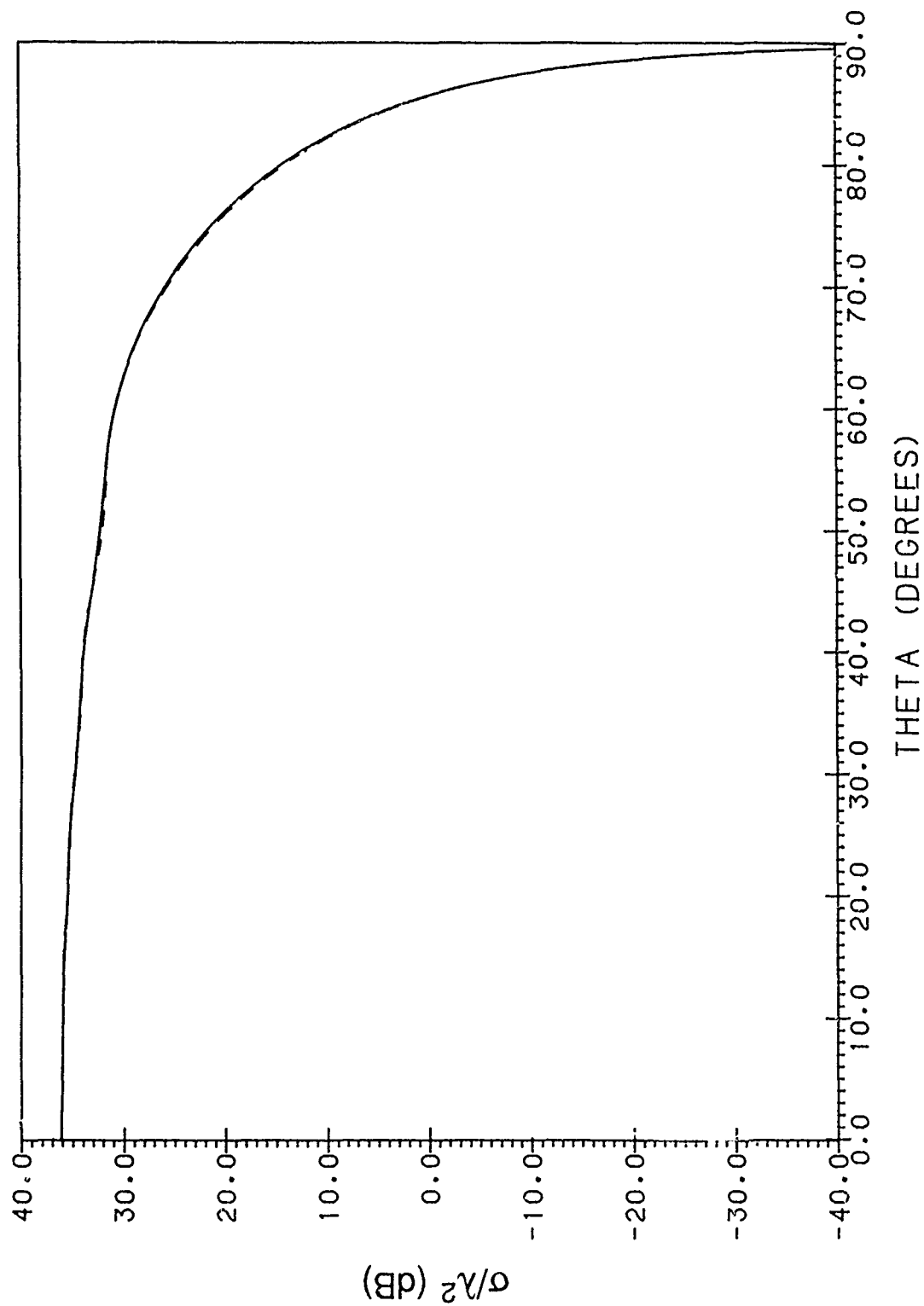


Figure 19b. Specular Scatter Cross Section Pattern of Disk,  $ka = 15$ , with Parallel Polarized Plane-Wave Illumination and Incremental Strips in Direction of Diffracted Rays; —: Exact, ----: PO + Approximate Nonuniform Current Field Obtained by Integrating IDC

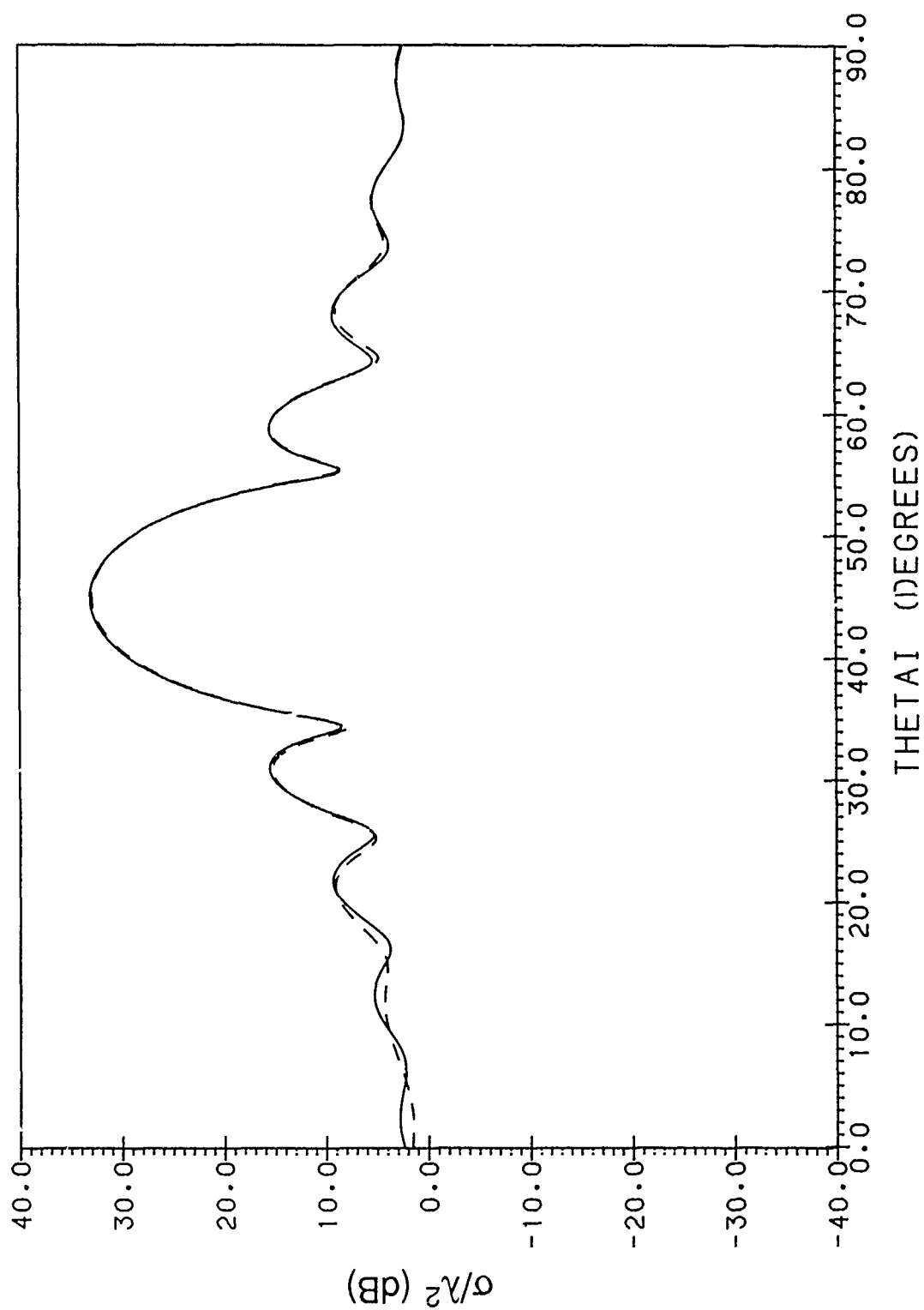


Figure 20a. Side Scatter Cross Section Pattern of Disk,  $ka = 15$ , with Perpendicular Polarized Plane-Wave Illumination and Incremental Strips Parallel to x-Axis; —: Exact, ----: PO + Approximate Nonuniform Current Field Obtained by Integrating IDC

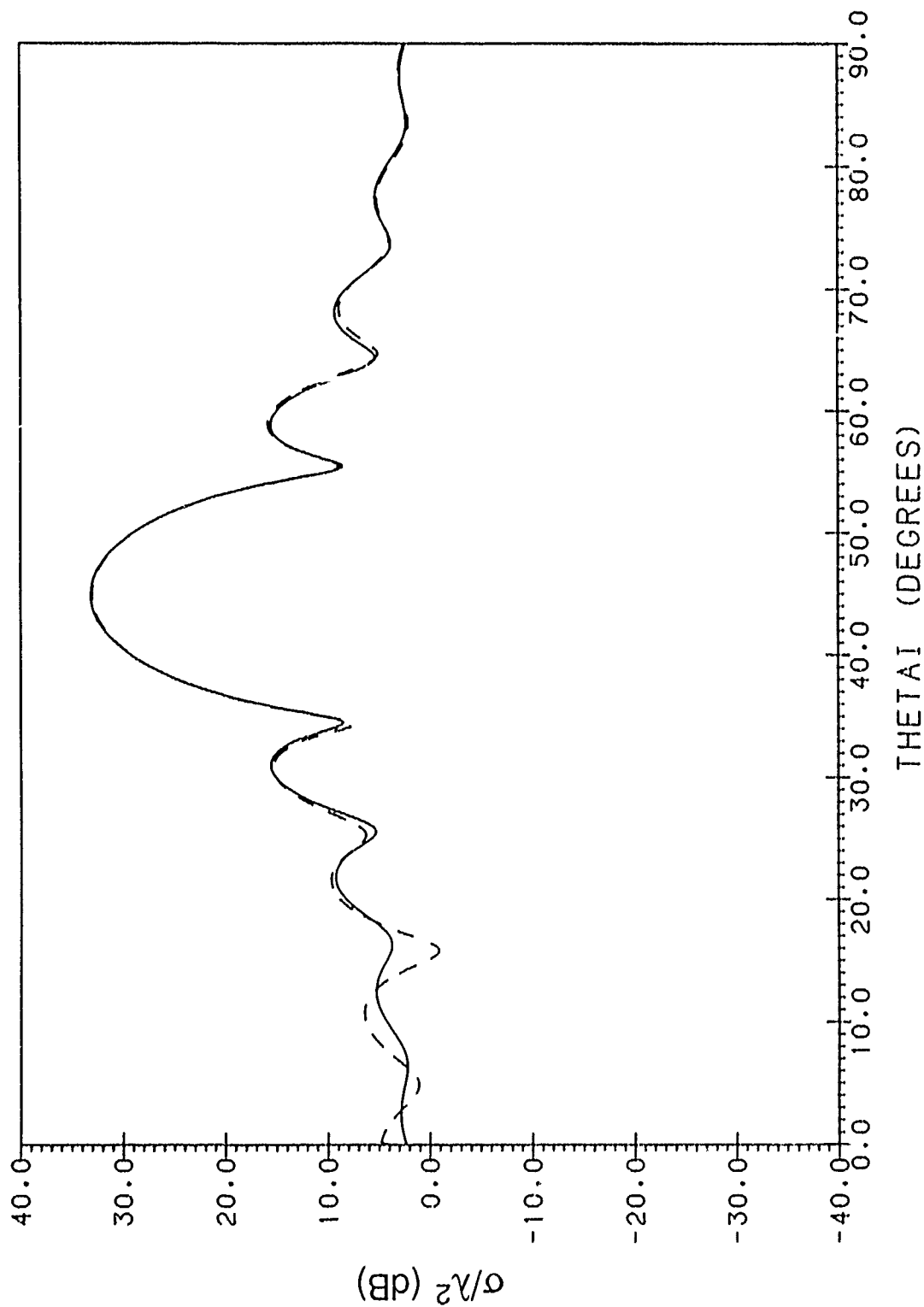


Figure 20b. Side Scatter Cross Section Pattern of Disk,  $ka = 15$ , with Perpendicular Polarized Plane-Wave Illumination and Incremental Strips in Direction of Diffracted Rays: — : Exact, - - - : PO + Approximate Nonuniform Current Field Obtained by Integrating IDC



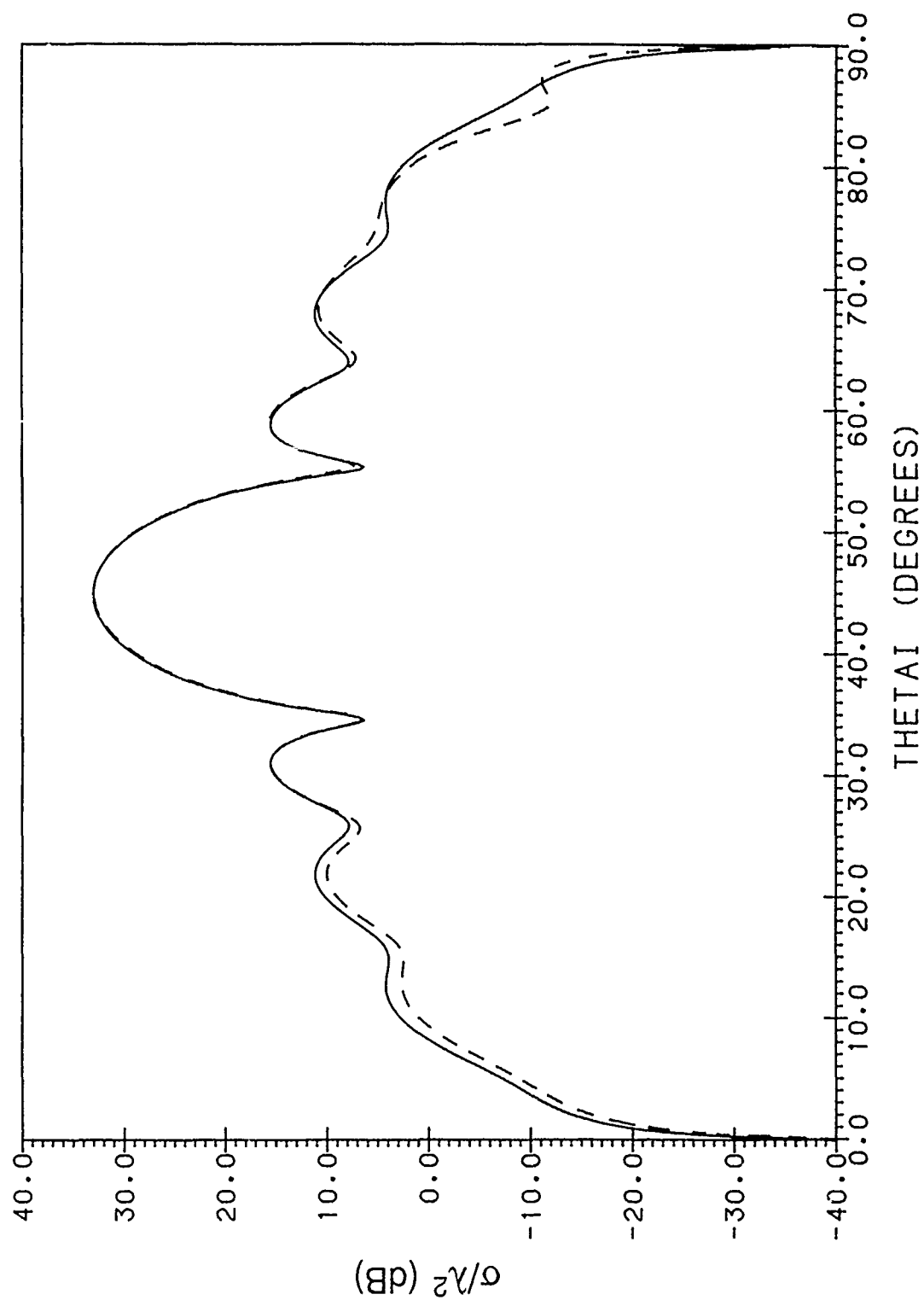


Figure 21a. Side Scatter Cross Section Pattern of Disk,  $ka = 15$ , with Parallel Polarized Plane-Wave Illumination and Incremental Strips Parallel to x-Axis; ———: Exact, - - - - - : PO + Approximate Nonuniform Current Field Obtained by Integrating IDC

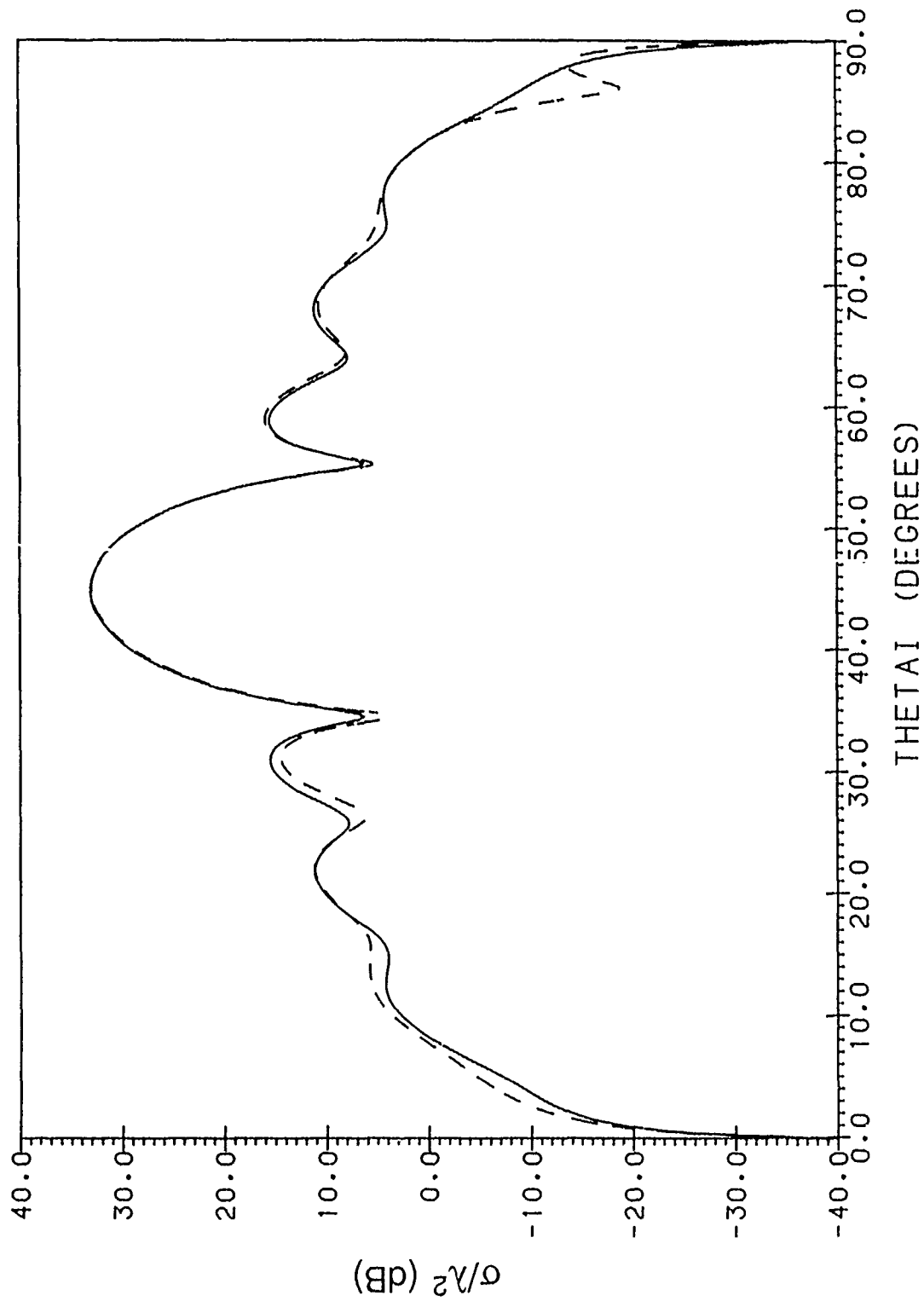


Figure 21b. Side Scatter Cross Section Pattern of Disk,  $ka = 15$ , with Parallel Polarized Plane-Wave Illumination and Incremental Strips in Direction of Diffracted Rays: —: Exact, - - - - -: PO + Approximate Nonuniform Current Field Obtained by Integrating IDC

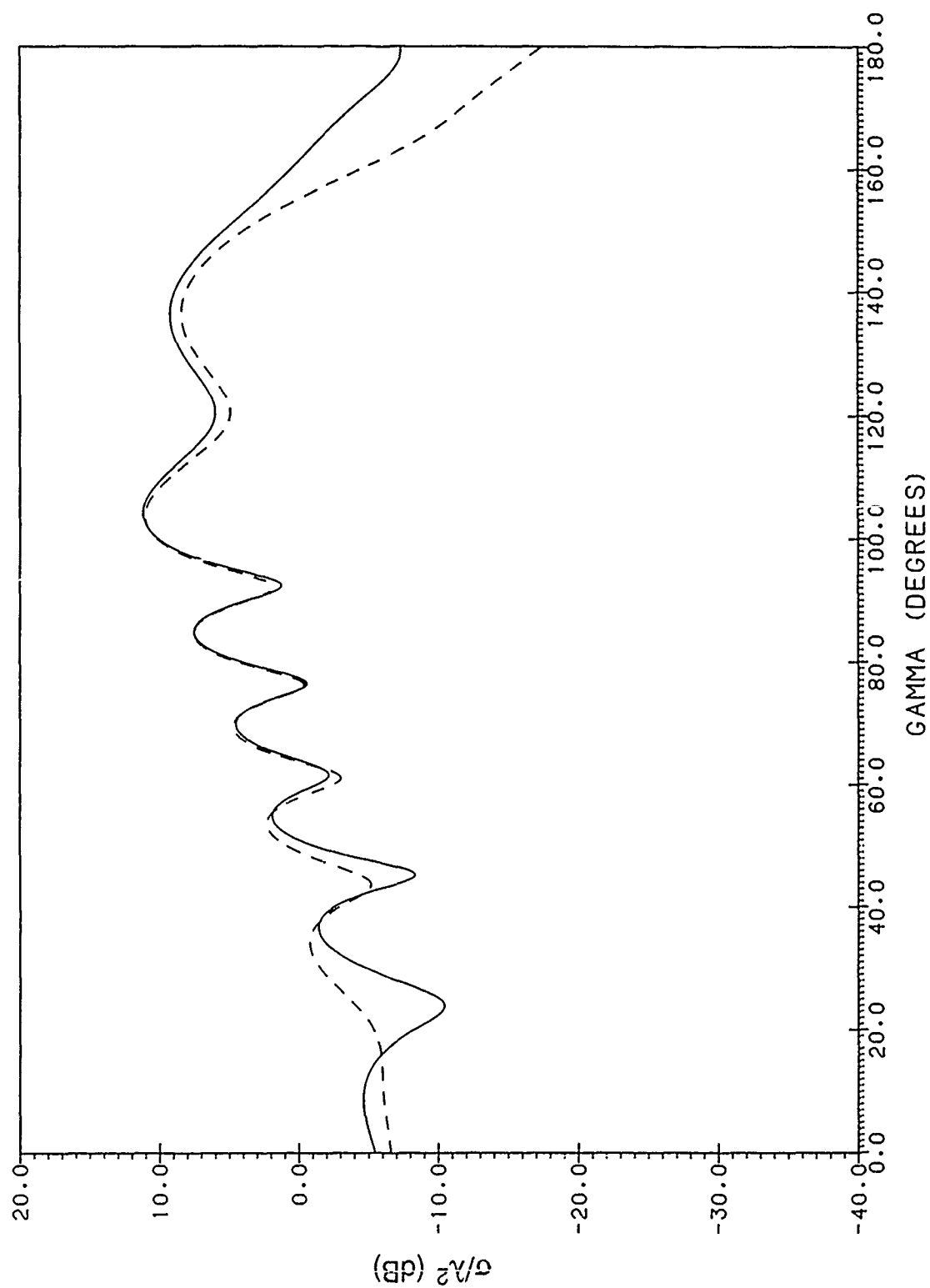


Figure 22a. Co-Polarized Cross Section Pattern of Disk,  $ka = 15$ , Illuminated by Perpendicular Polarized Plane Wave at  $\theta_i = 45^\circ$  in Plane Defined by  $\phi = 45^\circ$  and  $\phi = 225^\circ$ , with Incremental Strips Parallel to x-Axis; —: Exact, - - - - : PO + Approximate Nonuniform Current Field Obtained by Integrating IDC

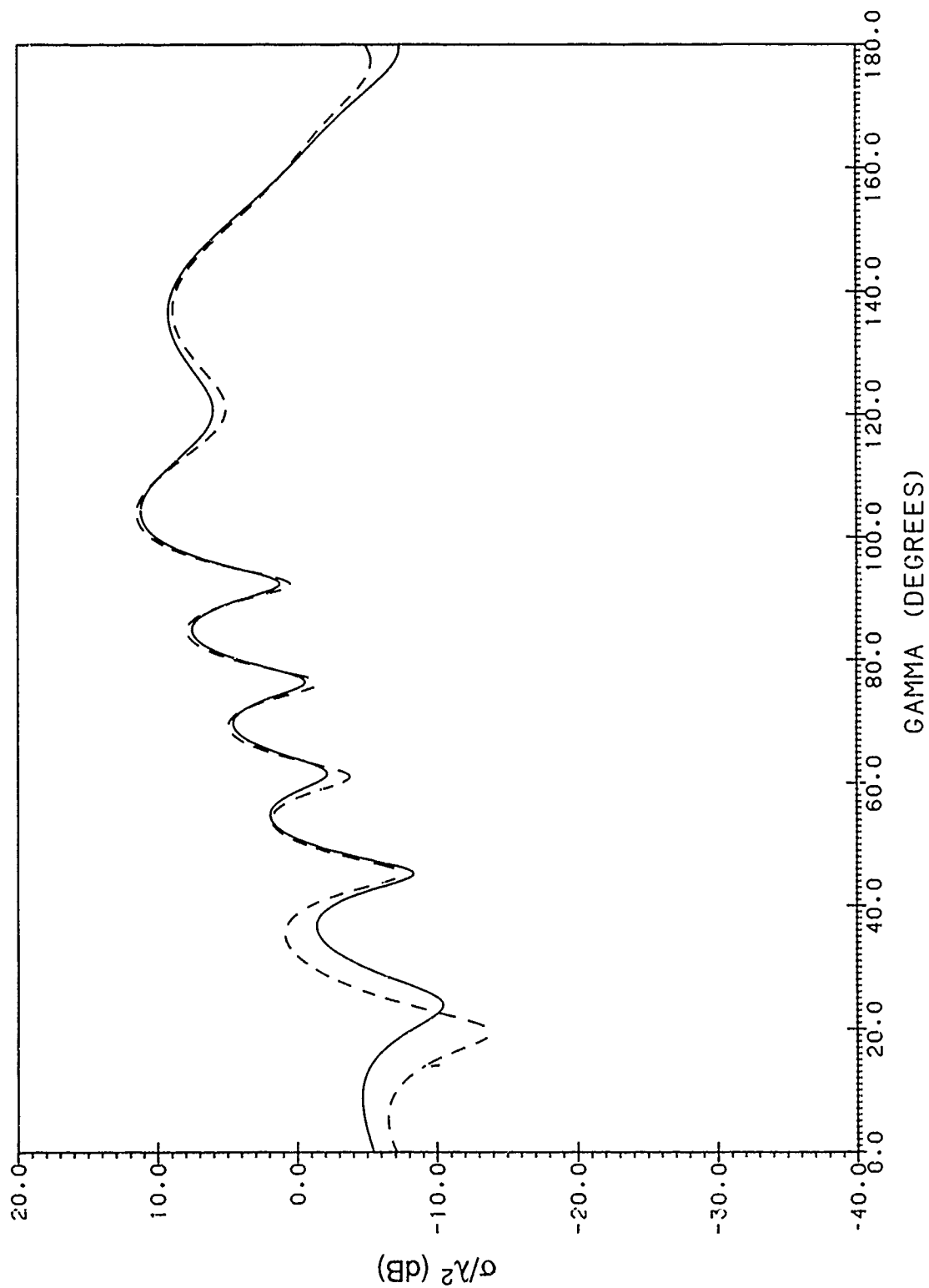


Figure 22b. Co-Polarized Cross Section Pattern of Disk,  $ka = 15$ , Illuminated by Perpendicular Polarized Plane Wave at  $\theta_i = 45^\circ$  in Plane Defined by  $\phi = 45^\circ$  and  $\phi = 225^\circ$ , with Incremental Strips in Direction of Diffracted Rays: ———: Exact, - - - - - : PO + Approximate Nonuniform Current Field Obtained by Integrating IDC

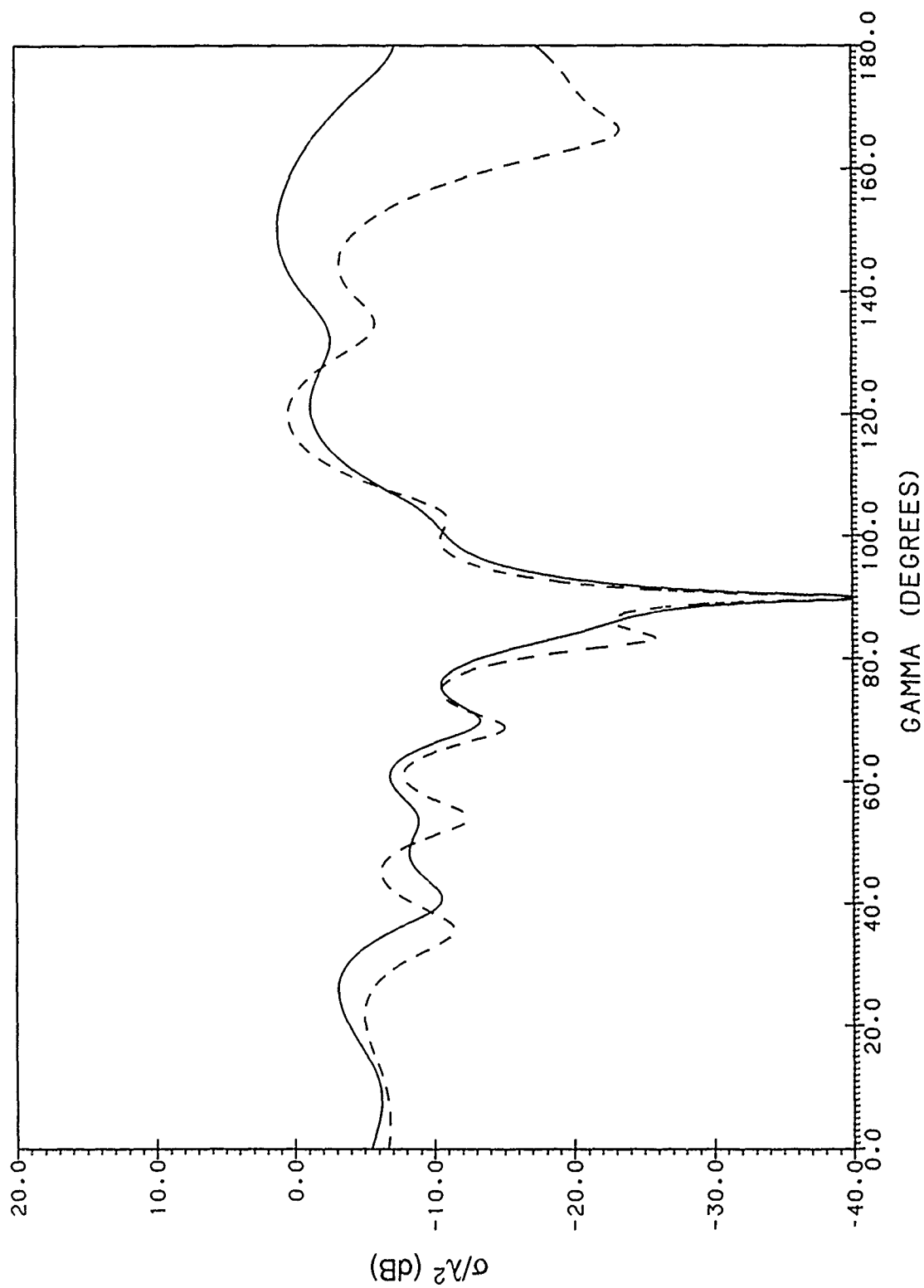


Figure 23a. Cross-Polarized Cross Section Pattern of Disk,  $ka = 15$ , Illuminated by Perpendicular Polarized Plane Wave at  $\theta_i = 45^\circ$  in Plane Defined by  $\phi = 45^\circ$  and  $\phi = 225^\circ$ , with Incremental Strips Parallel to x-Axis; —: Exact, - - - - -: PO + Approximate Nonuniform Current Field Obtained by Integrating IDC

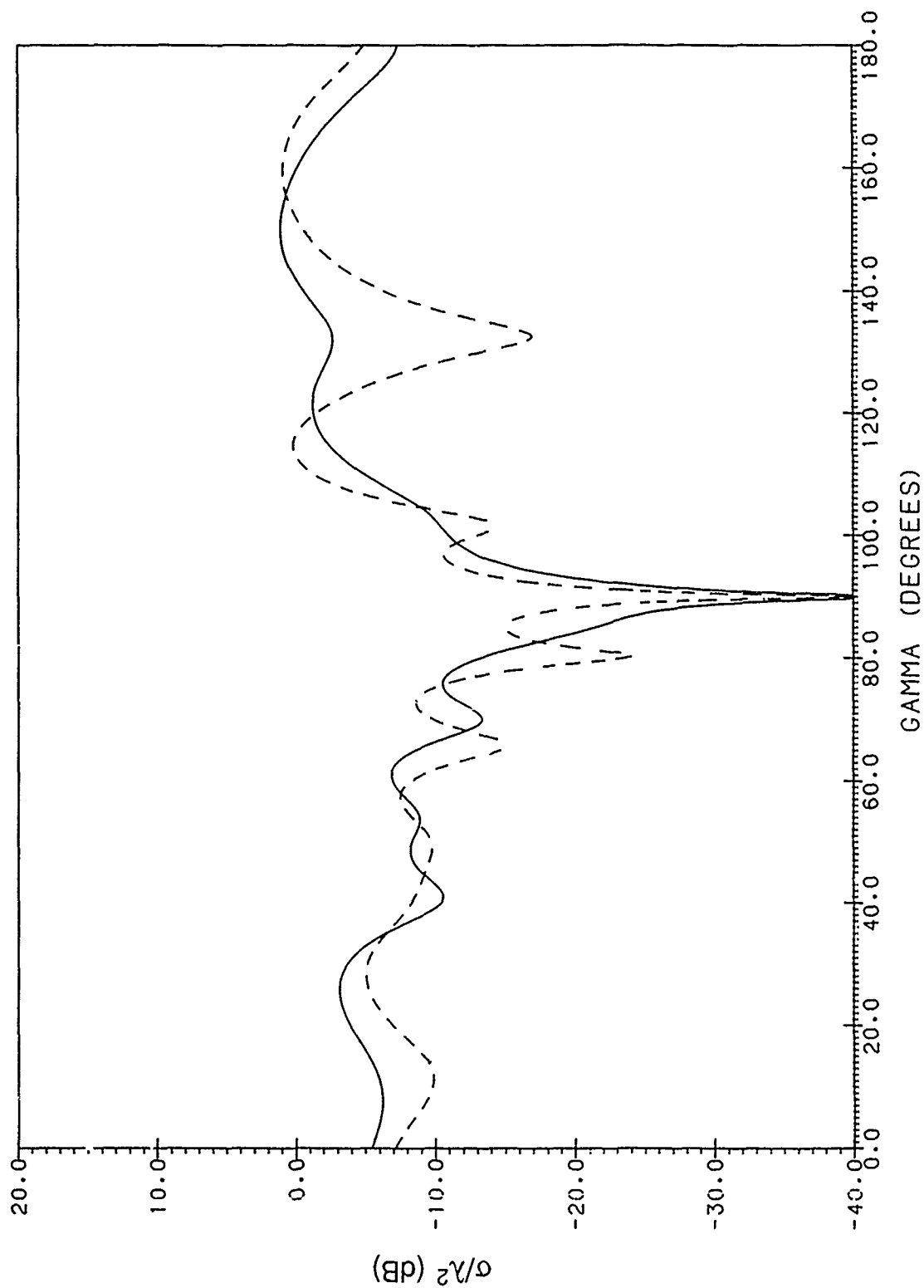


Figure 23b. Cross-Polarized Cross Section Pattern of Disk,  $ka = 15$ , Illuminated by Perpendicular Polarized Plane Wave at  $\theta_i = 45^\circ$  in Plane Defined by  $\phi = 45^\circ$  and  $\phi = 225^\circ$ , with Incremental Strips in Direction of Diffracted Rays; — : Exact, - - - : PO + Approximate Nonuniform Current Field Obtained by Integrating IDC

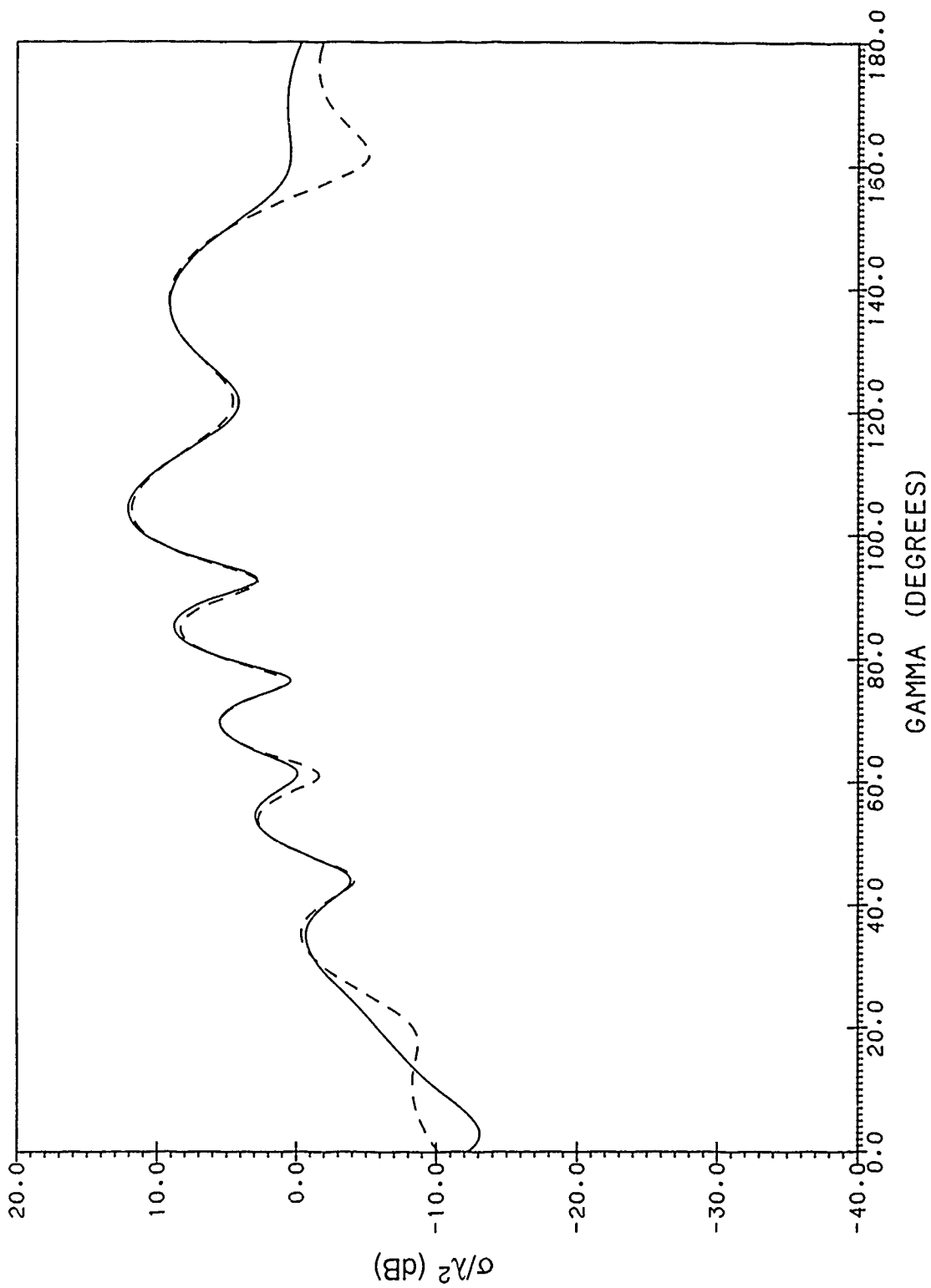


Figure 24a. Co-Polarized Cross Section Pattern of Disk,  $ka = 15$ , Illuminated by Parallel Polarized Plane Wave at  $\theta_i = 45^\circ$  in Plane Defined by  $\phi = 45^\circ$  and  $\phi = 225^\circ$ , with Incremental Strips Parallel to x-Axis; ———: Exact, - - - - - : PO + Approximate Nonuniform Current Field Obtained by Integrating IDC

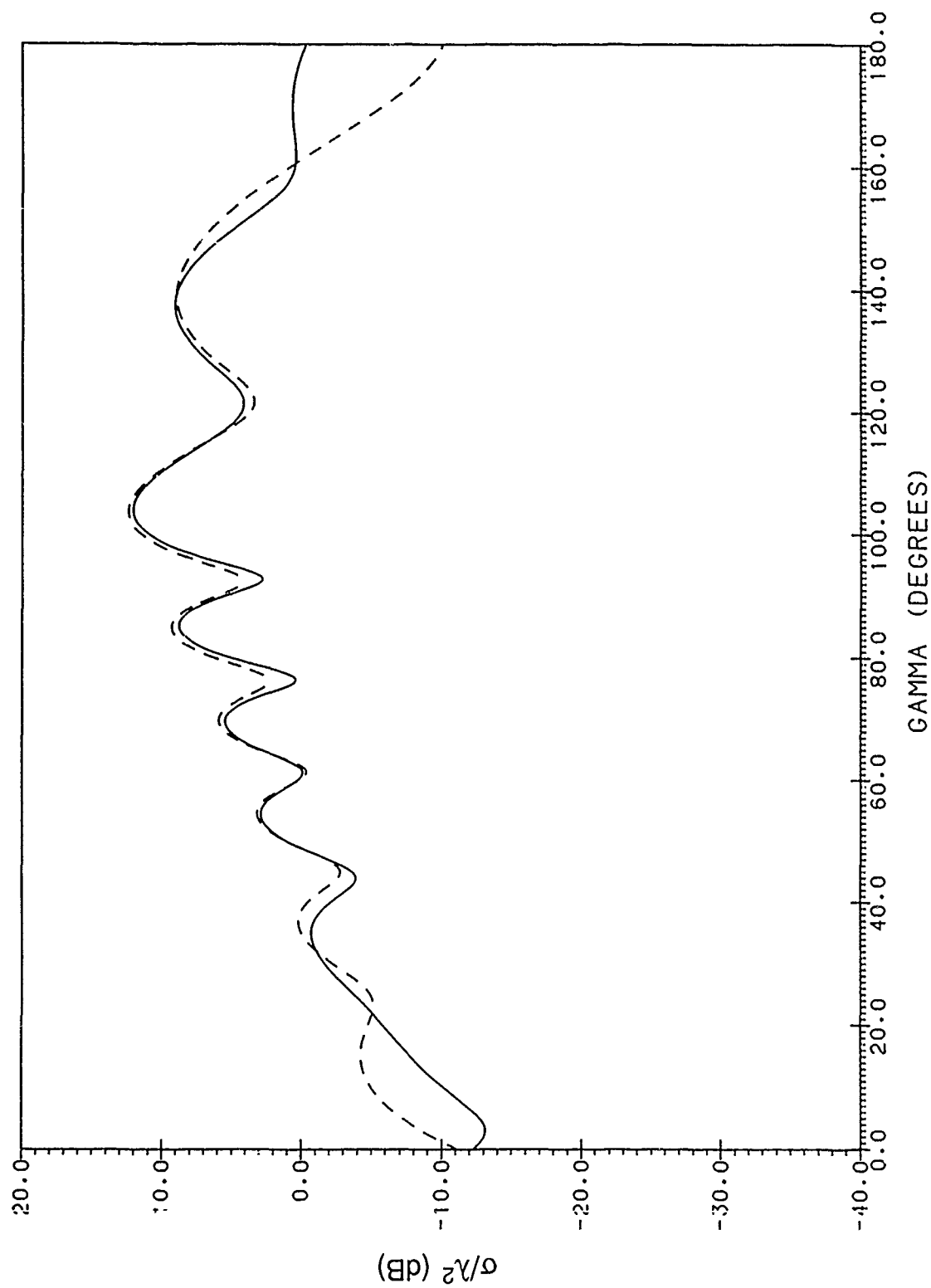


Figure 24b. Co-Polarized Cross Section Pattern of Disk,  $ka = 15$ , Illuminated by Parallel Polarized Plane Wave at  $\theta_i = 45^\circ$  in Plane Defined by  $\phi = 45^\circ$  and  $\phi = 225^\circ$ , with Incremental Strips in Direction of Diffracted Rays; —: Exact, - - - - -: PO + Approximate Nonuniform Current Field Obtained by Integrating IDC



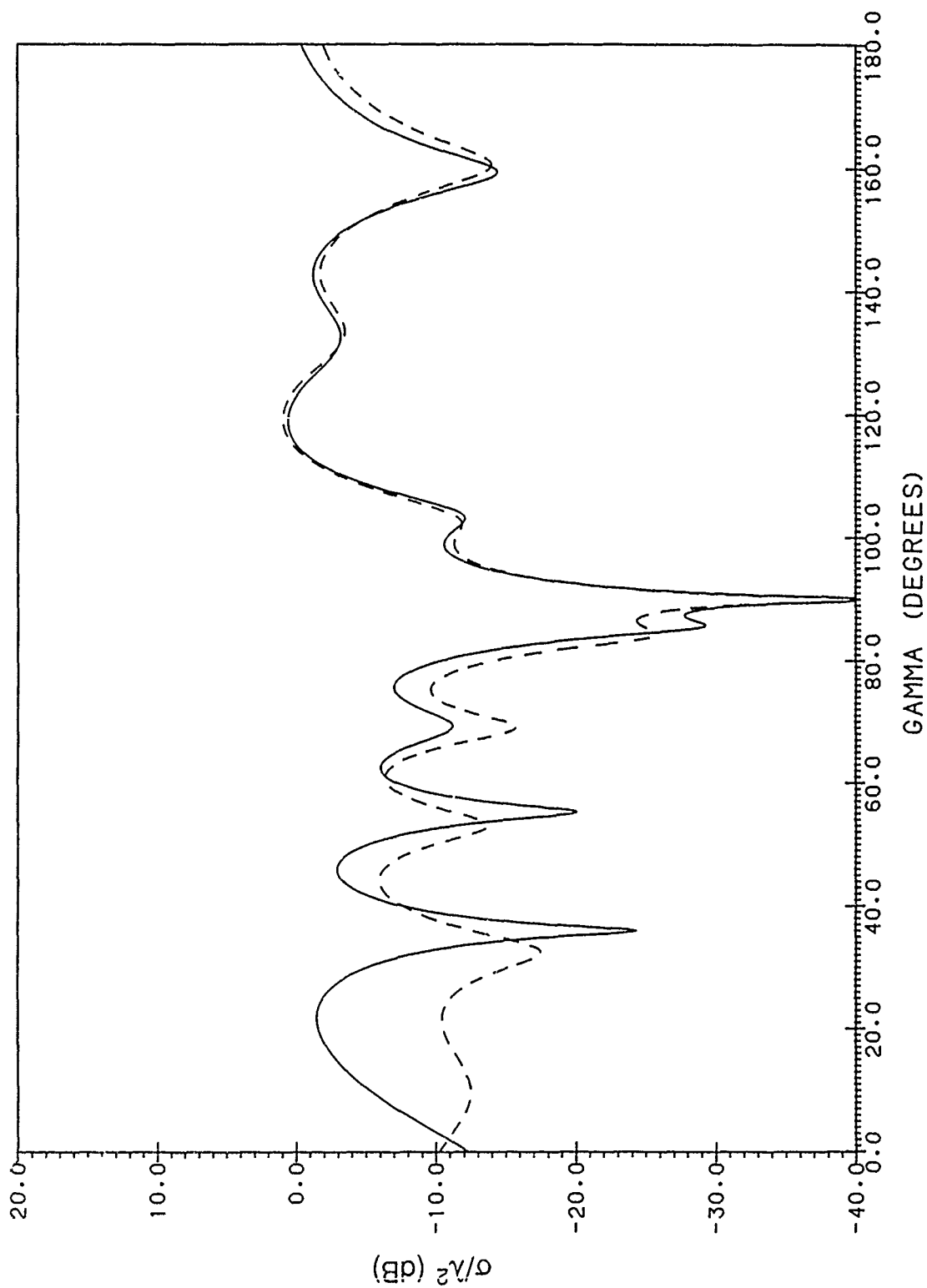


Figure 25a. Cross-Polarized Cross Section Pattern of Disk,  $ka = 15$ , Illuminated by Parallel Polarized Plane Wave at  $\theta_i = 45^\circ$  in Plane Defined by  $\phi = 45^\circ$  and  $\phi = 225^\circ$ , with Incremental Strips Parallel to x-Axis: — : Exact, - - - - : PO + Approximate Nonuniform Current Field Obtained by Integrating IDC

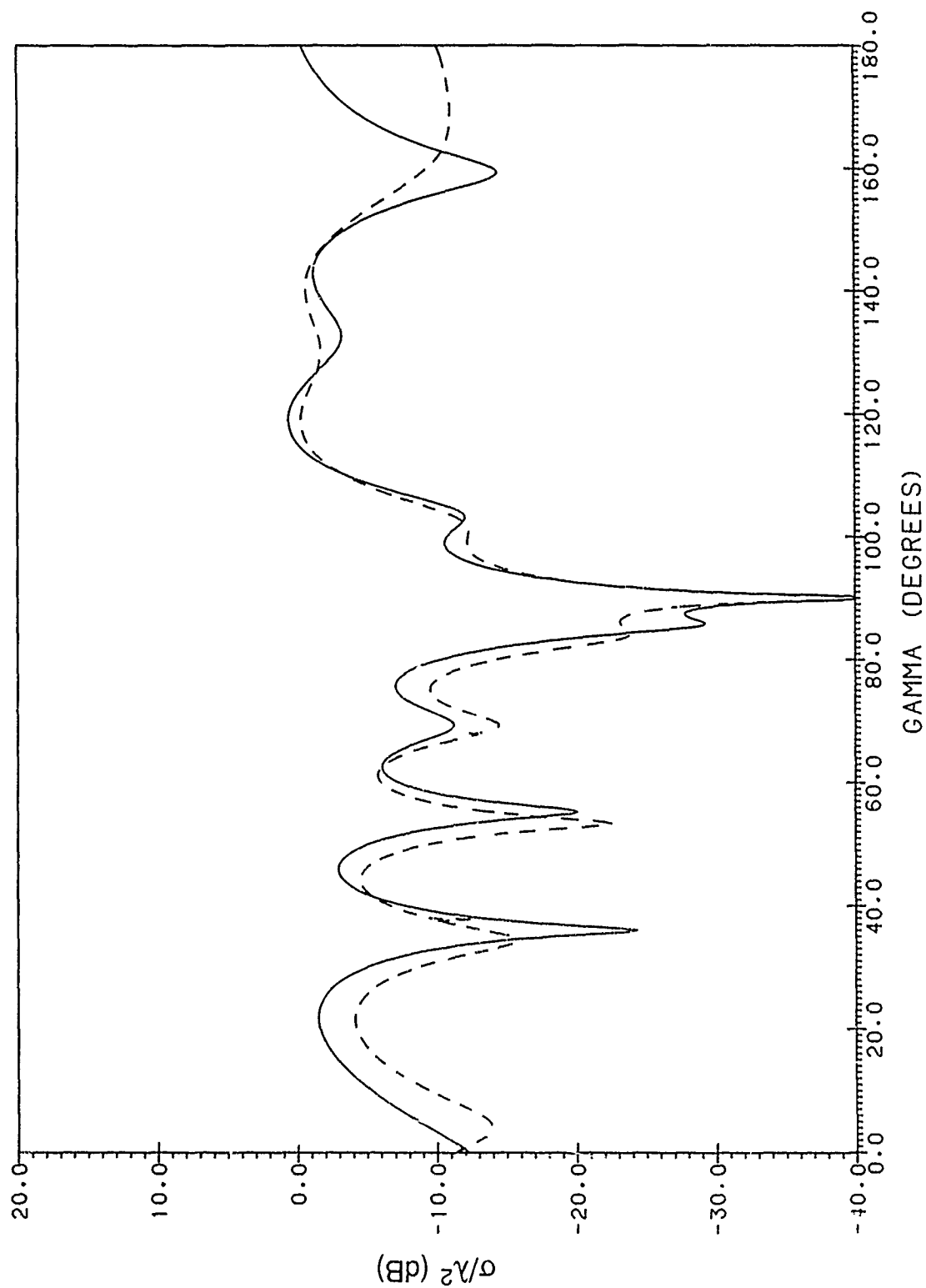


Figure 25b. Cross-Polarized Cross Section Pattern of Disk,  $ka = 15$ , Illuminated by Parallel Polarized Plane Wave at  $\theta_i = 45^\circ$  in Plane Defined by  $\phi = 45^\circ$  and  $\phi = 225^\circ$ , with Incremental Strips in Direction of Diffracted Rays; —: Exact, ----: PO + Approximate Nonuniform Current Field Obtained by Integrating IDC

these  $45^\circ$  patterns are caused by significant secondary diffraction between the leading and trailing edges that is not accurately accounted for away from grazing incident by the incremental strip approximation for the current on this disk of fairly small radius  $a = 15/2\pi \lambda \approx 2.4\lambda$ . This discrepancy diminishes for electrically larger disks. (See Appendix C.)

As with the strip, it is of interest to see the limitations of the PO approximation for the disk bistatic cross sections. In Figures 26a and b, 27a and b, and 28a and b, we compare the PO (-----) and exact (——) back scatter, specular scatter, and side scatter cross section patterns for perpendicular and parallel polarization of the illuminating plane wave. Figures 29a and b compare the co- and cross-polarized PO and exact patterns in the plane defined by  $\phi = 45^\circ$  and  $\psi = 225^\circ$  for a perpendicular polarized plane wave incident on the disk at an angle of  $\theta_i = 45^\circ$ . Figures 30a and b show the corresponding patterns for parallel polarization of the incident plane wave. It is apparent from these figures that the PO approximation does not, in general, give an accurate representation of the bistatic cross section patterns, especially in the vicinity of pattern minima. This, of course, serves to emphasize the importance of accounting for the nonuniform current field in calculating radar cross sections of objects with edge discontinuities.

To see how the accuracy of our approximation depends on the disk size, in Figures 31a and b, 32a and b, and 33a and b, we show the perpendicular and parallel polarization back scatter, specular scatter, and side scatter patterns for a disk of size  $ka = 1.5$ . For these patterns the incremental strips have been taken parallel to the x-axis. Although there are differences of a few dB between the exact and IDC solutions over much of the range of  $\theta$ , the pattern shapes are surprisingly accurate for this small disk of diameter less than one-half a wavelength.

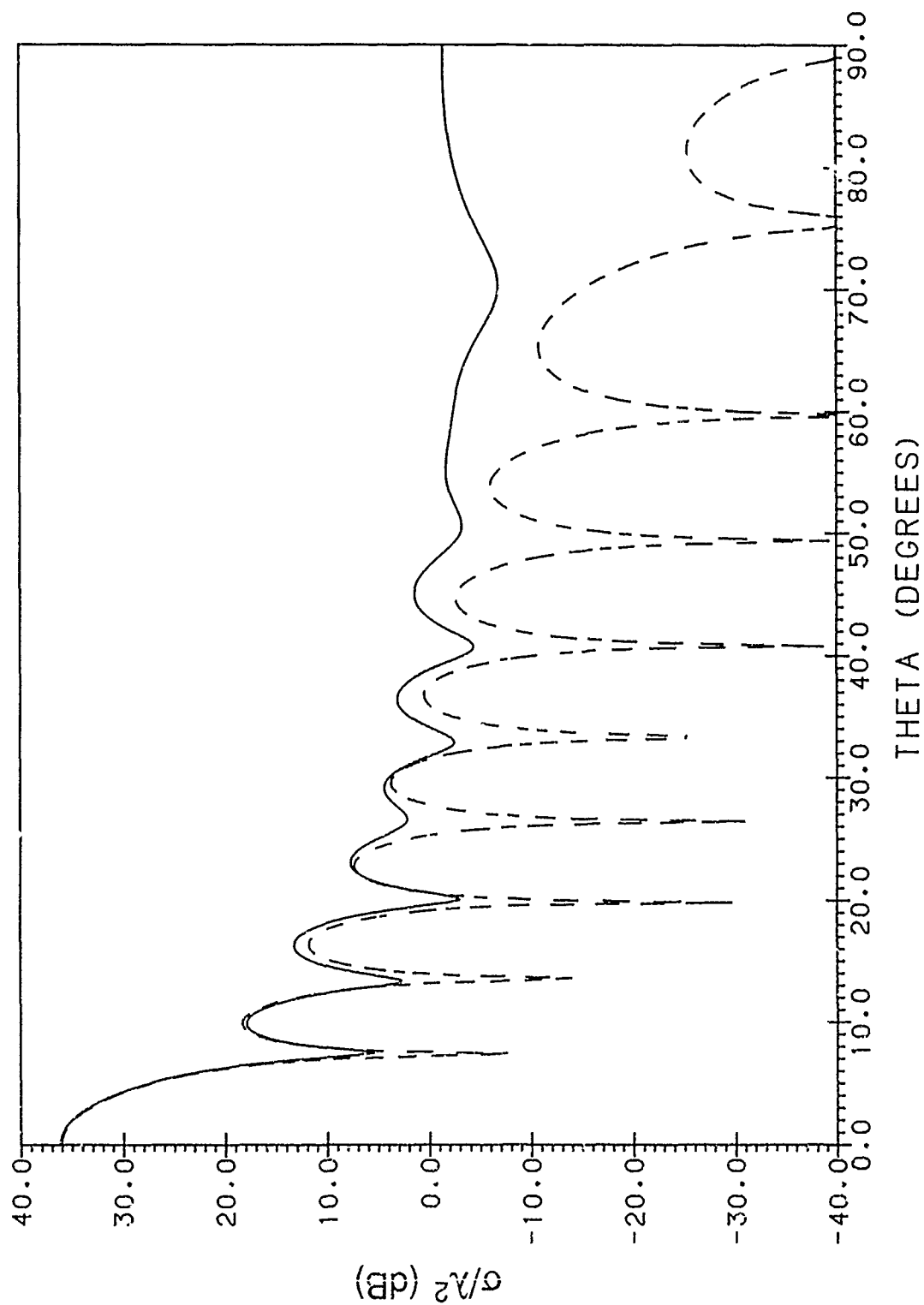


Figure 26a. Back Scatter Cross Section Pattern of Disk,  $ka = 15$ , with Perpendicular Polarized Plane-Wave Illumination;  
 —: Exact, ----: PO

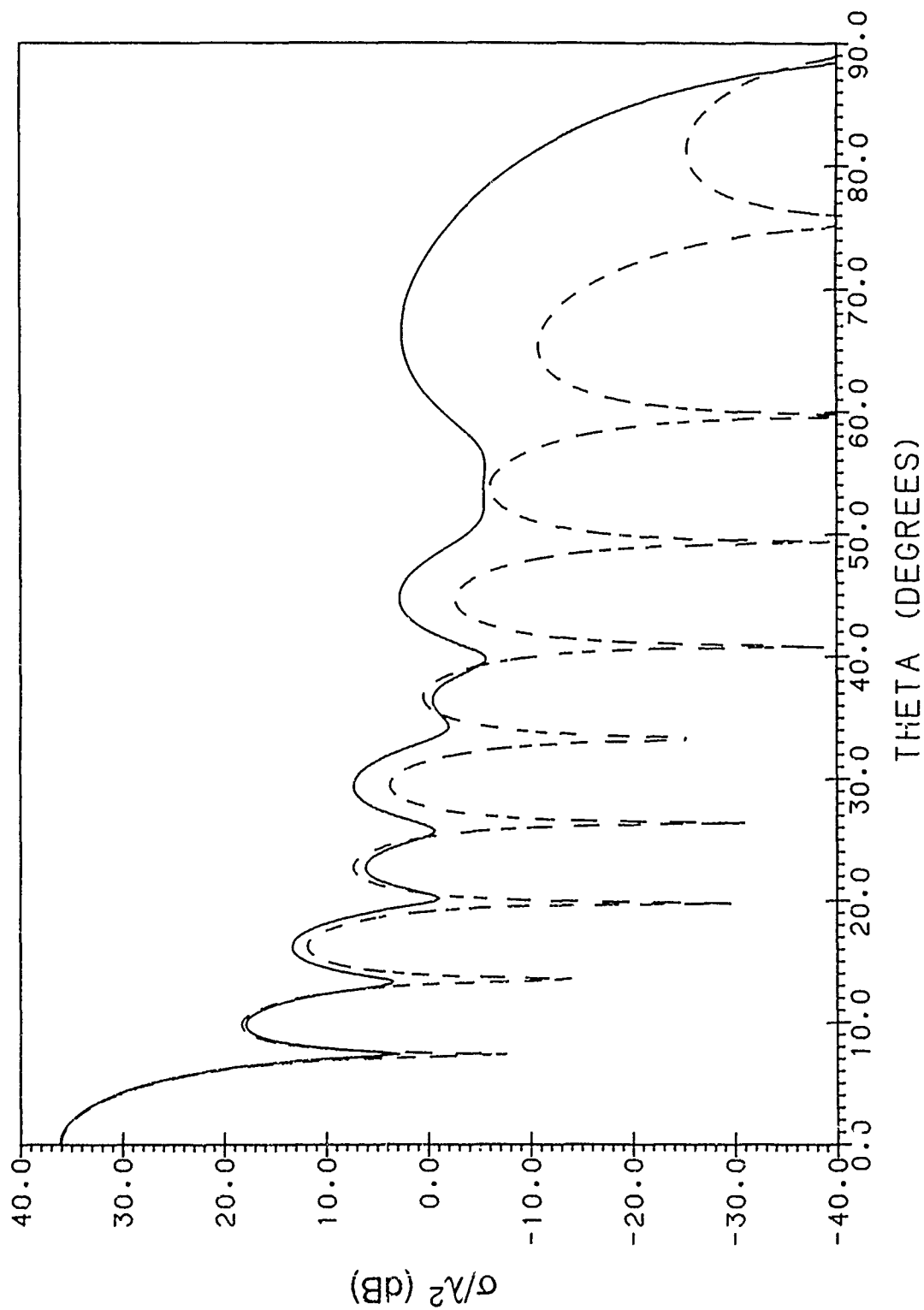


Figure 26b. Back Scatter Cross Section Pattern of Disk,  $ka = 15$ , with Parallel Polarized Plane-Wave Illumination;  
 — : Exact, - - - : PO

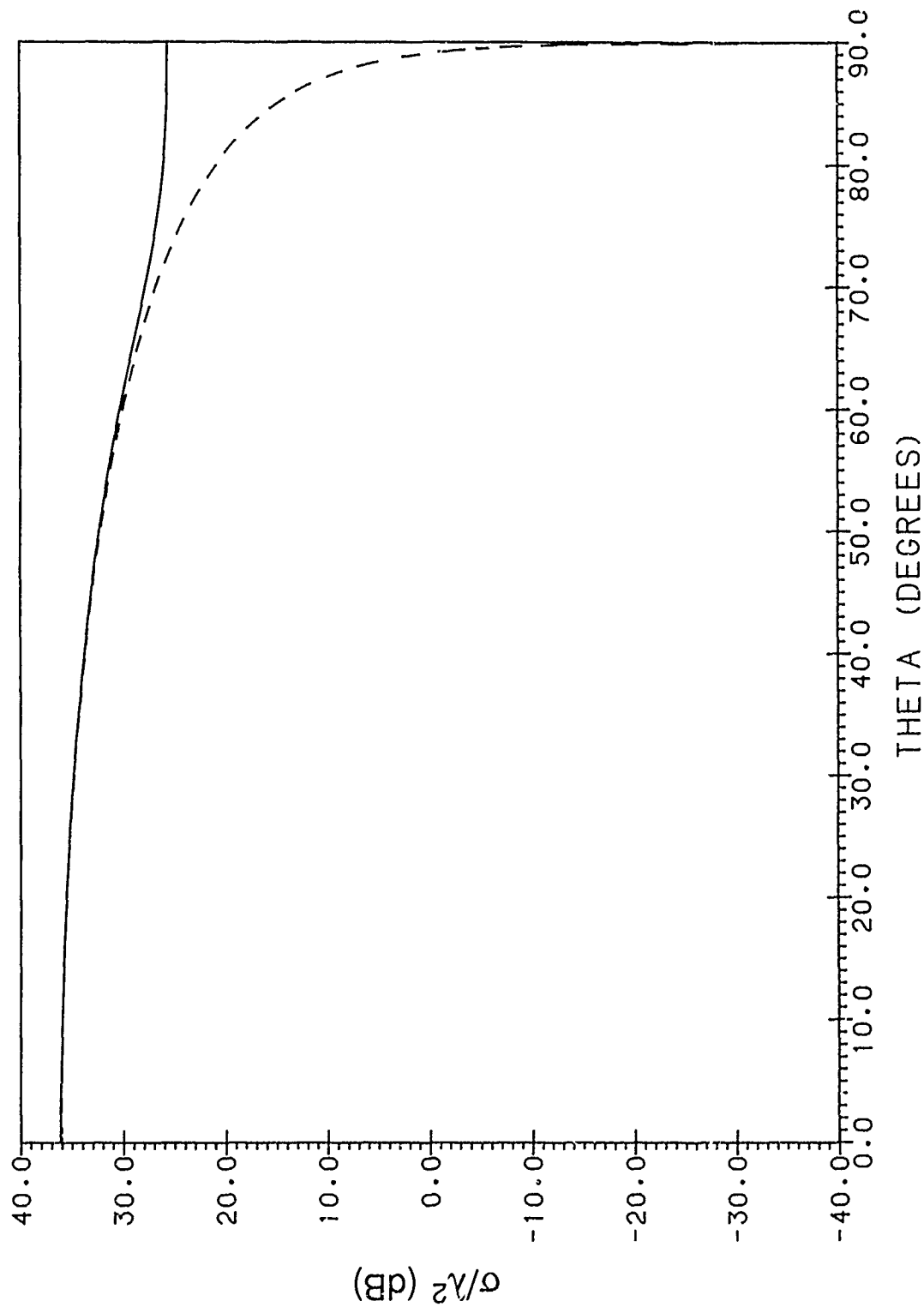


Figure 27a. Specular Scatter Cross Section Pattern of Disk,  $ka = 15$ , with Perpendicular Polarized Plane-Wave Illumination;  
 ---: Exact, ----: PO

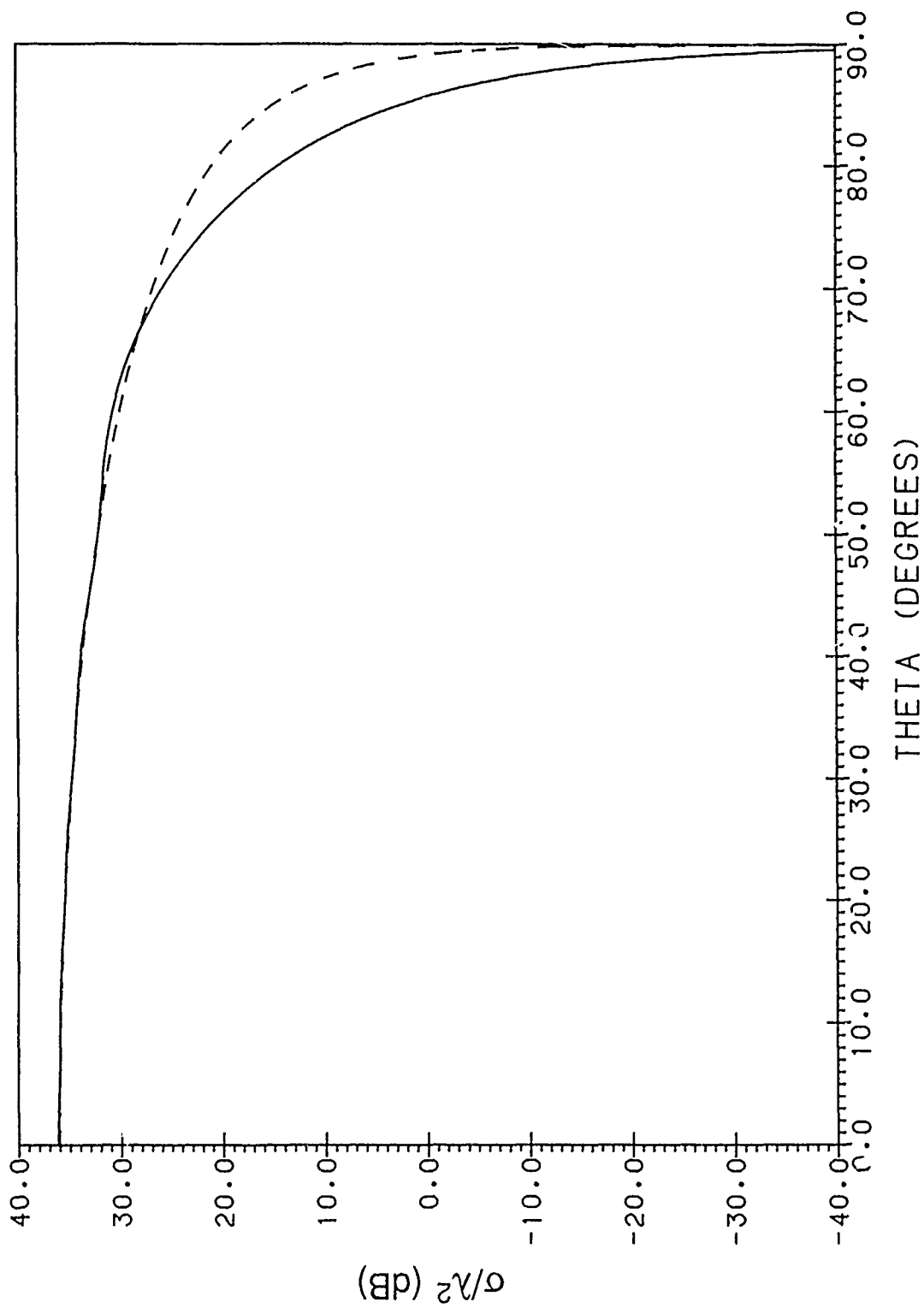


Figure 27b. Specular Scatter Cross Section Pattern of Disk,  $ka = 15$ , with Parallel Polarized Plane-Wave Illumination:  
 — : Exact, - - - - : PO

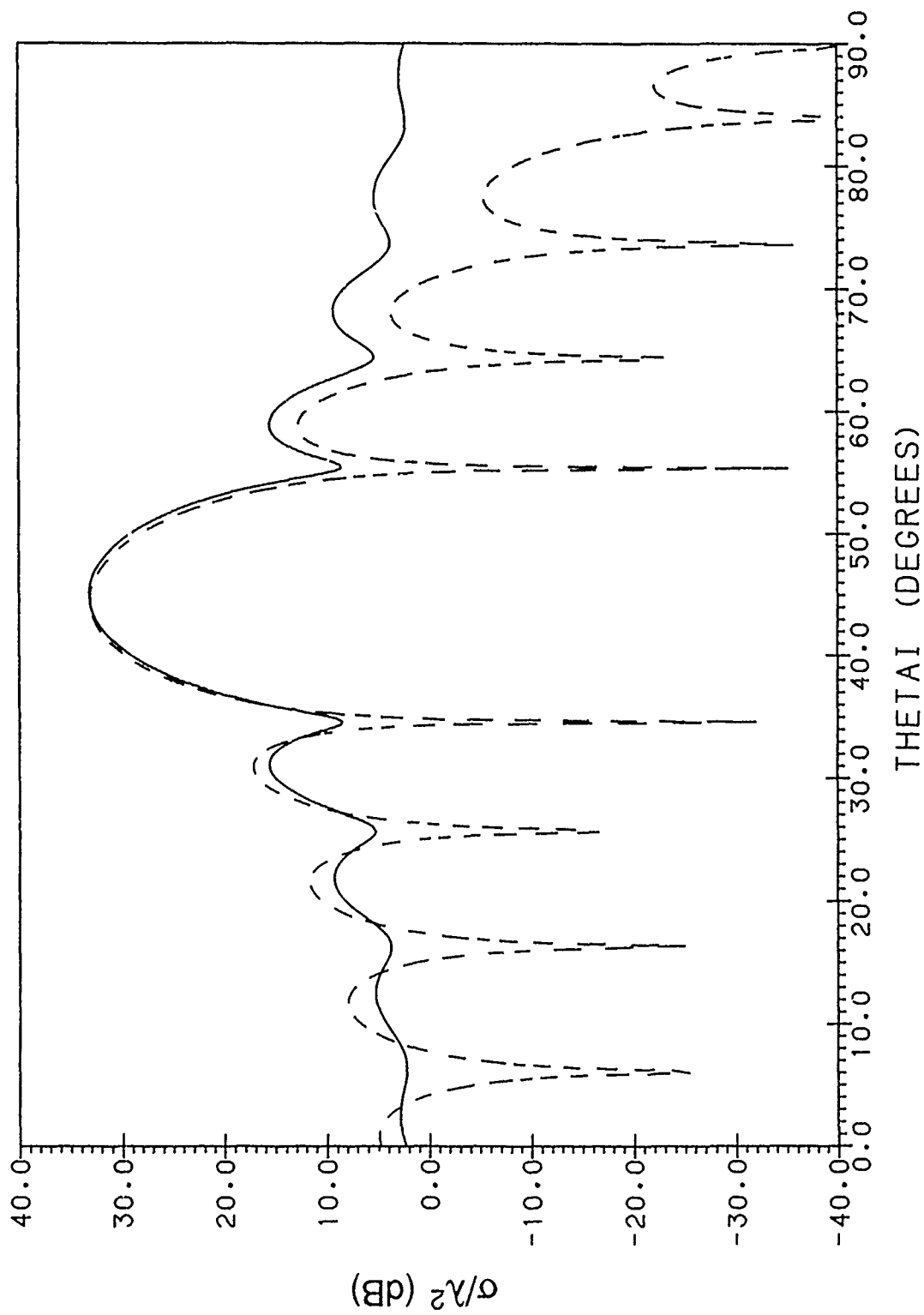


Figure 28a. Side Scatter Cross Section Pattern of Disk,  $ka = 15$ , with Perpendicular Polarized Plane-Wave Illumination;  
 —: Exact, ----: PO



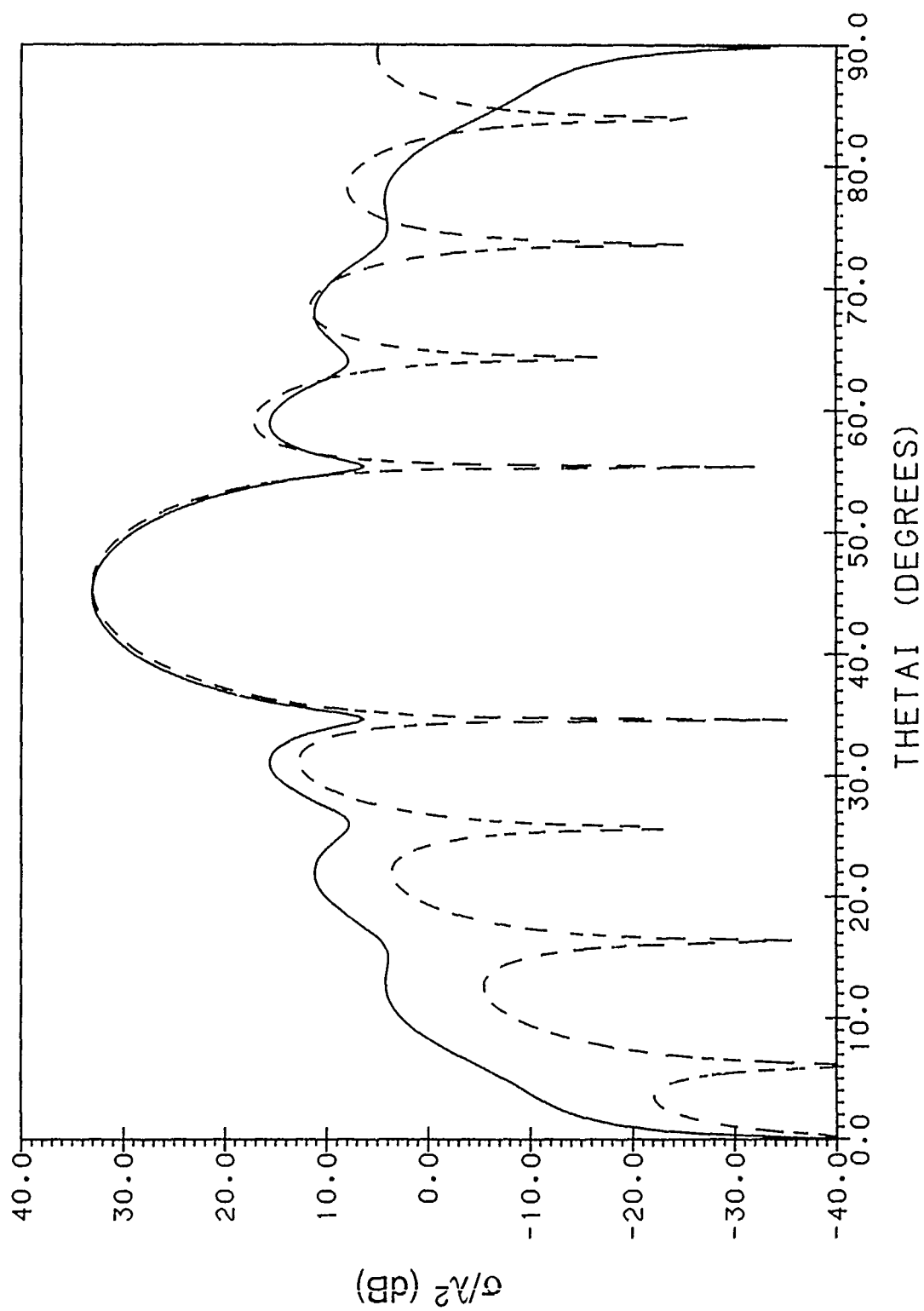


Figure 28b. Side Scatter Cross Section Pattern of Disk,  $ka = 15$ , with Parallel Polarized Plane-Wave Illumination;  
 — : Exact, - - - : PO

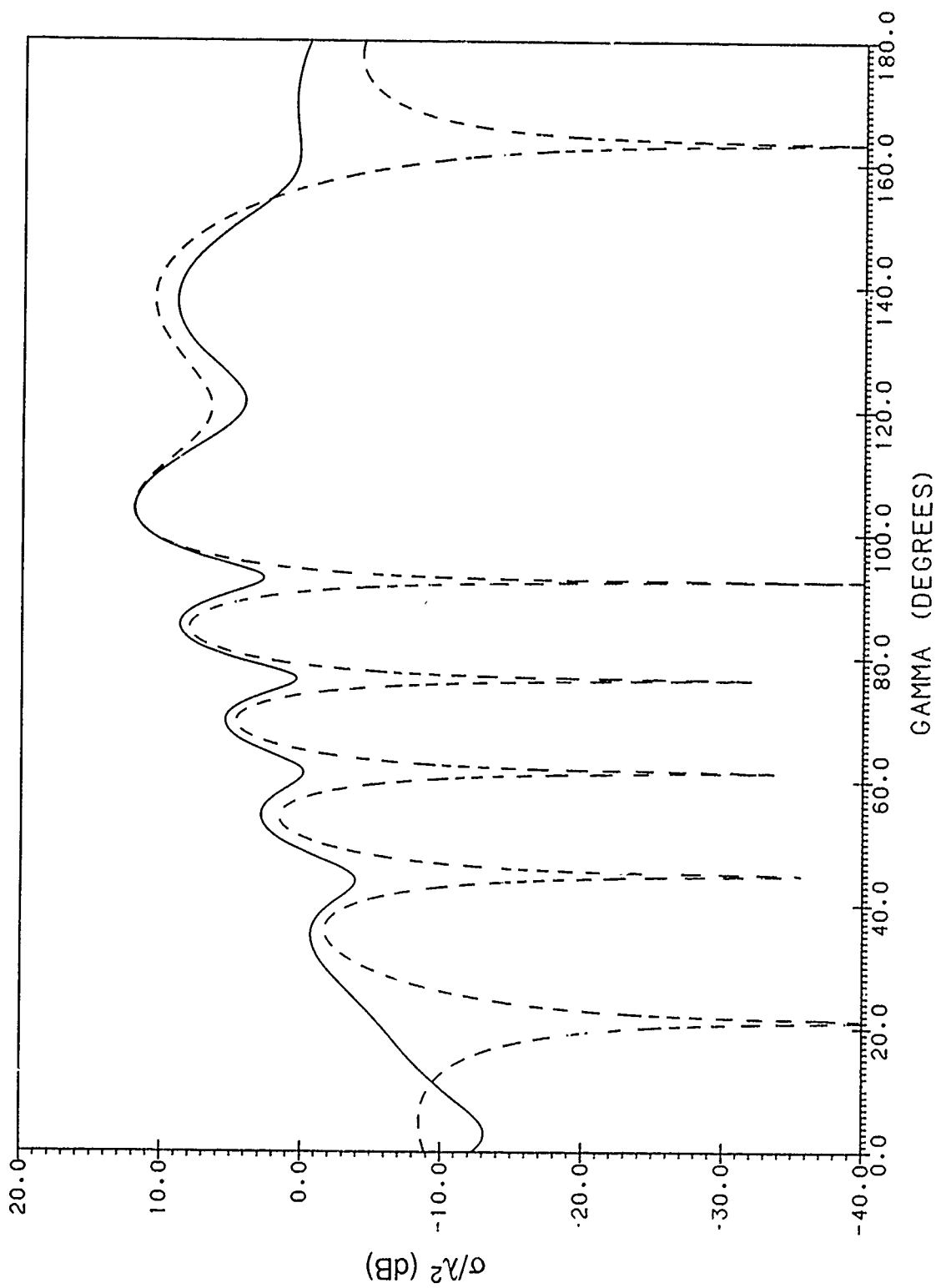


Figure 29a. Co-Polarized Cross Section Pattern of Disk,  $ka = 15$ , Illuminated by Perpendicular Polarized Plane Wave at  $\theta_i = 45^\circ$  in Plane Defined by  $\phi = 45^\circ$  and  $\phi = 225^\circ$ ; — : Exact, - - - : PO

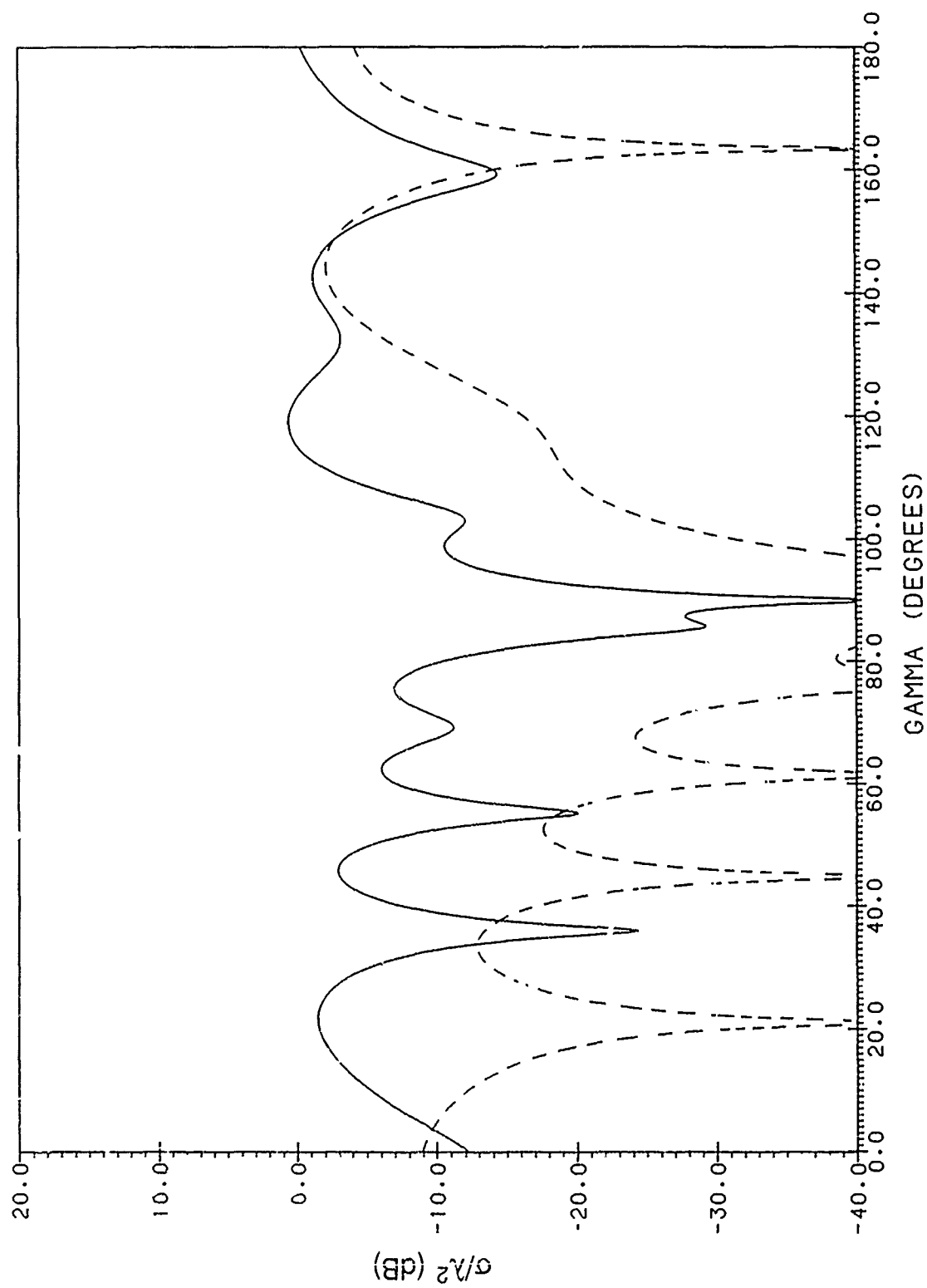


Figure 29b. Cross-Polarized Cross Section Pattern of Disk,  $ka = 15$ , Illuminated by Perpendicular Polarized Plane Wave at  $\theta_1 = 45^\circ$  in Plane Defined by  $\phi = 45^\circ$  and  $\phi = 225^\circ$ ; ———: Exact, - - - - - : PO

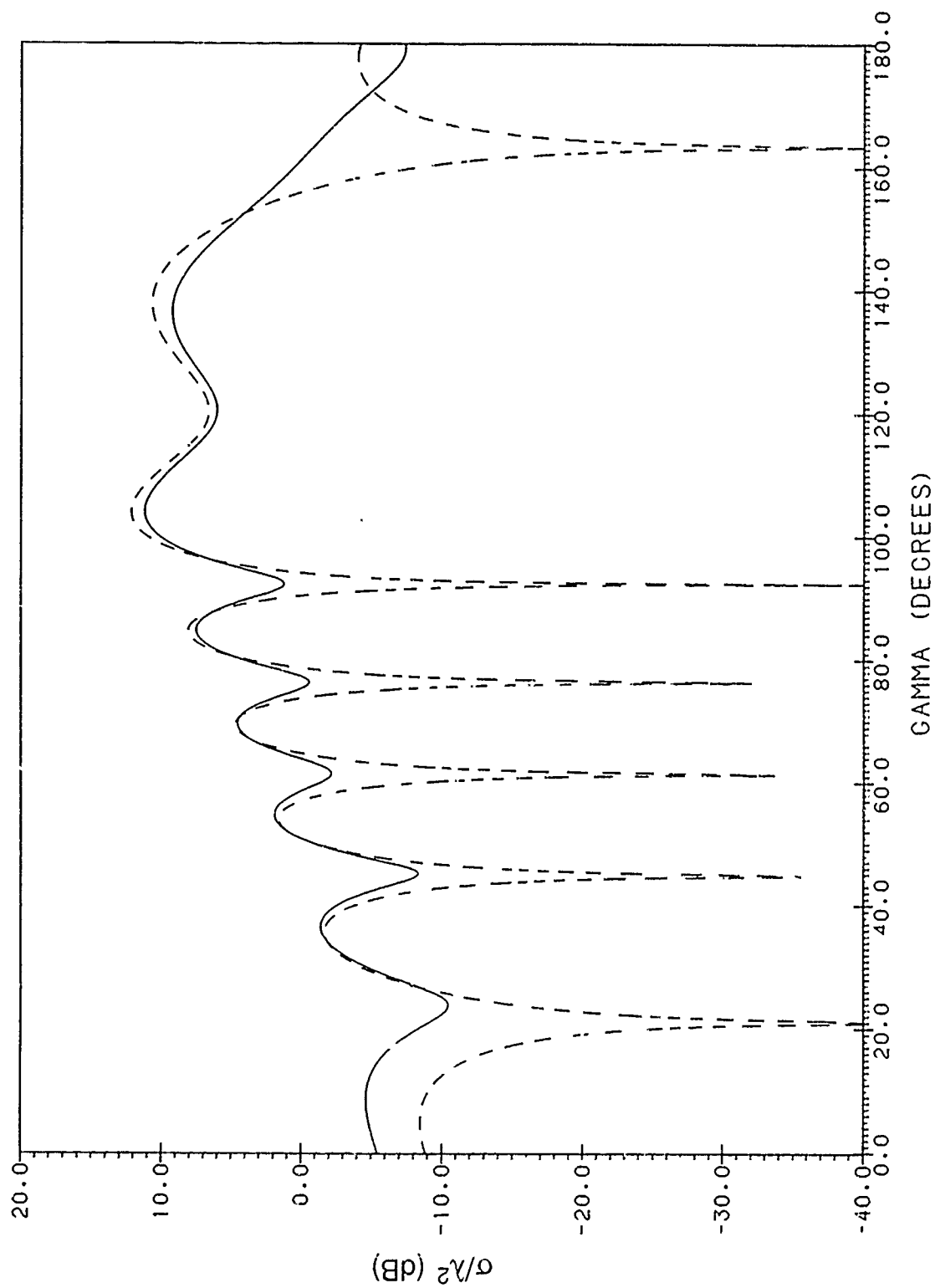


Figure 30a. Co-Polarized Cross Section Pattern of Disk,  $ka = 15$ , Illuminated by Parallel Polarized Plane Wave at  $\theta_i = 45^\circ$  in Plane Defined by  $\phi = 45^\circ$  and  $\phi = 225^\circ$ : — : Exact, ---- : PO

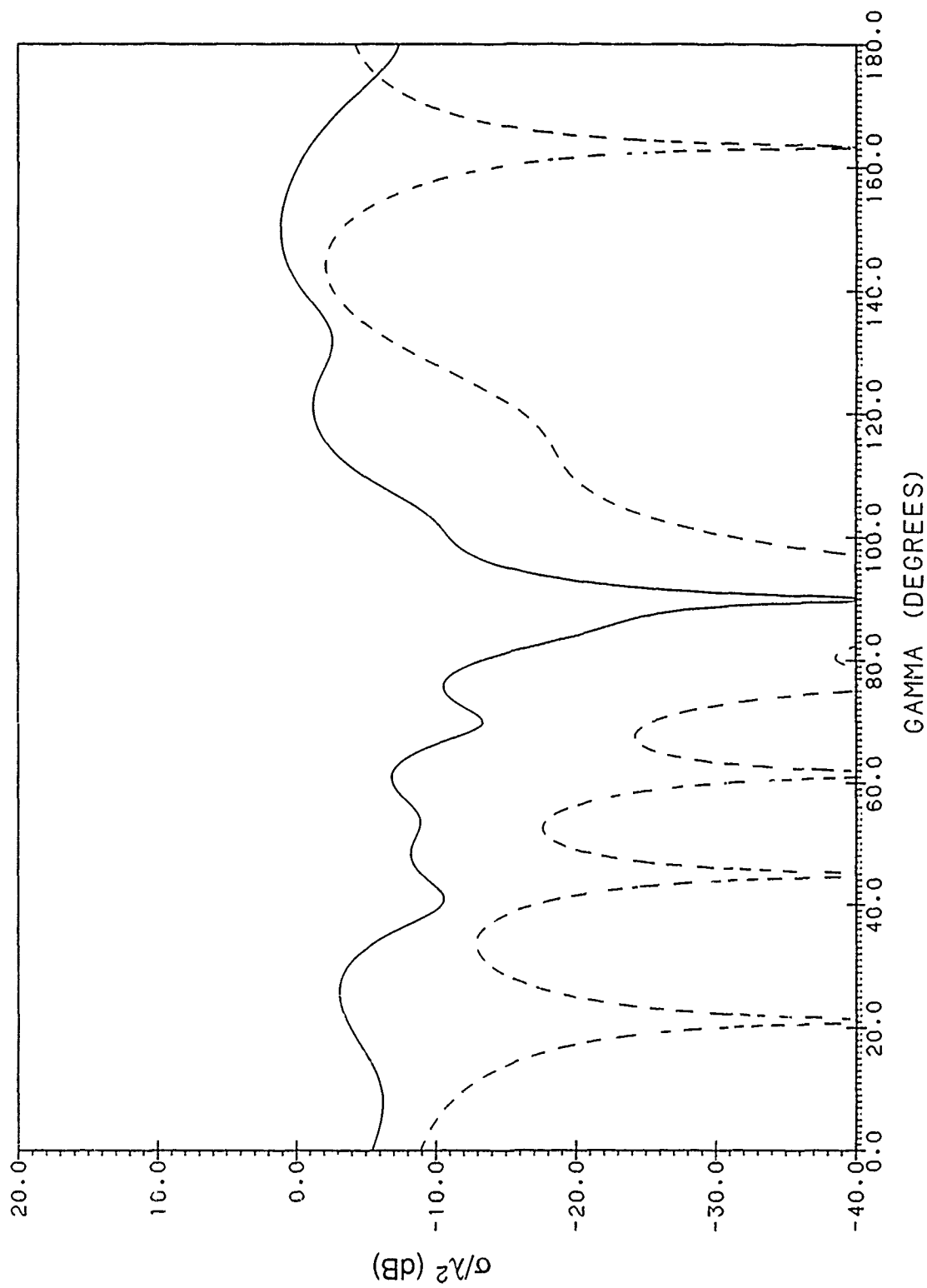


Figure 30b. Cross-Polarized Cross Section Pattern of Disk,  $ka = 15$ , Illuminated by Parallel Polarized Plane Wave at  $\theta_i = 45^\circ$  in Plane Defined by  $\phi = 45^\circ$  and  $\phi = 225^\circ$ ; — : Exact, - - - - : PO

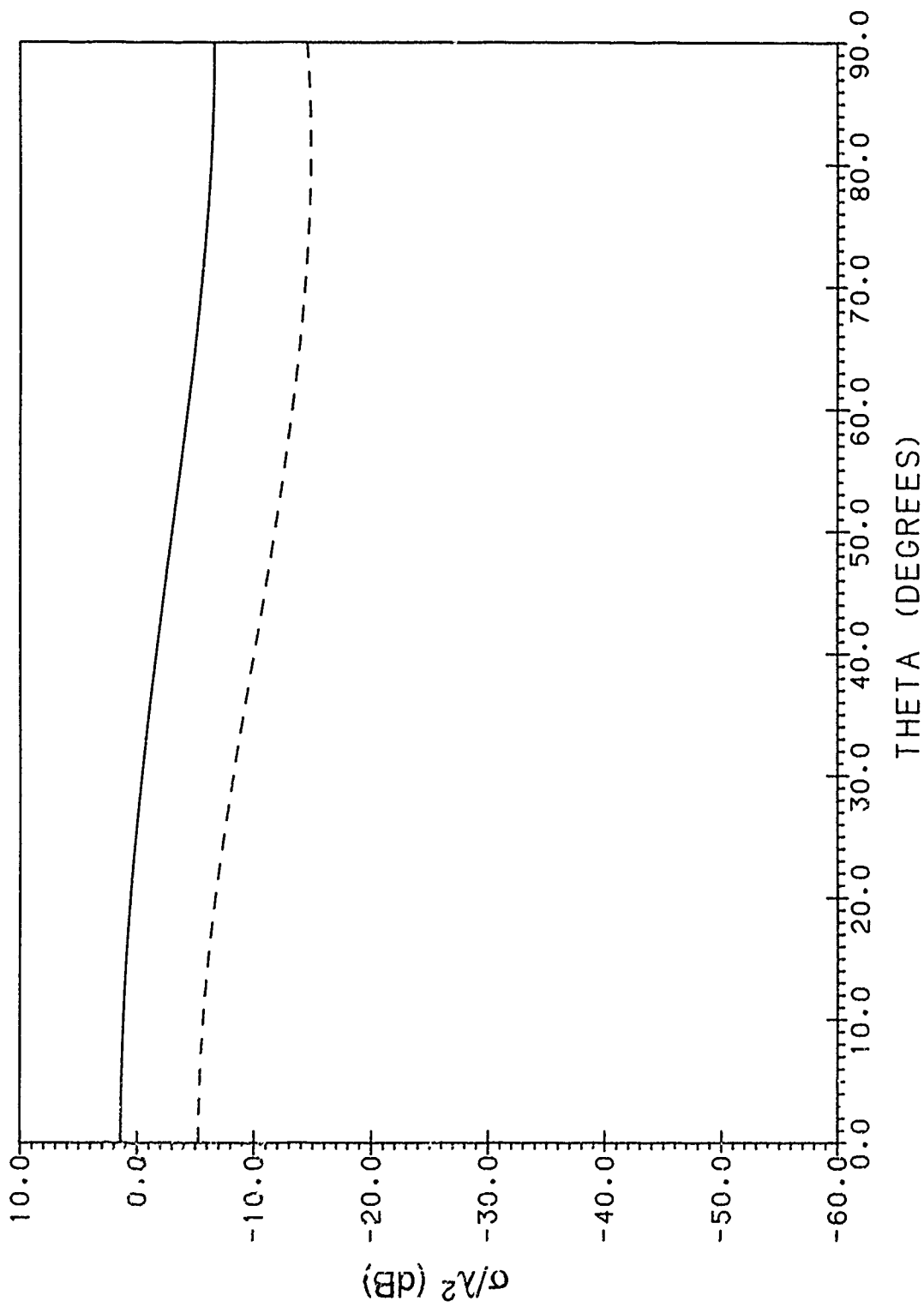


Figure 31a. Back Scatter Cross Section Pattern of Disk,  $ka = 1.5$ , with Perpendicular Polarized Plane-Wave Illumination and Incident Strips Parallel to x-Axis; —: Exact; ----: PO + Approximate Nonuniform Current Field Obtained by Integrating IDC

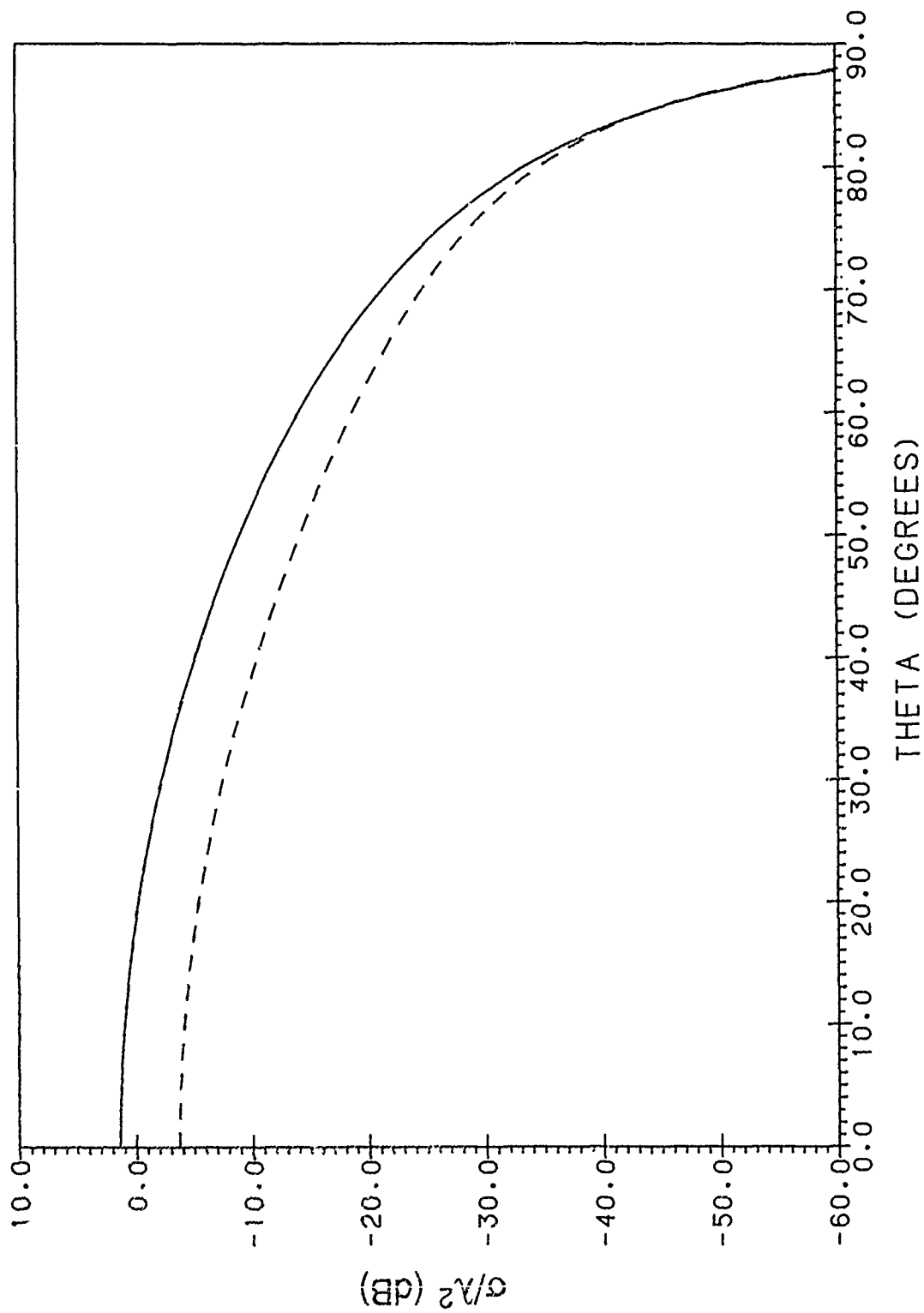


Figure 31b. Back Scatter Cross Section Pattern of Disk,  $ka = 1.5$ , with Parallel Polarized Plane-Wave Illumination and Incremental Strips Parallel to x-Axis; —: Exact; ---: PO + Approximate Nonuniform Current Field Obtained by Integrating IDC

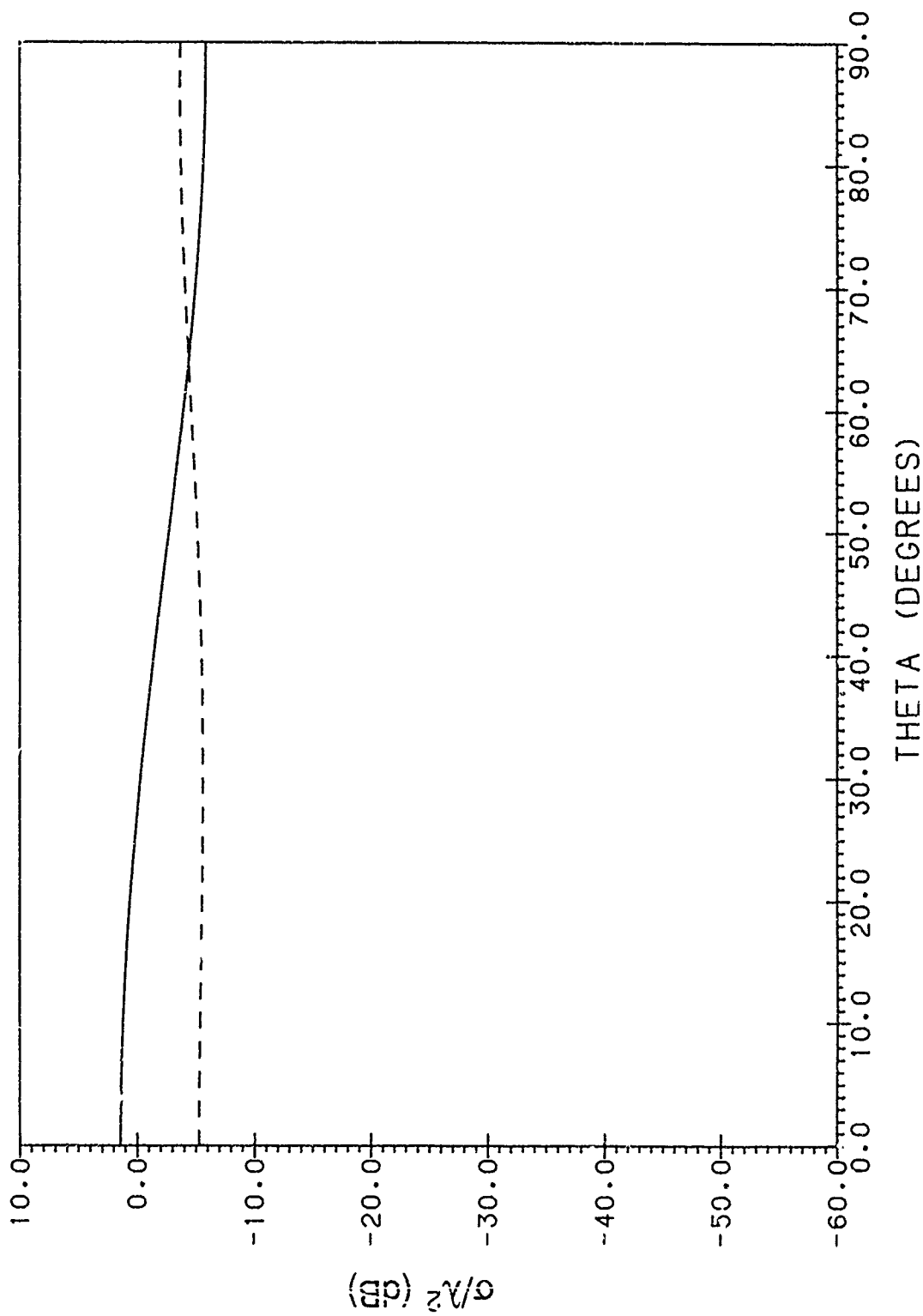


Figure 32a. Specular Scatter Cross Section Pattern of Disk,  $ka = 1.5$ , with Perpendicular Polarized Plane-Wave Illumination and Incremental Strips Parallel to x-Axis; ——— Exact, - - - - PO + Approximate Nonuniform Current Field Obtained by Integrating IDC



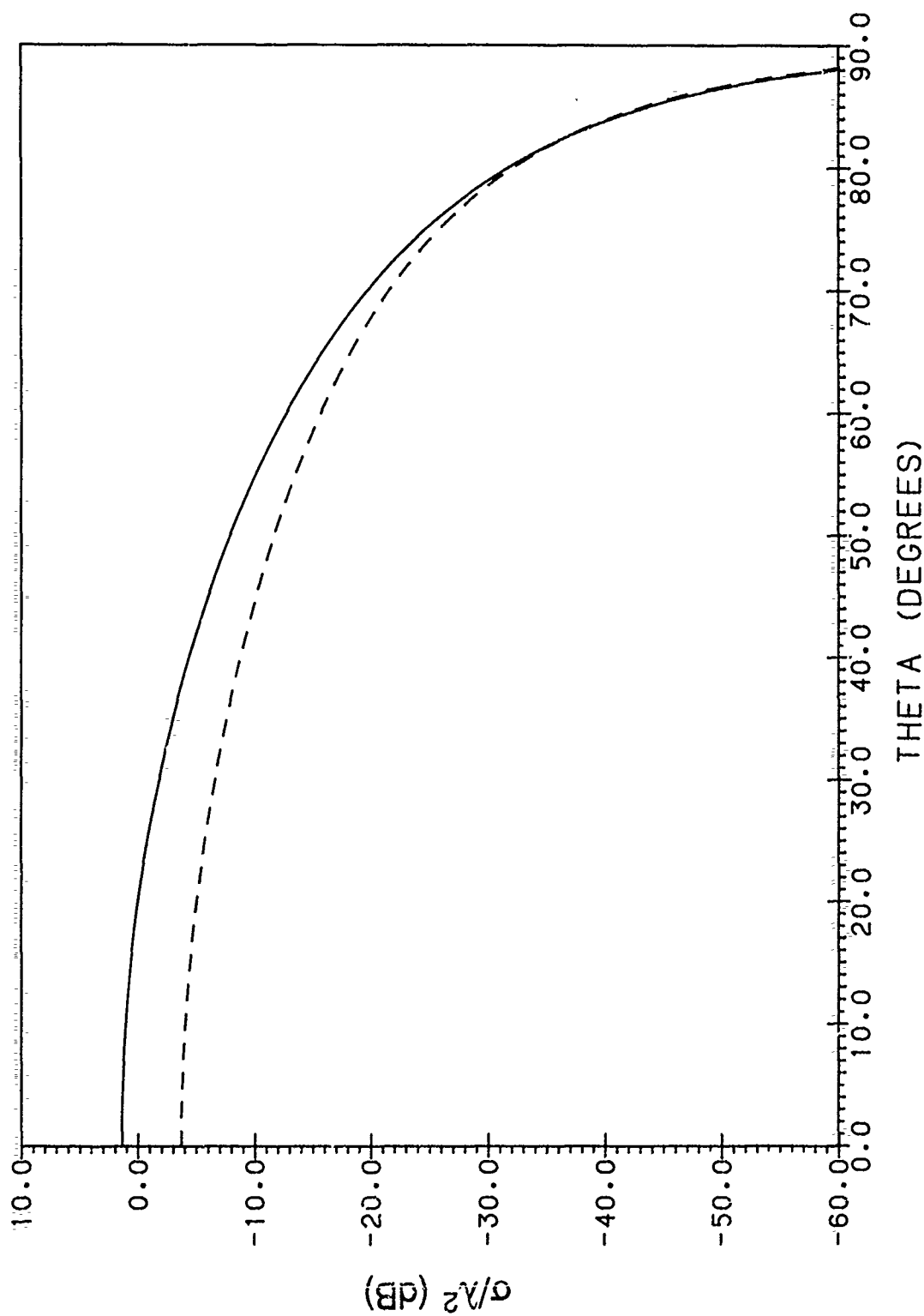


Figure 32b. Specular Scatter Cross Section Pattern of Disk,  $ka = 1.5$ , with Parallel Polarized Plane-Wave Illumination and Incremental Strips Parallel to x-Axis; —: Exact, ----: PO + Approximate Nonuniform Current Field Obtained by Integrating IDC

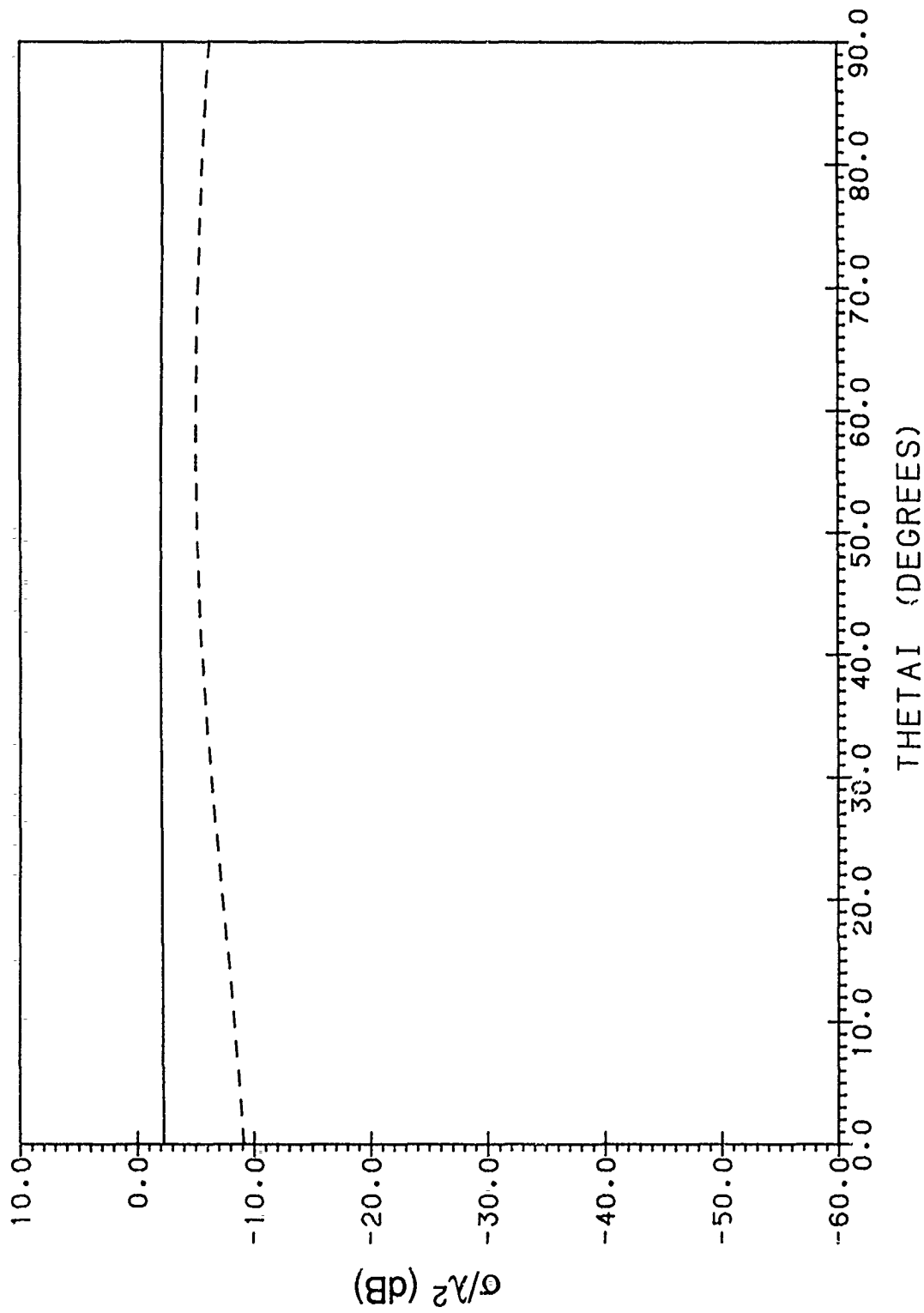


Figure 33a. Side Scatter Cross Section Pattern of Disk,  $ka = 1.5$ , with Perpendicular Polarized Plane-Wave Illumination and Incremental Strips Parallel to  $x$ -Axis; —: Exact, ----: PO + Approximate Nonuniform Current Field Obtained by Integrating IDC

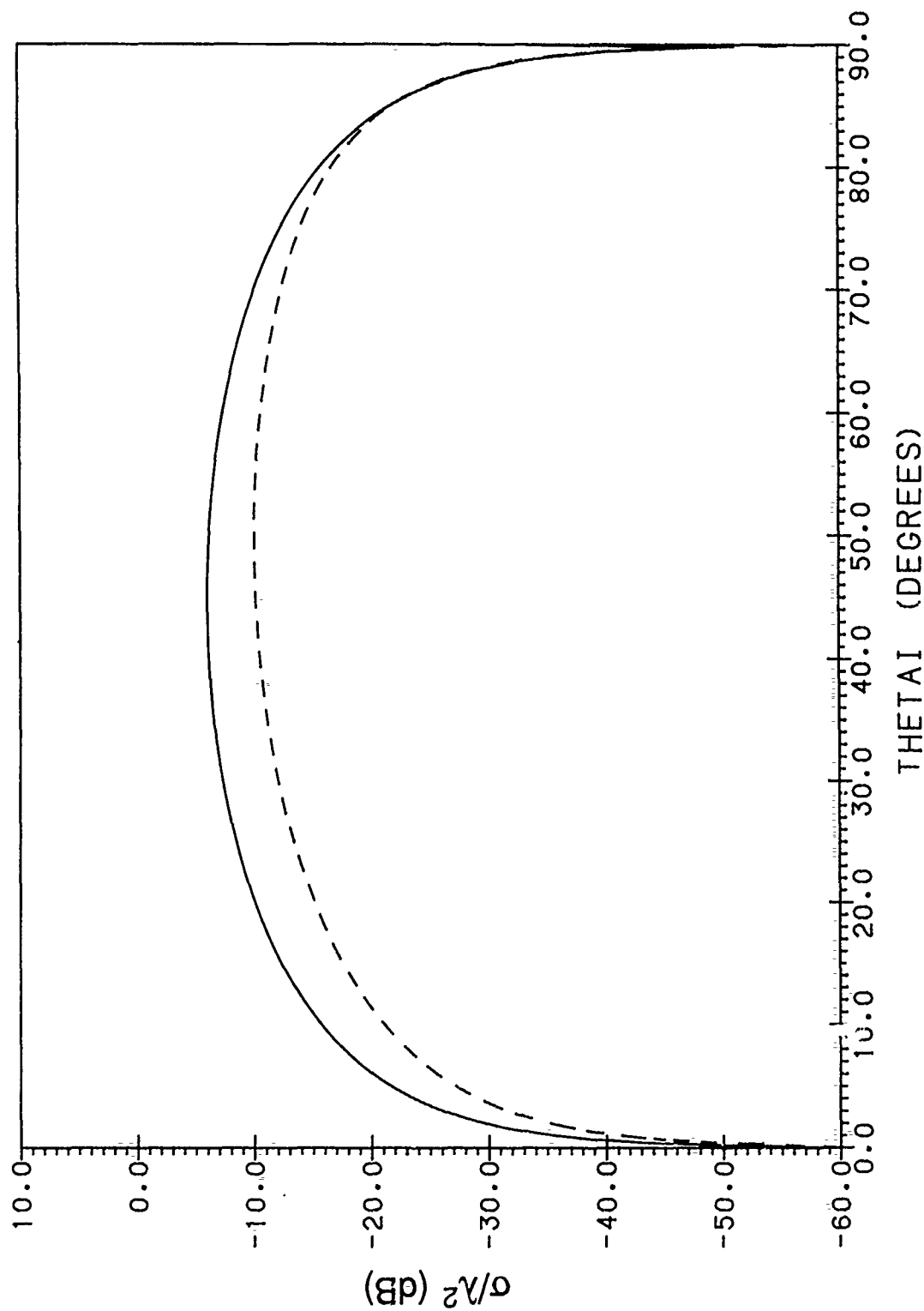


Figure 33b. Side Scatter Cross Section Pattern of Disk,  $ka = 1.5$ , with Parallel Polarized Plane-Wave Illumination and Incremental Strips Parallel to x-Axis; —: Exact, ----: PO + Approximate Nonuniform Current Field Obtained by Integrating IDC

## References

1. Mitzner, K.M. (1974) *Incremental Length Diffraction Coefficients*, Tech. Rep. No. AFAL-TR-73-296, (available from National Technical Information Service, Springfield, VA 22161, AD918861).
2. Michaeli, A. (1984) Equivalent edge currents for arbitrary aspects of observation, *IEEE Trans. Antennas Propagat.* **AP-32**:252-258, (correction, (1985) **AP-33**:227).
3. Shore, R.A. and Yaghjian, A.D. (1988) Incremental diffraction coefficients for planar surfaces, *IEEE Trans. Antennas Propagat.* **36**:55-70, (correction, (1989) **AP-37**:1342), also, *Incremental Diffraction Coefficients for Planar Surfaces, Part I: Theory*, RADC-TR-87-35, ADA208595.
4. Shore, R.A. and Yaghjian, A.D. (1987) *Incremental Diffraction Coefficients for Planar Surfaces, Part II: Calculation of Nonuniform Current Correction to PO Reflector Antenna Patterns*, RADC-TR-87-213, ADA208596.
5. Shore, R.A. and Yaghjian, A.D. (1988) *Incremental Diffraction Coefficients for Planar Surfaces, Part III: Pattern Effects of Narrow Cracks in the Surface of a Paraboloid Antenna*, RADC-TR-88-119, ADA207796.
6. Michaeli, A. (1986) Elimination of infinities in equivalent edge currents, Part I: fringe current components, *IEEE Trans. Antennas Propagat.* **AP-34**:912-918.
7. Knott, E.F. (1985) The relationship between Mitzner's ILDC and Michaeli's equivalent currents, *IEEE Trans. Antennas Propagat.* **AP-33**:112-114.
8. Coleman, J.R. (1973) *Investigation of Radar Scattering by Simulated Aircraft Duct/Engine Combinations*, Air Force Avionics Laboratory, AFAL-TR-73-361.
9. Sikta, F.A., Burnside, W.D., Chu, T.T., and Peters, L., Jr. (1983) First-order equivalent current and corner diffraction scattering from flat plate structures, *IEEE Trans. Antennas Propagat.* **AP-31**:584-589.
10. Michaeli, A. (1987) Equivalent currents for second-order diffraction by the edges of perfectly conducting polygonal surfaces, *IEEE Trans. Antennas Propagat.* **AP-35**:183-190.
11. Ufimtsev, P. Ya. (1958) Secondary diffraction of electromagnetic waves at a strip, *Journal of Technical Physics* **28** (No. 3).
12. Bowman, J.J., Senior, T.B.A., and Uslenghi, P.L.E. (1969) *Electromagnetic and Acoustic Scattering by Simple Shapes*, Amsterdam: North-Holland.

13. Dominek, A.K. (1988) Personal Communication, Ohio State University ElectroScience Laboratory.
14. Michaeli, A. (1984) A closed form physical theory of diffraction solution for electromagnetic scattering by strips and  $90^\circ$  dihedrals, *Radio Science* **19**:609-616.
15. Ufimtsev, P. Ya. (1969) Asymptotic investigation of the problem of diffraction on a strip, *Radio Engineering and Electronic Physics* **14**:1014-1025.
16. DeVore, R., Hodge, D.B., and Kouyoumjian, R.C. (1971) Backscattering cross sections of circular disks for arbitrary incidence, *J. Applied Physics* **42**:3075-3083.
17. Marsland, D.P., Balanis, C.A., and Brumley, S.A. (1987) Higher order diffractions from a circular disk, *IEEE Trans. Antennas Propagat.* **AP-35**:1436-1444.
18. Trott, K. (1988) *The Disk: A Comparison of Electromagnetic Scattering Solutions and Its Use as a Calibration Standard for Bistatic RCS Measurements*, RADC-TR-88-16, ADA200327.
19. Ludwig, A.C. (1973) The definition of cross polarization, *IEEE Trans. Antennas Propagat.* **AP-21**:116-119.
20. Hodge, D.B. (1979) *The Calculation of Far Field Scattering by a Circular Metal Disk*, Ohio State University ElectroScience Laboratory Report 710816-2.
21. Dominek, A.K. (1988) Personal Communication, Ohio State University ElectroScience Laboratory.

## Appendix A: Derivation of an Integral of the Fresnel Integral

In this Appendix we obtain a closed form expression for the following integral of the Fresnel integral:

$$\int_0^x F(u) e^{iau} du, \quad x > 0, \quad (A-1)$$

where  $F(u)$  is the Fresnel integral defined by

$$F(u) = \frac{1}{\sqrt{2\pi}} \int_0^u \frac{e^{it}}{\sqrt{t}} dt \quad (A-2)$$

To integrate (A-1), begin by integrating by parts to obtain

$$\int_0^x F(u) e^{iau} du = \frac{1}{ia} \left[ e^{iax} F(x) - \frac{1}{\sqrt{2\pi}} \int_0^x \frac{e^{i(a+1)u}}{\sqrt{u}} du \right]. \quad (A-3)$$

We now consider the following three cases: i)  $a+1 > 0$ ; ii)  $a+1 < 0$ ; and iii)  $a+1 = 0$ .

i)  $a+1 > 0$

For  $a+1 > 0$  let  $t = (a+1)u$ . Then from Eq. (A-3)

$$\begin{aligned} \int_0^x F(u) e^{iau} du &= \frac{1}{ia} \left[ e^{iax} F(x) - \frac{1}{(a+1)^{1/2}} \frac{1}{\sqrt{2\pi}} \int_0^{(a+1)x} \frac{e^{it}}{\sqrt{t}} dt \right] \\ &= \frac{1}{ia} \left[ e^{iax} F(x) - \frac{1}{(a+1)^{1/2}} F((a+1)x) \right]. \end{aligned} \quad (A-4)$$

ii)  $a+1 < 0$

Let  $t = |a+1|u$ . Then from Eq. (A-3)

$$\begin{aligned} \int_0^x F(u) e^{iau} du &= \frac{1}{ia} \left[ e^{iax} F(x) - \frac{1}{|a+1|^{1/2}} \frac{1}{\sqrt{2\pi}} \int_0^{(a+1)x} \frac{e^{-it}}{\sqrt{t}} dt \right] \\ &= \frac{1}{ia} \left[ e^{iax} F(x) - \frac{1}{|a+1|^{1/2}} F^*(|a+1|x) \right]. \end{aligned} \quad (A-5)$$

iii)  $a+1 = 0$  or  $a = -1$

From Eq. (A-3)

$$\begin{aligned} \int_0^x F(u) e^{-iu} du &= -\frac{1}{i} \left[ e^{-ix} F(x) - \frac{1}{\sqrt{2\pi}} \int_0^x \frac{1}{\sqrt{u}} du \right] \\ &= i \left[ e^{-ix} F(x) - \sqrt{\frac{2}{\pi}} \sqrt{x} \right]. \end{aligned} \quad (A-6)$$

Thus,

$$\int_0^x F(u) e^{iau} du = \begin{cases} \frac{1}{ia} \left[ e^{iax} F(x) - \frac{1}{(a+1)^{1/2}} F((a+1)x) \right], & a+1 > 0 \\ \frac{1}{ia} \left[ e^{iax} F(x) - \frac{1}{|a+1|^{1/2}} F^*(|a+1|x) \right], & a+1 < 0 \\ i \left[ e^{-ix} F(x) - \sqrt{\frac{2}{\pi}} \sqrt{x} \right], & a+1 = 0 \end{cases} \quad (A-7)$$

## Appendix B: Derivation of Incremental Strip Parameters

In this Appendix we derive expressions for the width,  $s$ , of the incremental strip in the IDC's given by Eqs. (40) and (42), and for  $\cot \psi_l$  in Eq. (41) where  $\psi_l$  is the angle between the axis of the incremental strip and the positive local  $z$ -direction. Both quantities depend on the choice of orientation of the incremental strips. We consider two choices: 1) incremental strips chosen parallel to the  $x$ -axis (the projection on the plane of the disk of the direction vector of the incident plane wave); and 2) incremental strips chosen in the direction of the diffracted rays on the disk.

### B1. Incremental Strips Parallel to the X-Axis

Referring to Figure B1a, we consider an incremental strip taken parallel to the  $x$ -axis at the point on the edge of the disk at  $\phi'$ ,  $-\pi \leq \phi' \leq \pi$ . Since the local unit  $z$ -vector,  $\hat{z}_l$ , is equal to  $\hat{\phi}'$ , [(Eq. (50c)],  $\phi_l$  is the angle between the chord parallel to the  $x$ -axis at  $\phi'$  and the tangent to the disk at  $\phi'$ . From elementary geometric considerations

$$\psi_l = \begin{cases} \frac{\pi}{2} - \phi', & -\frac{\pi}{2} \leq \phi' < \frac{\pi}{2}, \\ \frac{3\pi}{2} - \phi', & \frac{\pi}{2} \leq \phi' < \pi, \\ -\frac{\pi}{2} - \phi', & -\pi \leq \phi' < -\frac{\pi}{2}, \end{cases} \quad (\text{B1})$$

so that

$$\cot \psi_l = \tan \phi'. \quad (\text{B2})$$



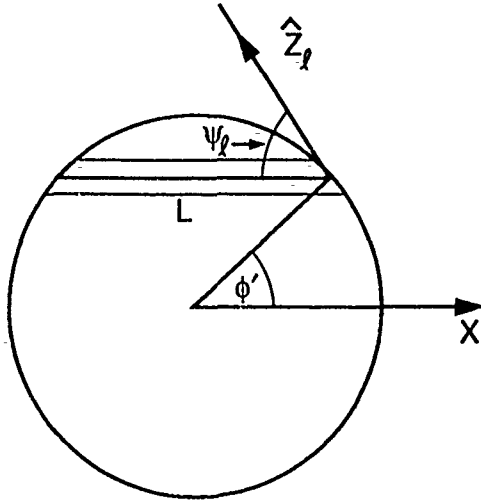


Figure B1a. Geometry of Disk with Incremental Strips Parallel to the x-Axis

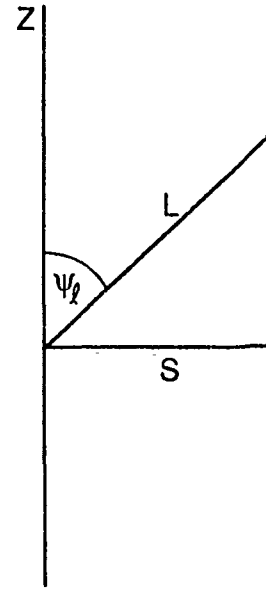


Figure B1b. Corresponding Strip Geometry

Since the disk is modelled locally by a strip whose edges are parallel to the local  $z$ -axis (see Figure B1b), the strip width  $s$  in the IDC's Eqs. (40) and (42) is related to the chord length  $L$  in Figure B1a by

$$s = L \sin \psi_l . \quad (B3)$$

Hence, with Eq. (B1)

$$s = L |\cos \phi'| . \quad (B4)$$

But

$$L = 2a |\cos \phi'| \quad (B5)$$

so that

$$s = 2a \cos^2 \phi' . \quad (B6)$$

## B2. Incremental Strips in the Direction of the Diffracted Rays

Let

$$\hat{r}_d = \alpha \hat{x} + \beta \hat{y} \quad (B7)$$

with

$$\alpha^2 + \beta^2 = 1 \quad (B8)$$

be the diffracted ray unit vector on the disk at the point  $(x', y') = (a \cos \phi', a \sin \phi')$ . The angle,  $\phi_l$  that  $\hat{r}_d$  makes with the local unit  $z$ -vector,  $\hat{\phi}'$  is given by

$$\psi_l = \pi - \theta_{0l} \quad (B9)$$

where  $\theta_{0l}$  is the angle between the local z-axis and the vector in the direction from which the illuminating plane wave is incident. Then from Eqs. (51a,b)

$$\cos \psi_l = -\cos \theta_{0l} = \sin \theta_i \sin \phi', \quad (\text{B10a})$$

$$\sin \psi_l = \sin \theta_{0l} = (1 - \sin^2 \theta_i \sin^2 \phi')^{1/2}, \quad (\text{B10b})$$

so that

$$\cot \psi_l = -\cot \theta_{0l}. \quad (\text{B11})$$

To determine the length of the chord,  $L$ , made by the diffracted ray on the disk we first need expressions for the direction cosines  $\alpha$  and  $\beta$  in Eq. (B7).

Since

$$\hat{\mathbf{r}}_d \cdot \hat{\boldsymbol{\phi}}' = \cos \psi_l \quad (\text{B12})$$

it follows from Eq. (B10a) that

$$-\alpha \sin \phi' + \beta \cos \phi' = \sin \theta_i \sin \phi' \quad (\text{B13})$$

or

$$\beta = \tan \phi' (\alpha + \sin \theta_i). \quad (\text{B14})$$

Substituting Eq. (B14) into (B8), solving the resulting quadratic equation for  $\alpha$ , and substituting  $\alpha$  in Eq. (B14) gives

$$\alpha = -\sin \theta_i \sin^2 \phi' \pm \cos \phi' (1 - \sin^2 \theta_i \sin^2 \phi')^{1/2}, \quad (\text{B15a})$$

$$\beta = \sin \phi' \left[ \sin \theta_i \cos \phi' \pm (1 - \sin^2 \theta_i \sin^2 \phi')^{1/2} \right]. \quad (\text{B15b})$$

Now let

$$x = a \cos \phi' + \alpha u, \quad (\text{B16a})$$

$$y = a \sin \phi' + \beta u, \quad (\text{B16b})$$

be the parametric representation of points on the diffracted ray. Substituting for  $\alpha$  and  $\beta$  from Eq. (B15) in Eq. (B16), setting

$$x^2 + y^2 = a^2 \quad (\text{B17})$$

and letting  $L$  be the resulting solution for  $u$ , yields

$$L = -2a \cdot \pm (1 - \sin^2 \theta_i \sin^2 \phi')^{1/2} \quad (\text{B18})$$

where the  $\pm$  corresponds to that in Eq. (B15). It follows that the minus sign must be chosen in Eq. (B15) and

$$L = 2a (1 - \sin^2 \theta_i \sin^2 \phi')^{1/2} \quad (\text{B19})$$

Hence, using Eqs. (B3) and (B10b),

$$s = 2a (1 - \sin^2 \theta_i \sin^2 \phi'). \quad (\text{B20})$$



## Appendix C: Conditions for Incremental Current Strips to Accurately Predict Fields Diffracted from the Trailing Edge

In Section 2.5 we modified the TE fields incident upon the trailing edge of a truncated half-plane to account for the nonuniform TE current that emanates from the leading edge and diffracts at the trailing edge. (The nonuniform TM currents decay rapidly away from the leading edge for all angles of incidence, and thus, produce negligible diffracted fields at the trailing edge of a truncated half-plane a few or more wavelengths across.) In applying the TE modification derived in Section 2.5 to the disk, we assume that the incremental nonuniform current strips maintain a constant width across the disk. Although this assumption is valid for the infinitely long straight edges of a truncated half-plane, it may not yield an accurate representation of the actual nonuniform currents beyond a certain distance from the leading edge of a finite dimensional flat plate such as the disk. The purpose of this Appendix is to establish the distance from the leading edge of a flat plate that the nonuniform current predicted by incremental half-plane current strips remains a good approximation to the actual current.

When the incident plane-wave is grazing, the magnitude of the nonuniform TE current remains constant across the flat plate and the nonuniform incremental-strip current agrees exactly with the actual current. For an incident plane-wave far from grazing, the actual TE nonuniform current,  $K_{\text{actual}}$ , emanating from the leading edge of the plate can be evaluated approximately by a stationary phase evaluation of the diffraction integral. This evaluation leads to the usual geometric factor in the edge-diffracted rays<sup>C1</sup>; specifically

---

C1. Kouyoumjian, R.G. (1975) The geometrical theory of diffraction and its application, Chapter 6 in Vol. 3 of Topics in Applied Physics (*Numerical and Asymptotic Techniques in Electromagnetics*), R. Mittra, Ed., New York: Springer Verlag.

$$K_{\text{actual}}^{\text{nu(TE)}} = A \sqrt{\frac{q}{d(q+d)}} e^{ikd} \quad (\text{C1})$$

where  $d$  is the distance from the leading edge (diffraction point) along the diffracted ray to the observation point in the plate, and  $q$  is the focal length along this diffracted ray measured from the leading edge. The focal length is determined by the curvature of the leading edge at the diffraction point and the direction of incidence of the illuminating plane wave. The constant  $A$  is a complex amplitude proportional to the amplitude of the incident plane wave. The derivation of Eq. (C1) assumes that the distance  $d$  from the leading edge to the observation point is greater than about a wavelength, and that the incident plane-wave is sufficiently far from grazing for the nonuniform TE current to decay as  $1/\sqrt{d}$  for  $\lambda < d \ll q$ .

The nonuniform TE current,  $K_{\text{incr}}^{\text{nu(TE)}}$ , predicted by incremental half-plane current strips of constant width, taken along the directions of the diffracted rays through the trailing edge points, is given approximately by

$$K_{\text{incr}}^{\text{nu(TE)}} = A \sqrt{\frac{1}{d}} e^{ikd} \quad (\text{C2})$$

for  $d \geq \lambda$  and the incident plane-wave far from grazing. The  $1/\sqrt{d}$  factor can be derived by subtracting the PC current from the total current in Eq. (32a) and then letting  $2k \sin \theta_0 \cos^2(\phi_0/2)$  be much larger than unity.

Comparing Eq. (C2) with Eq. (C1), we see that the nonuniform TE current predicted by the incremental half-plane strips of current is a reasonable approximation to the actual TE current when  $|d/q| \geq 1/4$ ; that is, when the distance from the leading edge along the diffracted ray is less than about one-quarter of the focal length. Thus, secondary diffraction at the trailing edge of the nonuniform current emanating from the leading edge will be accurately determined by the half-plane incremental current strips when the distance along the diffracted ray is less than about one-quarter of the focal length. Of course, for a plane wave incident along a direction far from grazing, the secondary diffraction of the nonuniform current will become negligible with increasing plate size. Moreover, as mentioned above, near grazing incidence the incremental nonuniform current closely approximates the actual current across the plate, and secondary diffraction is accurately predicted. Interestingly, near grazing incidence the focal length of the diffracted rays approaches infinity. Hence, although the expressions for current in Eqs. (C1) and (C2) are not valid close to grazing, they correctly predict equality at grazing incidence between the actual and incremental half-plane strip nonuniform current.

## Reference

- C1. Kouyoumjian, R.G. (1975) The geometrical theory of diffraction and its application, Chapter 6 in Vol. 3 of Topics in Applied Physics (*Numerical and Asymptotic Techniques in Electromagnetics*), R. Mittra, Ed., New York: Springer Verlag.



## *MISSION of Rome Air Development Center*

RADC plans and executes research, development, test and selected acquisition programs in support of Command, Control, Communications and Intelligence (C<sup>3</sup>I) activities. Technical and engineering support within areas of competence is provided to ESD Program Offices (POs) and other ESD elements to perform effective acquisition of C<sup>3</sup>I systems. The areas of technical competence include communications, command and control, battle management, information processing, surveillance sensors, intelligence data collection and handling, solid state sciences, electromagnetics, and propagation, and electronic, maintainability, and compatibility.